NASA CR-175,836

Polytechnic Institute of New York

NASA-CR-175836
19850018678

POLYTECHNIC INSTITUTE OF NEW YORK

FINAL REPORT

to

NASA-AMES RESEARCH CENTER

on

CHARACTERIZATION-CURING-PROPERTY STUDIES OF HBRF 55A RESIN FORMULATIONS

Co-principal Investigators:

Eli M. Pearce
Dean of Arts and Sciences
Director, Polymer Research Institute

Jovan Mijovic
Associate Professor of Chemical Engineering

JANUARY 31, 1985

POLYTECHNIC INSTITUTE OF NEW YORK

FINAL REPORT

to

NASA-AMES RESEARCH CENTER

on

CHARACTERIZATION-CURING-PROPERTY STUDIES OF HBRF 55A RESIN FORMULATIONS

Co-principal Investigators:

Eli M. Pearce
Dean of Arts and Sciences
Director, Polymer Research Institute

Jovan Mijovic
Associate Professor of Chemical Engineering

JANUARY 31, 1985

Additional Research Team Members:

1. Y. Okamoto
   Professor of Chemistry

2. A. Moroni
   Post-doctoral Fellow

3. C.C. Foun
   Ph.D. Candidate

4. H. Mei
   Ph.D. Candidate

FOREWORD

The information compiled herein presents the final report of our research into characterization-curing-property investigations on HBRF 55A resin formulations.

The first part of this report reviews our initial studies on "as-received" cured samples cut from a full-size FWC. Results are presented in condensed form. Inadequacies of "as-received" and aged samples are pointed out. Additional electron microscopic evidence, not included in preceding progress reports, is offered herein.

The second part of the report describes our results of characterization of "as-received" ingredients of HBRF 55A formulation. Specifically, Epon 826, Epon 828, EpiRez 5022, RD-2 and various amines, including Tonox and Tonox 60/40, were characterized. GPC, NMR and FTIR were among techniques used in the characterization study.

The third part of our report deals with investigation of cure kinetics of various formulations. Hitherto, studies done using isothermal DSC runs at various high temperatures yielded reliable kinetic models.

The fourth part of our report describes changes in physical/thermal properties (viscosity, specific heat, thermal conductivity and density) during cure. Preliminary results were obtained at several temperatures between 25° - 50°C and can be used in modeling of cure.

PART I

PHYSICAL/MECHANICAL PROPERTIES, DAMAGE TOLERANCE AND AGING OF THE "AS-RECEIVED" GRAPHITE/EPOXY COMPOSITES USED FOR FWC

EXPERIMENTAL

The first set of experiments was conducted on various samples cut from a large block of a full size FWC and supplied to us by NASA-Ames. The samples were cut on July 29 and the various sample configurations are described in previous reports. The "as-received" samples were first visually inspected for flaws, i.e., voids, imperfections, etc. The largest voids were visually detected and mapped on each sample. We initially planned to try to correlate the failure during testing to the original location of voids. The existence of numerous voids was more clearly seen in the micrographs presented in our progress reports. A Bausch and Lomb Bench Metallographer Model 32 was used for light microscopy. Samples for scanning electron microscopy (SEM) were gold shadowed and an AMR-1200 scanning electron microscope was used to investigate composite surfaces.

All "as-received" samples were divided into three groups, each characterized by a different thermal history, as described in Table 1. To prevent damage from occurring in the grips during tensile testing of mechanical properties, aluminum end-tabs were bonded to all samples. The end-tabs for samples for tensile and fracture energy measurements were described in our previous reports.

After the initial calculation of samples' areas for tensile testing, wires were soldered to the strain gages and the terminals, and then connected to the strain indicator. A model P-3500 strain indicator (Measurements Group Inc.) was used in connection with an X-Y

recorder. An Instron tensile tester was used throughout our experimental work. Tests were run at crosshead speeds of 0.05 and/or 0.005 in./min. The Instron chart recorded the load while the X-Y recorder connected to the strain indicator measured the strain. The corresponding stress-strain (σ-ε) curves were obtained for every sample and an example is shown Figure 1. The best fit of data to a straight line was obtained by the least squares analysis. The values of Young's modulus were determined from the slope of the σ-ε curve.

Uniform double cantilever (UDCB) samples (type D) were also described previously. The beams were placed in Instron and pins were put through the holes in end-tabs. Stress was applied and the crack was then allowed to propagate to a certain length. The stress was released at that point, the load recorded and then the stress was reapplied. This cycle was repeated at least seven times for every sample tested. The displacement was calculated from the crosshead speed and the corresponding time for each run. The compliance was calculated by dividing the displacement by the critical load. Detailed calculation of the critical value of the strain energy release rate in mode I (G_{Ic}) was described in our progress report.

RESULTS AND DISCUSSION

We first present Table 2 in which we summarize the observed changes in tensile properties (E, σ_F and ε_F) as a function of the type and thermal history of the sample. It is clearly seen from Table 2 that thermal aging reduces the ultimate tensile strength of samples. The "as- received" type A samples had ultimate tensile strength

(UTS) ranging from 8.1×10^3 to 1.26×10^4 psi. On the other hand, the vacuum heated samples had UTS between 5.35×10^3 and 6.88×10^3 psi and the air heated samples between 2.68×10^3 and 7.65×10^3 psi.

Our results also show that the vacuum oven heated type A samples had higher elongation at break (strain at failure) than their air oven heated counterparts.

The most likely reason for the difference in UTS values of aged samples is oxidative degradation. As a result of the network degradations, one observes a reduction in mechanical properties. Photomicroscopic investigation of thermally aged type A samples has revealed interesting results. Cracks were observed in the direction perpendicular to the direction of fiber axis, as clearly seen in Figures 2-4. These cracks appear to start from the voids initially present in the composite. Fracture surfaces obtained in tensile tests were then investigated by scanning electron microscopy (SEM). Results obtained on several samples thermally aged in air, are shown in Figures 5 and 6. Two general observations were made. First, fiber failure was detected mostly in the regions near the sample edge. And second, little evidence was obtained for the existence of strong adhesion between the fibers and the matrix throughout the sample.

The experimentally determined values of G_{Ic} were similar to those reported in the literature. Thermal aging had no apparent effect on the values of Young's moduli. This observation was not surprising for both stress and strain were reduced by a similar relative amount, i.e., along the σ-ε curve, without changing its slope.

The study of the effect of thermal again on the critical strain energy release rate (G_{Ic}) did not produce conclusive results. Six samples (three different thermal histories) were tested in the UDCB specimen configuration and the values of G_{Ic} were calculated. The results are summarized in Table 3. No definite trend in G_{Ic} as a function of thermal history was observed. Unfortunately, only two samples of each kind (thermal history) were available, too small a number for reliable evaluation of fracture characteristics. It is also possible that the thickness of the sample has retarded the time-dependent degradation. The fracture tests were useful in the sense that they have provided preliminary information about the value of G_{Ic}. Fracture surfaces obtained in UDCB tests were also investigated by scanning electron microscopy (SEM). Results obtained on samples aged in air are shown in Figures 7-9. A large void is clearly seen in Figure 7. Fibers appear smooth and devoid of readily detectable damage, as seen in Figures 8 and 9. There are sporadic sites on the surface where an indication of resin deformation was noted. There are also places where there appears to be hardly any resin present, suggesting a low resin content in the composite and/or nonuniform resin distribution. The smooth fiber surfaces suggest the absence of strong fiber-matrix adhesion at those sites.

In another set of preliminary experiments, four samples were tested by Acoustic Emission (AE) technique. The instrumentation was supplied by the Physical Laboratories in Princeton, New Jersey. The AE technique is of interest for the in situ measurements of development of flaws in samples under external stress. It was our intent to test the applicability of AE to studies on graphite/epoxy composites.

In the test, a sensor was placed on the sample which was then loaded. Various "events" were recorded during the test as a result of formation and/or extension of flaws. Obviously, a determined effort is needed in order to fully utilize the AE technique. Different flaws develop during testing (as measured by different sound waves) but precise calibration is needed to attribute them to a particular type of failure mechanism in the sample. A set of Figures obtained in our analysis was presented in our progress report. We concluded that a careful calibration and a well established data base are needed for the physical interpretation of the AE data.

TABLE 1

Thermal Histories to Which Samples Were Exposed Prior to Testing

Sample	Thermal History
I	"As-received"
II	24.5 days/350°F in Air Oven
III	24.5 days/350°F in Vacuum Oven

TABLE 2

Mechanical Properties as a Function
of the Type of Sample and its Thermal History

Sample	Crosshead Speed	σ_F	ε_F	E
A6	.05 inch/min.	4.73×10^3 psi	0.196%	2.82×10^6 psi
Air heat at 350°F		3.26×10^7 Pa		1.94×10^{10} Pa
24½ days				
A7	.05 inch/min.	7.65×10^3 psi	0.255%	3.17×10^6 psi
same		5.27×10^7 Pa		2.19×10^{10} Pa
A8	.05 inch/min.	2.68×10^3 psi	0.108%	2.41×10^6 psi
same		1.85×10^7 Pa		1.66×10^{10} Pa
A9	.05 inch/min.	3.39×10^3 psi	0.149%	2.24×10^6 psi
same		2.34×10^7 Pa		1.54×10^{10} Pa

TABLE 2 - Continued

Sample	Crosshead Speed	σ_F	ε_F	E
A10	.05 inch/min.	5.35×10^3 psi	0.264%	1.77×10^6 psi
Vacuum heat at		3.69×10^7 Pa		1.22×10^{10} Pa
350°F - 24½ days				
A11	.05 inch/min.	6.88×10^3 psi	0.260%	2.33×10^6 psi
same		4.74×10^7 Pa		1.61×10^{10} Pa
A12	.05 inch/min.	6.82×10^3 psi	0.304%	2.28×10^6 psi
same		4.70×10^7 Pa		1.57×10^{10} Pa
A13	.05 inch/min.	5.03×10^3 psi	0.200%	2.11×10^6 psi
same		3.47×10^7 Pa		1.45×10^{10} Pa
C6	.05 inch/min.	1.17×10^4 psi	0.576%	1.88×10^6 psi
same as A6-10		8.06×10^7 Pa		1.30×10^{10} Pa

TABLE 2 - Continued

Sample	Crosshead Speed	σ_F	ε_F	E
C7	.05 inch/min.	1.04×10^4 psi	0.392%	2.59×10^6 psi
same		7.17×10^7 Pa		1.78×10^{10} Pa
C8	.05 inch/min.	6.94×10^3 psi	0.180%	4.18×10^6 psi
same		4.79×10^7 Pa		2.88×10^{10} Pa
C9	.05 inch/min.	1.14×10^4 psi	0.475%	2.34×10^6 psi
same		7.88×10^7 Pa		1.61×10^{10} Pa
C10	.05 inch/min.	1.92×10^4 psi	0.600%	3.15×10^6 psi
same as A10-13		13.25×10^7 Pa		2.17×10^{10} Pa
C11	.05 inch/min.	6.98×10^3 psi	N.A.	N.A.
same		4.82×10^7 Pa		

TABLE 2 - Continued

Sample	Crosshead Speed	σ_F	ε_F	E
C12	.05 inch/min.	9.27×10^3 psi	N.A.	N.A.
same		6.39×10^7 Pa		
C13	.05 inch/min.	1.13×10^4 psi	0.375%	3.41×10^6 psi
same		7.82×10^7 Pa		2.35×10^{10} Pa
C3	.05 inch/min.	2.71×10^4 psi	N.A.	N.A.
no treatment		1.89×10^8 Pa		
C4	.005 inch/min.	3.32×10^4 psi	N.A.	N.A.
same		2.29×10^8 Pa		
A2	.05 inch/min.	8.10×10^3 psi	N.A.	N.A.
same		5.58×10^7 Pa		

TABLE 2 - Continued

Sample	Crosshead Speed	σ_F	ε_F	E
A3 same	.005 inch/min.	1.03×10^4 psi 7.08×10^7 Pa	N.A.	N.A.
A1 no treatment	.05 inch/min.	1.26×10^4 psi 8.7×10^7 Pa	0.170%	7.42×10^6 psi 5.12×10^{10} Pa
A5 same	.005 inch/min.	1.19×10^4 psi 8.2×10^7 Pa	N.A.	N.A.
C1 same	.05 inch/min.	1.51×10^4 psi 10.4×10^7 Pa	N.A.	N.A.
C2 same	.005 inch/min.	1.60×10^4 psi 10.1×10^7 Pa	0.403%	3.97×10^6 psi 2.73×10^{10}

TABLE 3

Critical Strain Energy Release Rate as a Function of Sample Thermal History

Sample	Width(in.)	A_1(lb^{-1} in^2)	A_2(lb in.)	G_{Ic} (J/m^2)
01	.5000	1.04×10^{-4}	154.50	1.31×10^3
02	.5240	2.06×10^{-4}	86.29	7.69×10^2
ATA* 03	.5195	9.04×10^{-5}	158.64	1.15×10^3
ATA 04	.5113	1.55×10^{-5}	168.70	1.92×10^3
VTA**05	.5170	9.12×10^{-5}	104.30	5.04×10^2
VTA 06	.5079	1.16×10^{-4}	137.07	1.13×10^3

* ATA - Air Oven Thermal Aging

**VTA - Vacuum Oven Thermal Aging

Figure Captions

Figure 1. Stress-strain curve for sample A-9

Figure 2. Photomicrograph of a cross-section of type A sample thermaly aged in vacuum oven. Magnification 80X.

Figure 3. Same as Figure 2. Magnification 400X.

Figure 4. Same as Figure 2. Magnification 400X.

Figure 5. Scanning electron micrograph of fracture surface of tensile specimen thermally aged in air.

Figure 6. Same as Figure 5.

Figure 7. Scanning electron micrograph of fracture surface of UDCB specimen thermally aged in air.

Figure 8. Same as Figure 7.

Figure 9. Same as Figure 7.

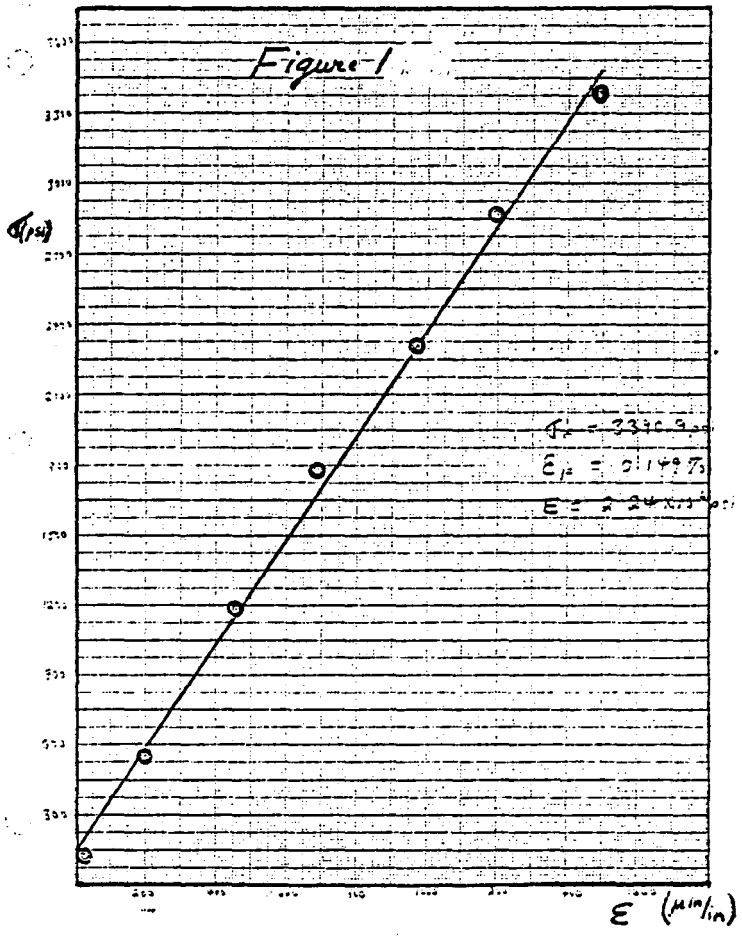

Figure 1

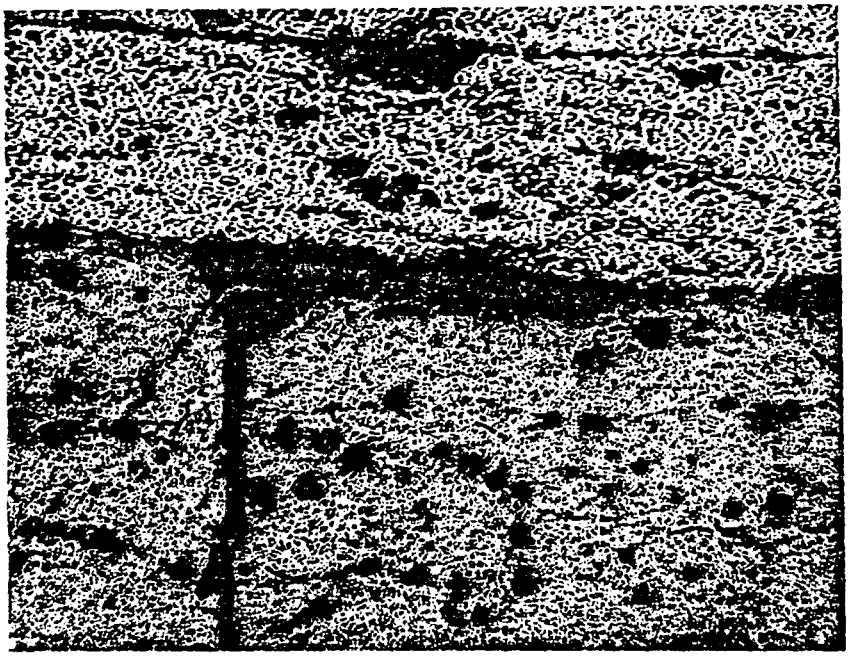

Figure 2

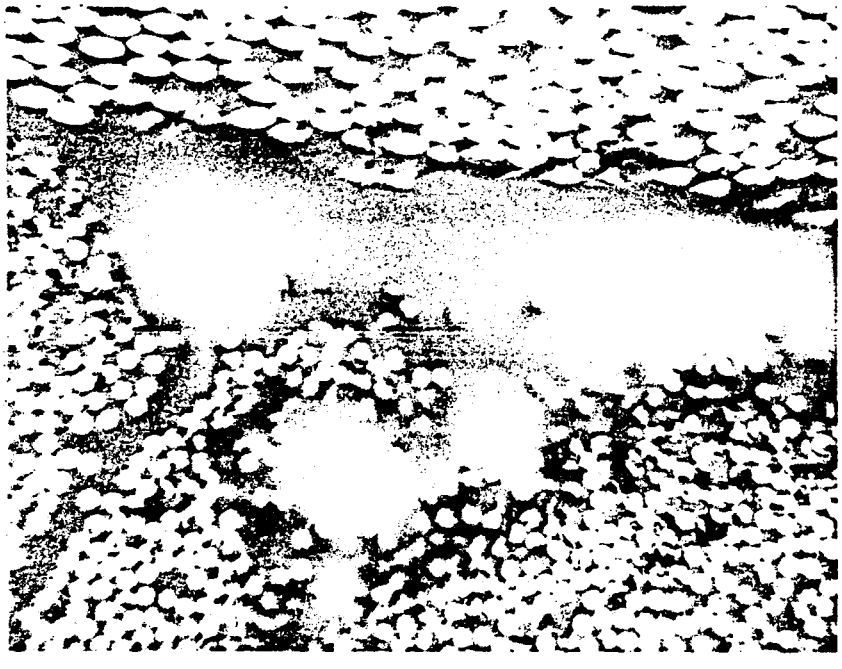

Figure 3

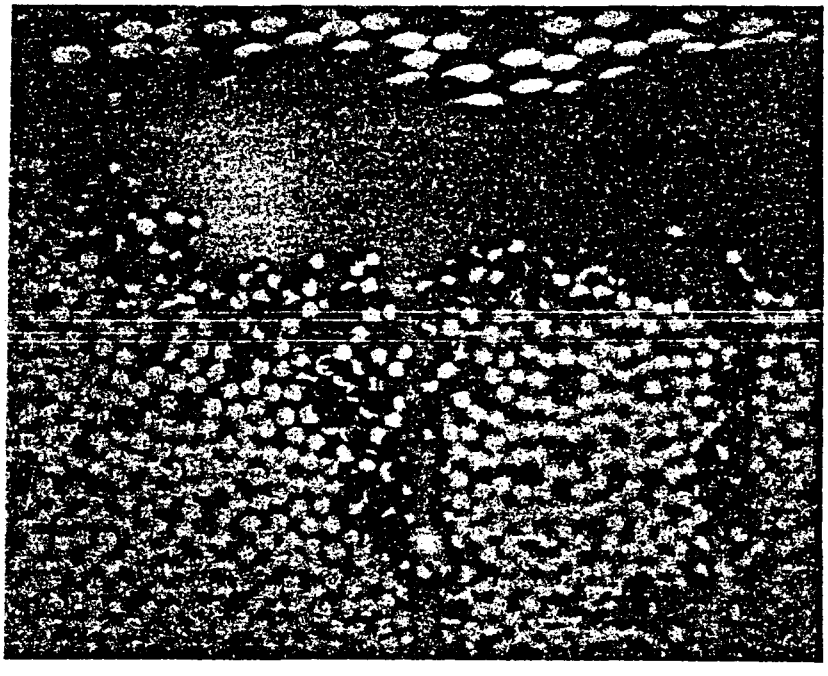

Figure 4

Figure 5

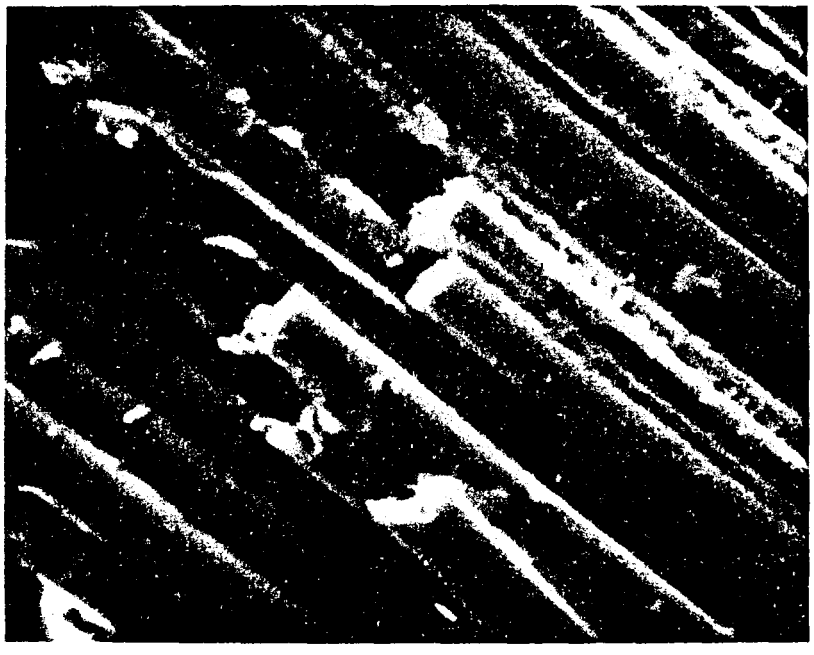

Figure 6

Figure 7

Figure 8

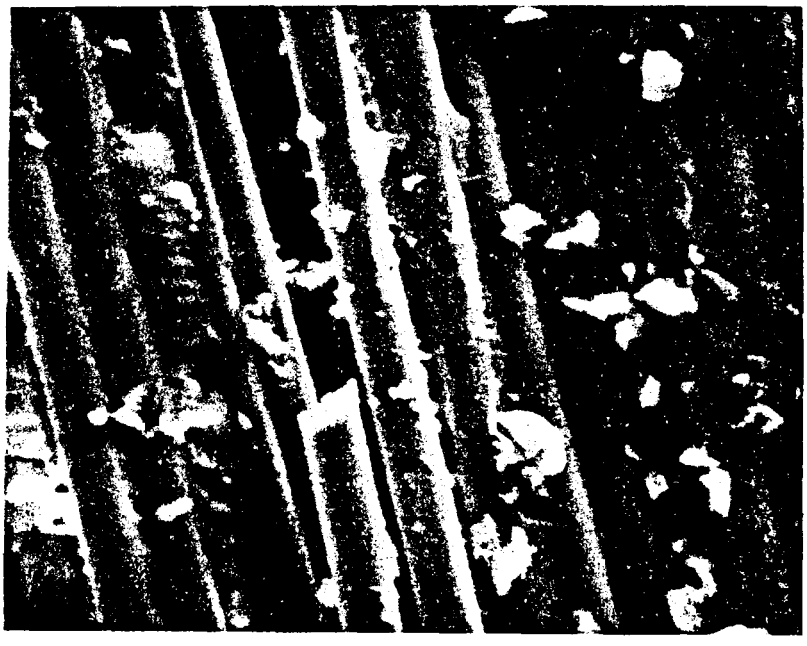

Figure 9

PART II

CHARACTERIZATION OF HBRF 55A RESIN FORMULATIONS

OBJECTIVE

Analyze the composition of raw materials and determine the chemical structure of every component for the following studies:

1. The influence of moisture, solvent, impurities on the curing behavior and physical/mechanical properties of final products.
2. The effect of molecular weight distribution to the curing behavior.
3. The curing kinetics of epoxy resin with different aromatic amine component.

INTRODUCTION

The composition of epoxy resins EpiRez 5022, RD-2, Epon 826 and Epon 828 and of curing agents Tonox and Tonox 60/40 was determined by analytical techniques such as Gel Permeation Chromatography (GPC), ^1H NMR and Fourier Transform Infrared Spectroscopy (FT-IR). GPC analysis were run on a Water Associates HPLC instrument model ALC / CPC 244 equipped with M 6000 A solvent delivery, 660 solvent programmer and 7100 WISP autoinjection system. Column used was a 100 Å pore size Ultrastyragel with an upper exclusion limit of Mn=1000. Solvent was HPLC grade tetrahydrofuran at a flow rate of 1 ml/min. A differential refractive index detector model R 400 was used together with an UV detector model 440 at a wavelength of 254 nm.

The NMR instrument used was a 60 MHz Varian A60 Spectrometer and the epoxy equivalent weight of epoxy resins (EEW) was determined adding a known amount of 1,1,2,2-tetrachloroethane (TCE) as internal standard.

The FT-IR spectra was taken on a Digilab FTS 20 B infrared spectrophotometer; the viscous liquid samples were smeared on the surface of a KBr plate while the solid samples were mixed with equal amount of anhydrous KBr and pressed in order to make a tiny sheer pellet.

Epoxy equivalent weights of epoxy resins were also determined by dissolving a known amount of resin in chlorobenzene and titrating it with HBr/AcOH 0.1 N using crystal violet indicator solution (0.1%); the acid solution was standardized against potassium acid phthalate ($KHC_8H_4O_4$). The titration was carried out according to ASTM 1652-73.

Results shown by these analyses were in accord with data reviewed from the literature for the diglycidil ether of bisphenol A (DGEBA) (1) (2) and for Tonox and Tonox 60/40 (3).

E P I R E Z 5 0 2 2

The GPC analysis of Epirez 5022 shows it to be a mixture of 1,4-butanediol diglycydil ether (n=0) and higher oligomers (n=1,2, ⩾3) .

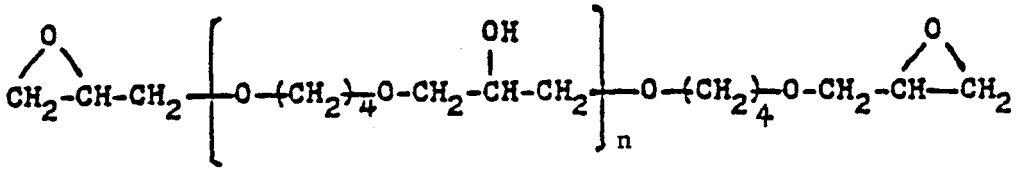

n=0 MN = 202
n=1 MN = 348
n=2 MN = 494
n=3 MN = 640

It also contains a small amount of Xylene.

GPC chromatogam of Epirez 5022

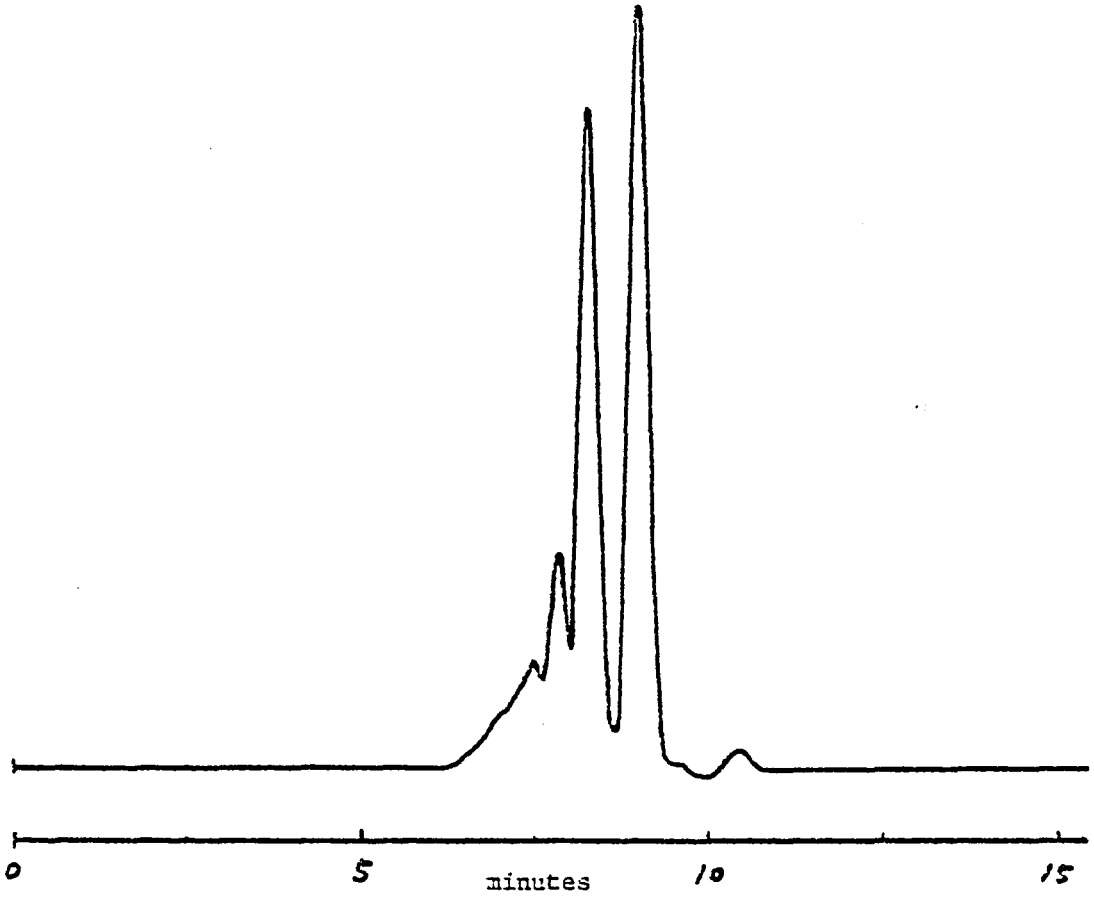

Table 1 **GPC Separation of EpiRez 5022. Column, Ultra Styragel 100 Å Mobile Phase, THF; Flow Rate, 1ml/min; Detector, RI**

Sample	Peak #	Retention time (mins.)	Composition(%)	Components
EpiRez 5022	1	7.5	15.46	Oligomers n>3
	2	7.9	11.23	n=2
	3	8.4	32.94	n=1
	4	9.0	39.46	1,4-butanediol diglycidyl ether n= 0
	5	10.4	0.9	Xylene

Using percentages reported in table 1 for the various fractions of Epirez 5022 the $\overline{MN}$ results are :

$$\overline{MN} = \sum_{n=0}^{3} MN_n N_n \Big/ \sum_{n=0}^{3} N_n = 296 \qquad \text{where } N_n = \text{Weight } \%_n / MN_n$$

This value disagrees with values obtained as a result of titration ($\overline{MN}$ = EEW . 2 = = 131 · 2 = 262) and NMR analysis ($\overline{MN}$ = EEW · 2 = 126 · 2 = 252).

It was hypothesized that the relative percentages of the fractions of Epirez 5022 were not exact, the source of error being the higher refractive index for fractions with $n \geq 1$ than $n = 0$.

To measure the difference in refractive index of different fractions, samples of known concentration of fraction #4, #3 , and #2 were injected again in the instrument and their peak areas measured and related to concentration in order to calculate RI .

Assuming RI of fraction #4 = 1.0 , fraction #3 showed RI = 1.3 and fraction #2 RI= 1.6 .

Fraction # 1 was of too low concentration to give appreciable results, thus its RI was assumed to be the same as fraction # 2 (RI = 1.6) .

Correction of peak areas with the values shown gave a different percentage composition as shown in table 1 A .

Table 1 A . Fractions of Epirez 5022 .

Fraction #	Retention time (min.)	MN	Differential RI	Weight % (corrected)	Component	n
1	7.5	640	1.6	4.38	Oligomers	3
2	7.9	494	1.6	9.16	Oligomer	2
3	8.4	348	1.3	34.29	Oligomer	1
4	9.0	202	1.0	51.26	1,4-butanediol diglycydil ether	0
5	10.4	106	-	0.9	Xylene	

Using these corrected fraction percentage values, the new $\overline{MN}$ and $\overline{MW}$ were

$$\overline{MN} = \sum_{n=0}^{3} MN_n N_n \; / \sum_{n=0}^{3} N_n = 262$$

and

$$\overline{MW} = \sum_{n=0}^{3} (MN_n)^2 N_n \; / \sum_{n=0}^{3} MN_n N_n = 299 \qquad \text{where } N_n = \text{Weight \%}_n \; / \; MN_n$$

$\overline{MN}$ value agrees with results obtained from titration ($\overline{MN}$ = 262) and NMR ($\overline{MN}$ = 252). In order to further characterize different fractions of Epirez 5022 they were separated by vacuum distillation.

It was very difficult to achieve good separation between various fractions because they gave azeotropic mixtures . However it was possible to collect a small amount of almost pure samples which were identified by injecting into the GPC instrument as components of Epirez 5022. A fraction corresponding to GPC peak # 4 (B.P. 135° C @ 0.3 mm Hg) and a fraction corresponding to peak #3 (B.P. 175°@ 0.3 mm Hg) were 95 % pure while a fraction corresponding to peak #2 (B.P. 215° @ 0.3 mm Hg) contained impurities of fractions #3 and #1. A very small amount of fraction #1 was collected (B.P. >230 @ 0.3 mm Hg) .

After GPC analysis to prove their identity and purity, the four fractions where characterized by FT-IR, NMR and titration with HBr/AcOH in order to determine their EEW. Spectra obtained from FT-IR and NMR analysis are reported.
The presence of the OH bands and the EEW values were slightly higher than the theoretical values in fraction # 4 of Epirez 5022, corresponding to 1,4-butanediol diglycydil ether (n=0) and indicates that some epoxy group may have undergone to hydrolysis.

GPC Separation of Fraction 4 from EpiRez 5022. Column, Ultra Styragel 100 Å; Mobile Phase, THF; Flow Rate, 1ml/min; Detector, RI.

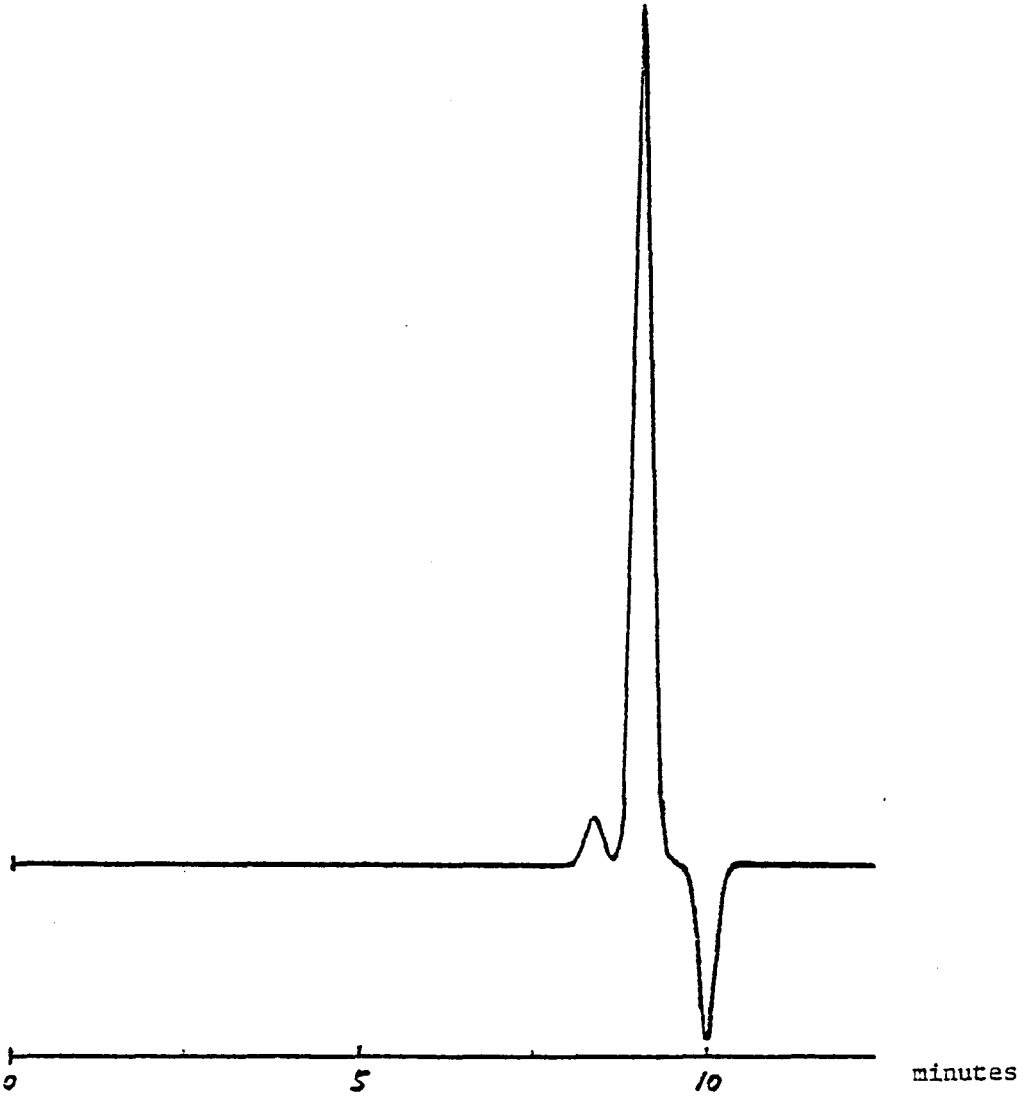

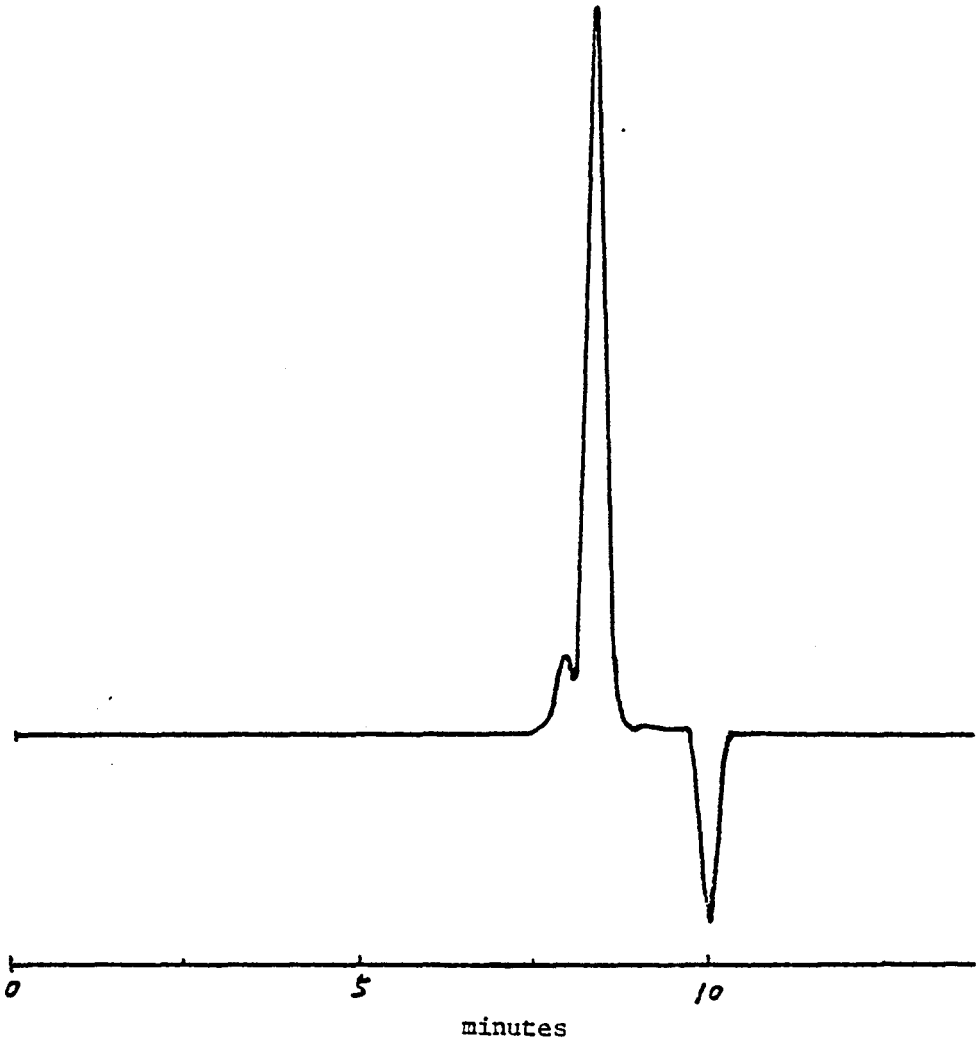

GPC Separation of Fraction 3 from EpiRez 5022. Column, Ultra Styragel 100 Å; Mobile Phase, THF; Flow Rate, 1ml/min; Detector, RI.

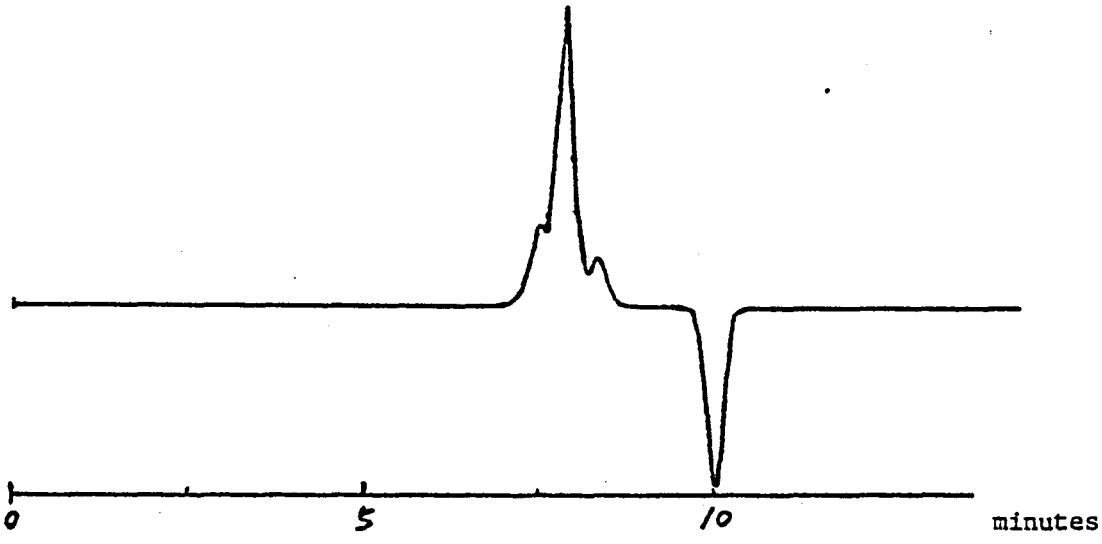

GPC Separation of Fraction 2 from EpiRez 5022. Column, Ultra Styragel 100 Å; Mobile Phase, THF; Flow Rate, 1ml/min; Detector, RI.

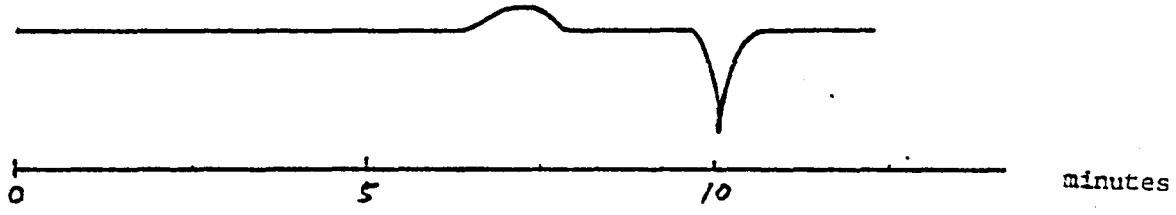

GPC Separation of Fraction 1 from EpiRez 5022. Column, Ultra Styragel 100 Å; Mobile Phase, THF; Flow Rate, 1ml/min; Detector, RI.

Calibration curve of GPC column ultra Styragel 100 Å . MW versus retention time. Flow rate 1 ml/min. Theoretical values of MW of Epirez 5022.

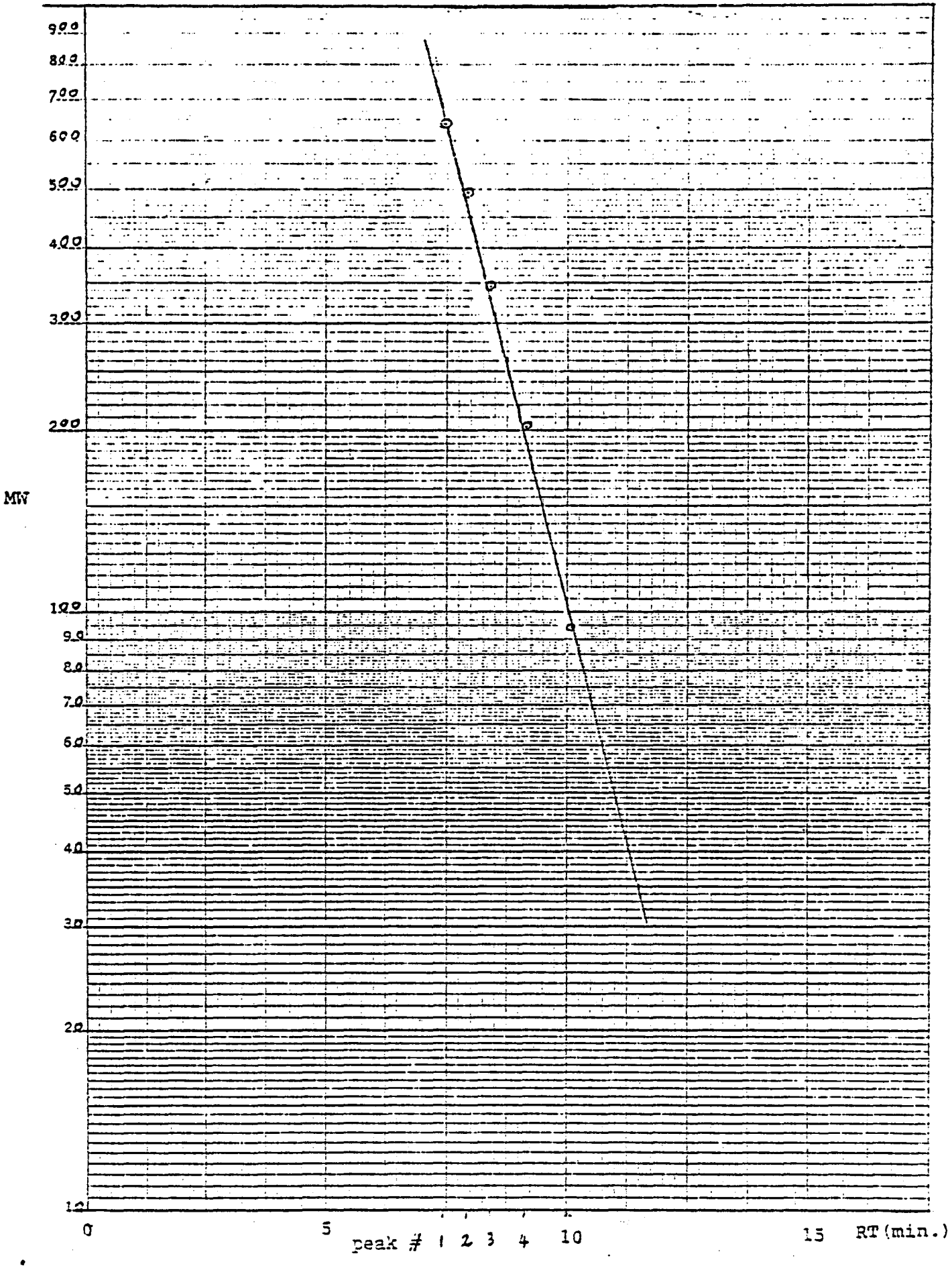

FT-IR spectrum of Epirez 5022.

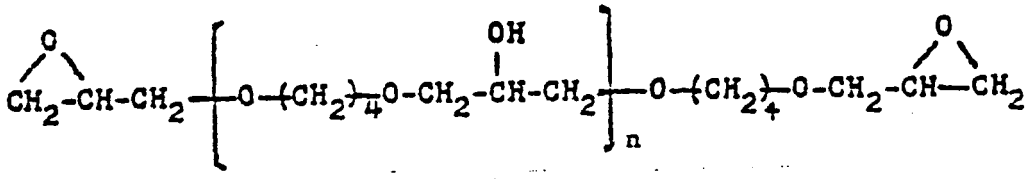

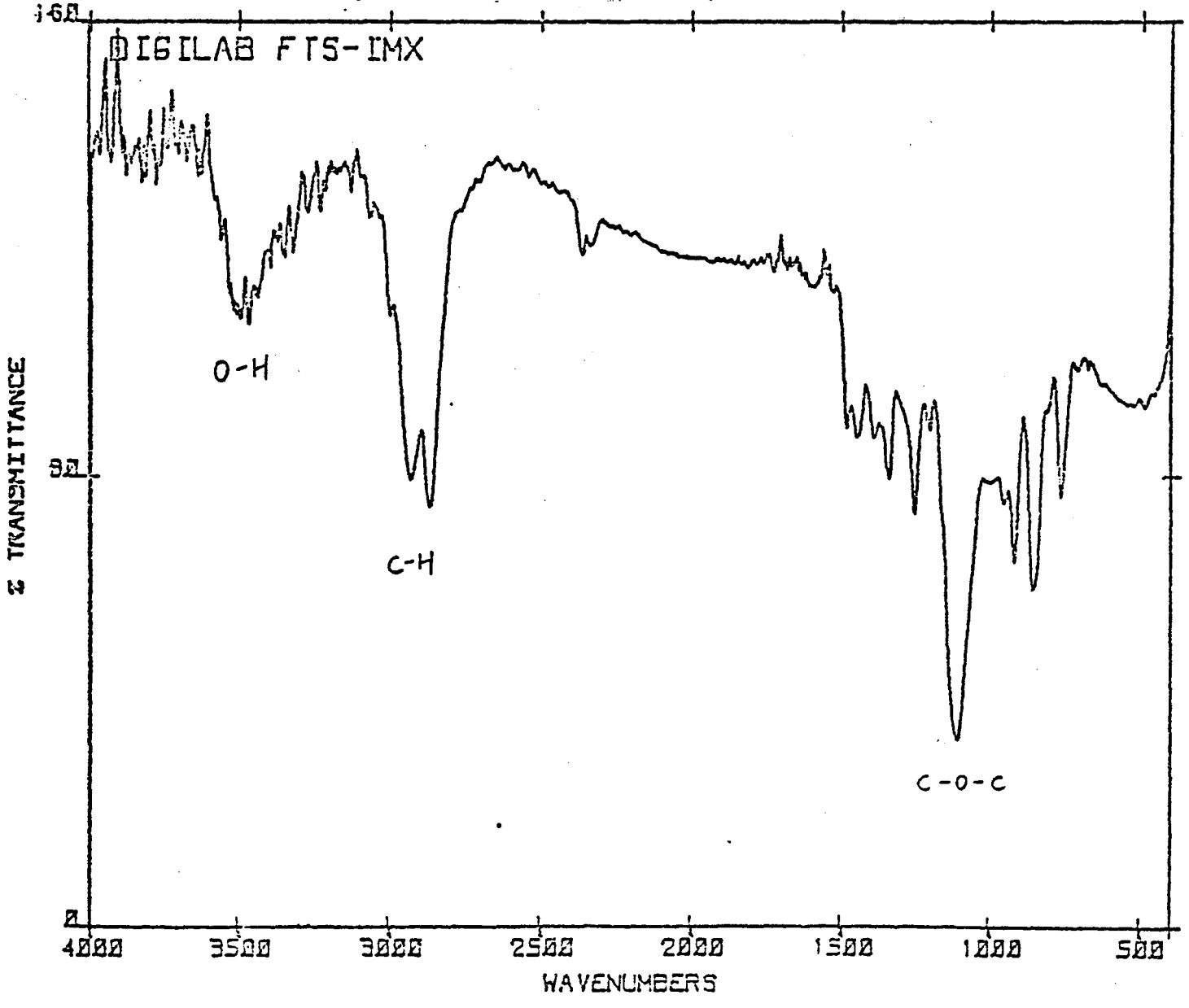

FT-IR spectrum of peak #4 of Epirez 5022.

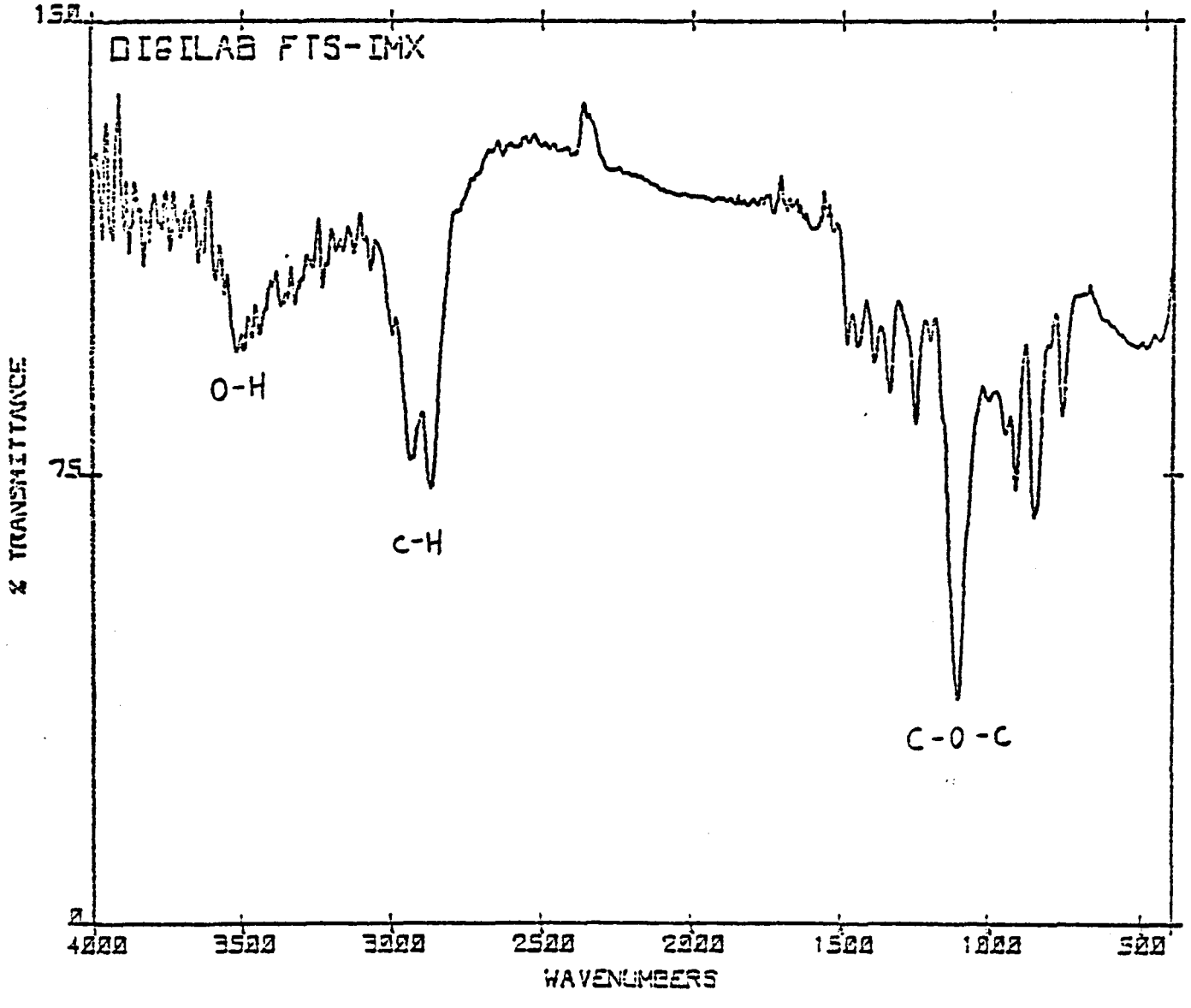

FT-IR spectrum of peak #3 of Epirez 5022.

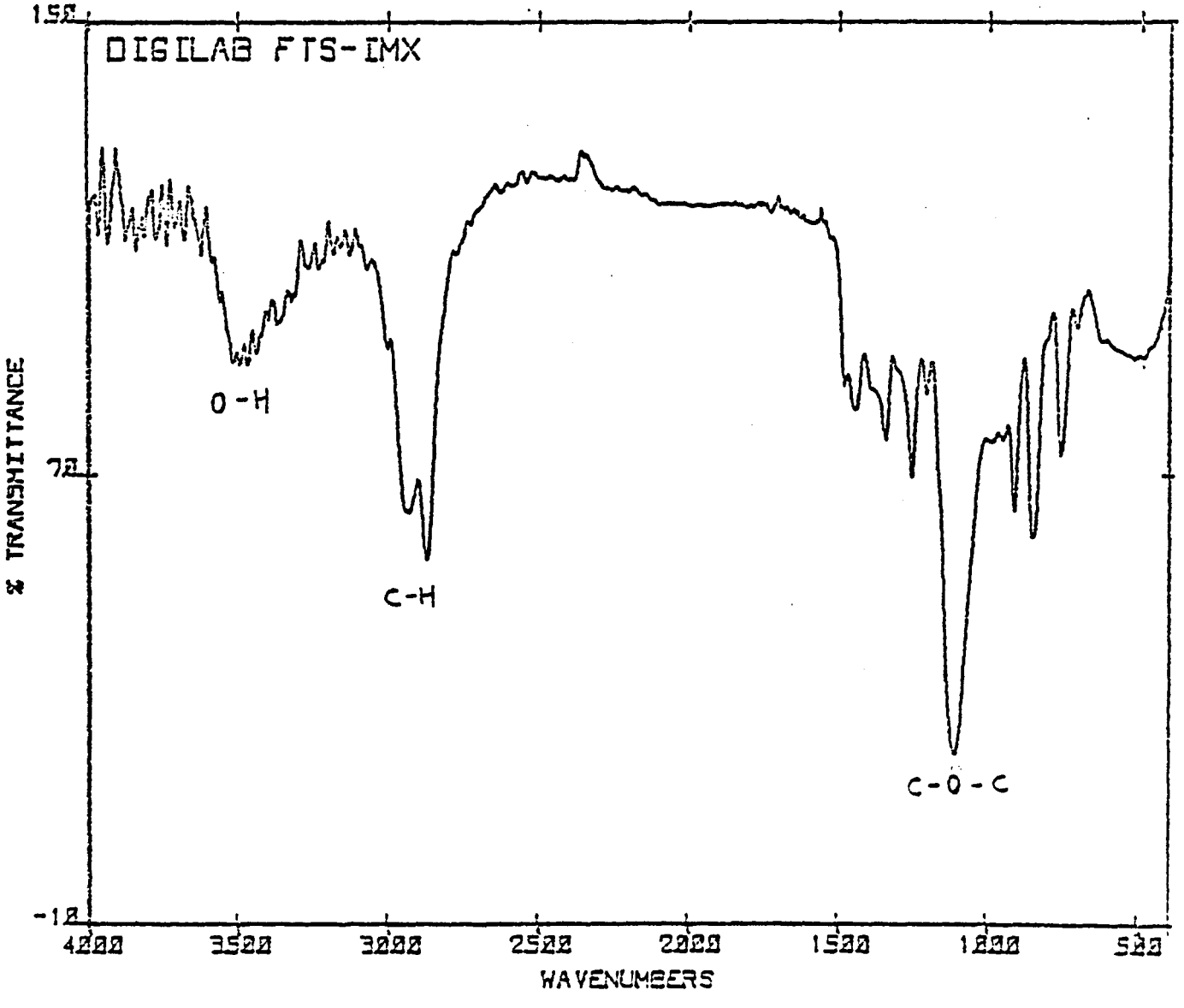

FT-IR spectrum of peak #2 of Epirez 5022.

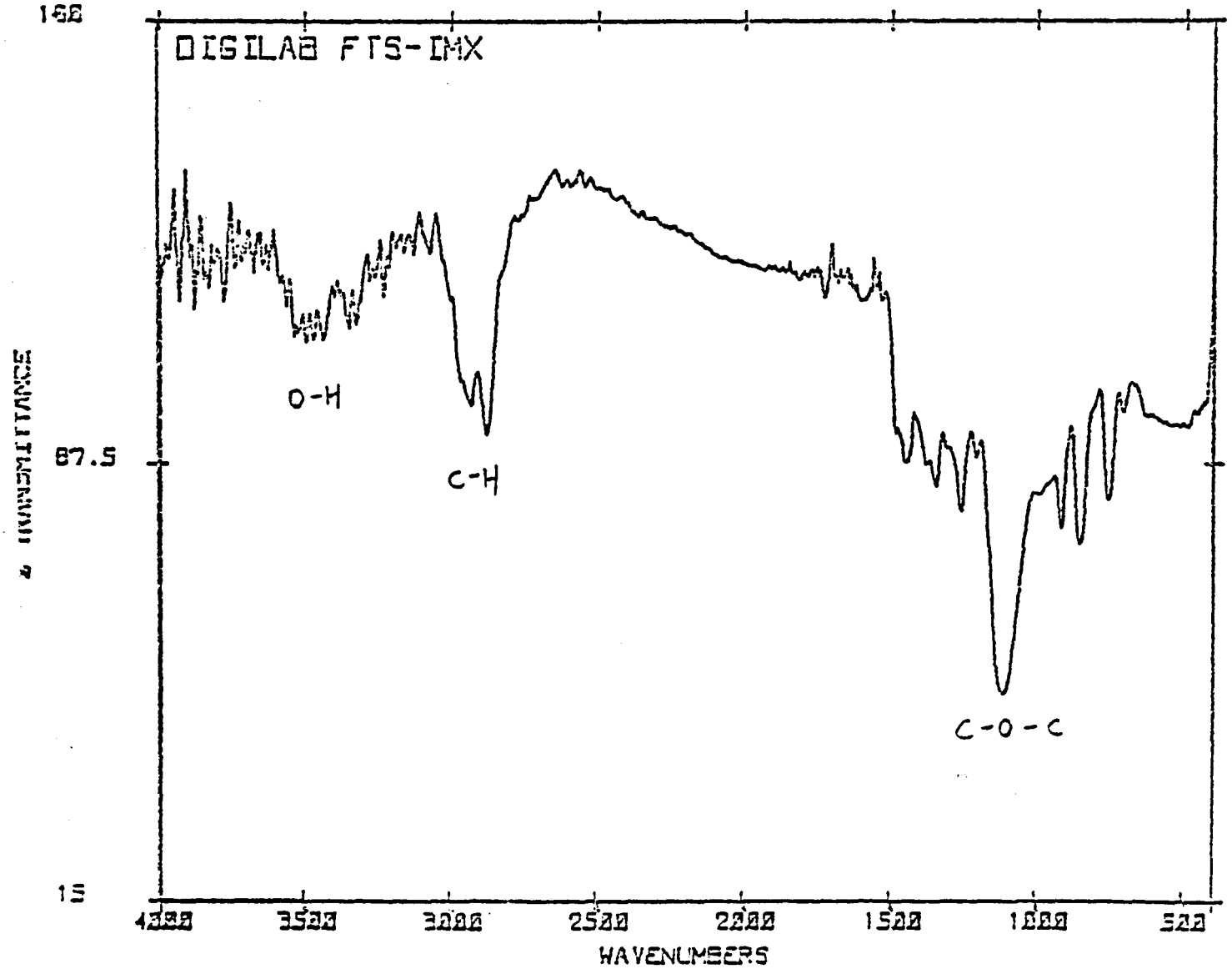

FT-IR spectrum of peak #1 of Epirez 5022.

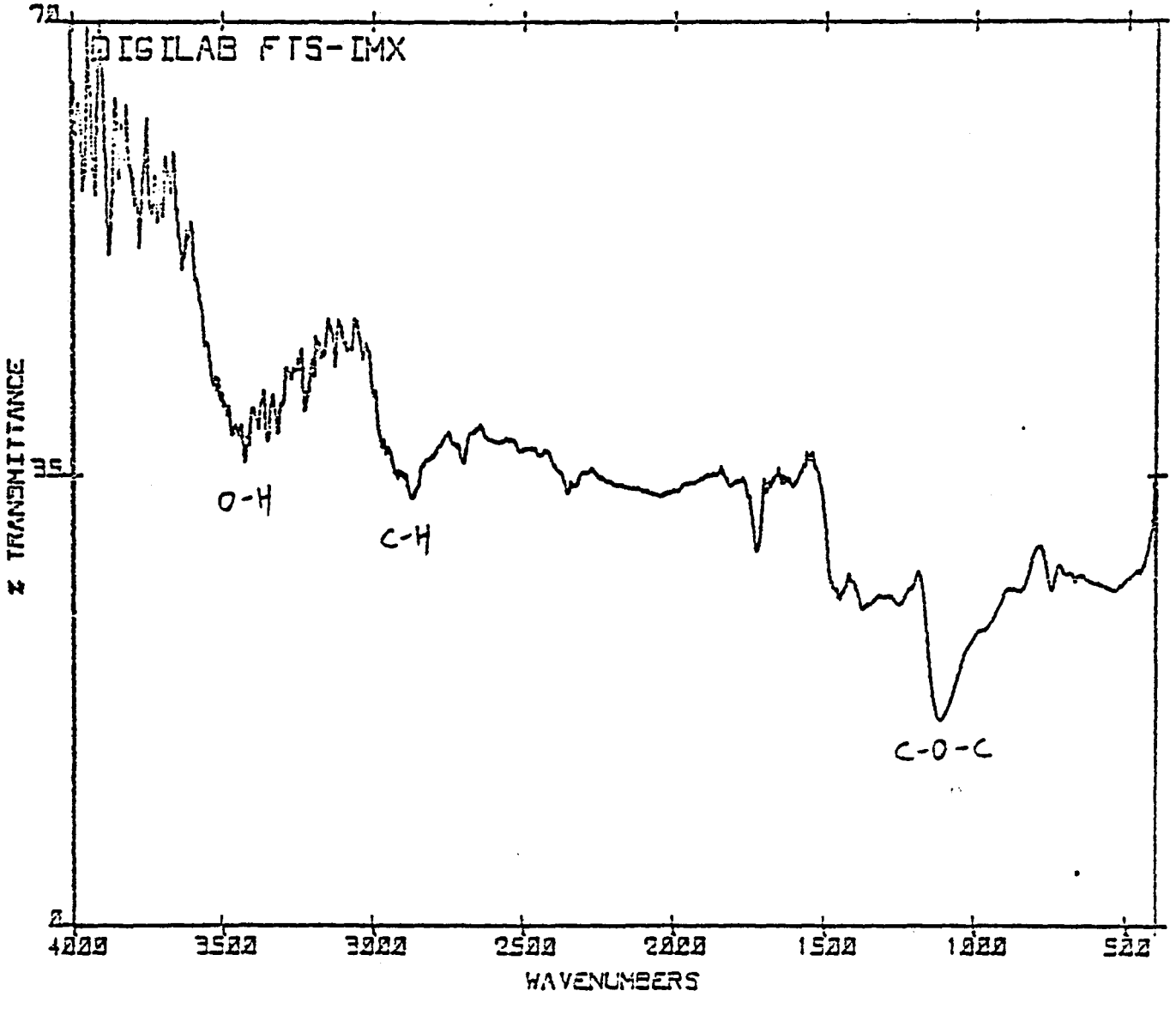

$$EEW = \frac{I_F}{I_B}\left(\frac{\text{Weight of Resin}}{\text{Weight of TCE}}\right)\left(\text{Molecular Weight of TCE}\right)$$

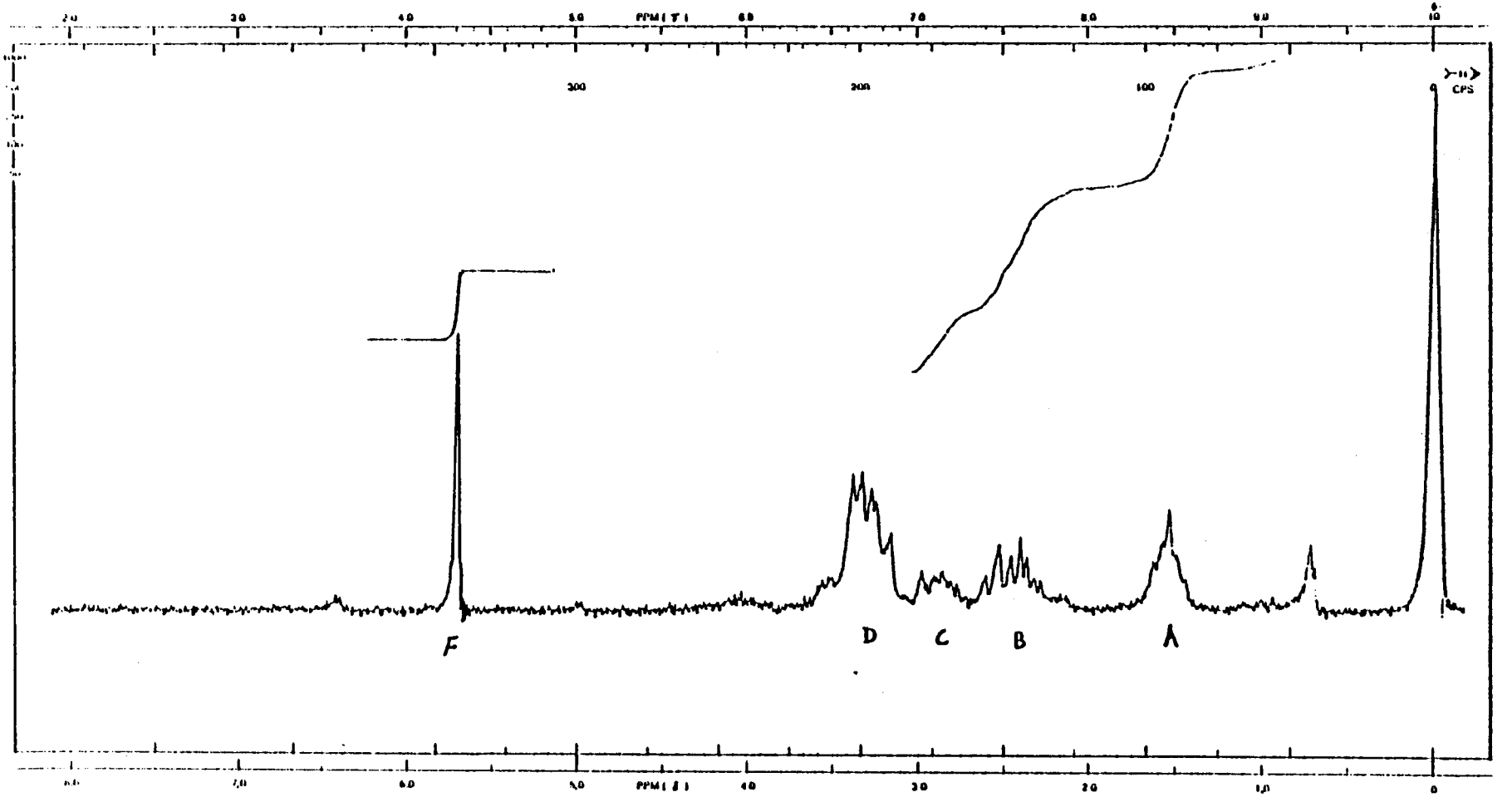

60 MHz proton NMR spectrum of EpiRez 5022 with 1,1,2,2-tetrachloroethane (TCE) added as internal standard.

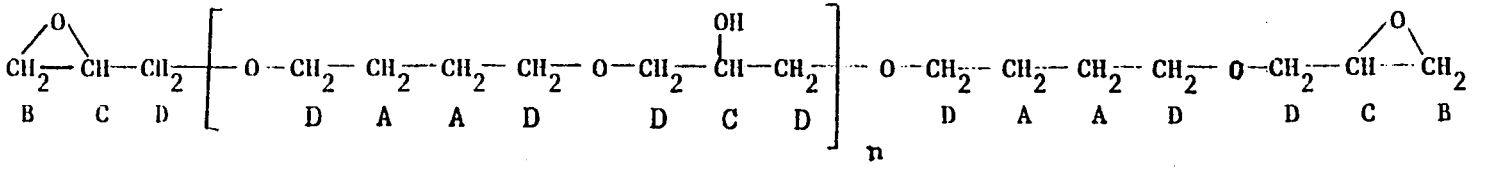

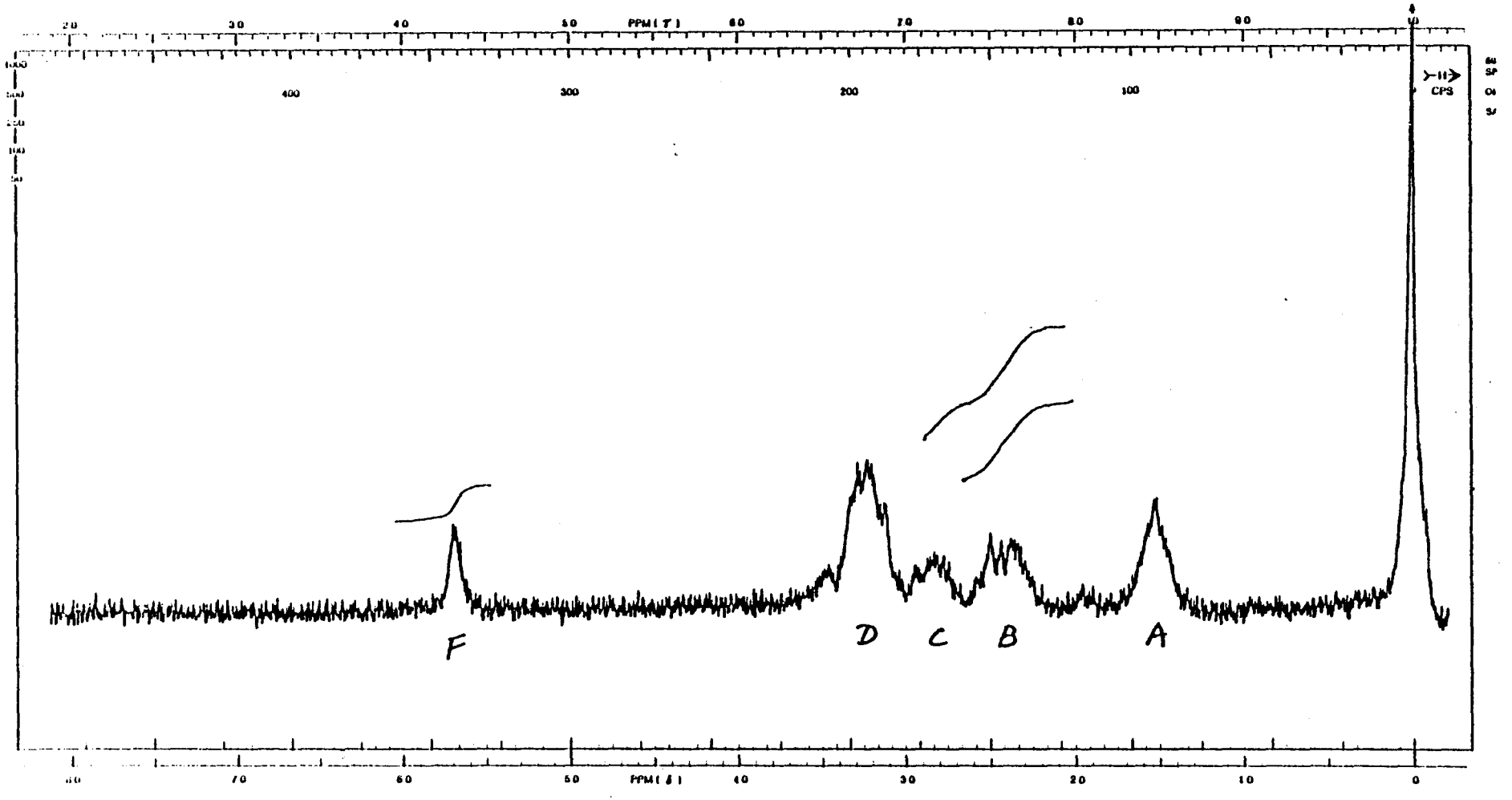

60 MHz Proton NMR spectrum of peak #4 of Epirez 5022 with 1,1,2,2-tetra chloroethane (TCE) added as intrnal standard.

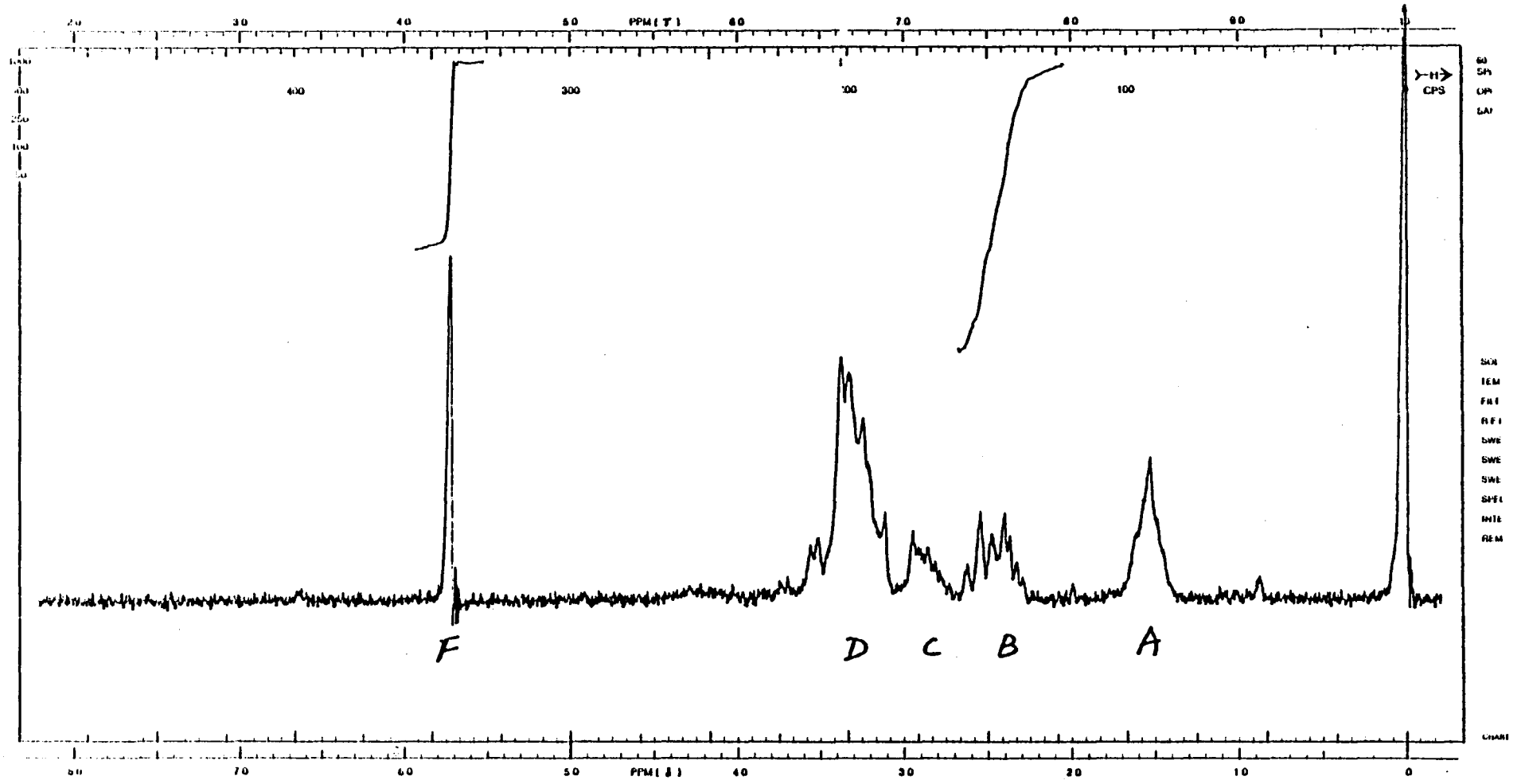

60 MHz Proton NMR spectrum of peak #3 of Epirez 5022 with 1,1,2,2-tetra chloroethane (TCE) added as internal standard.

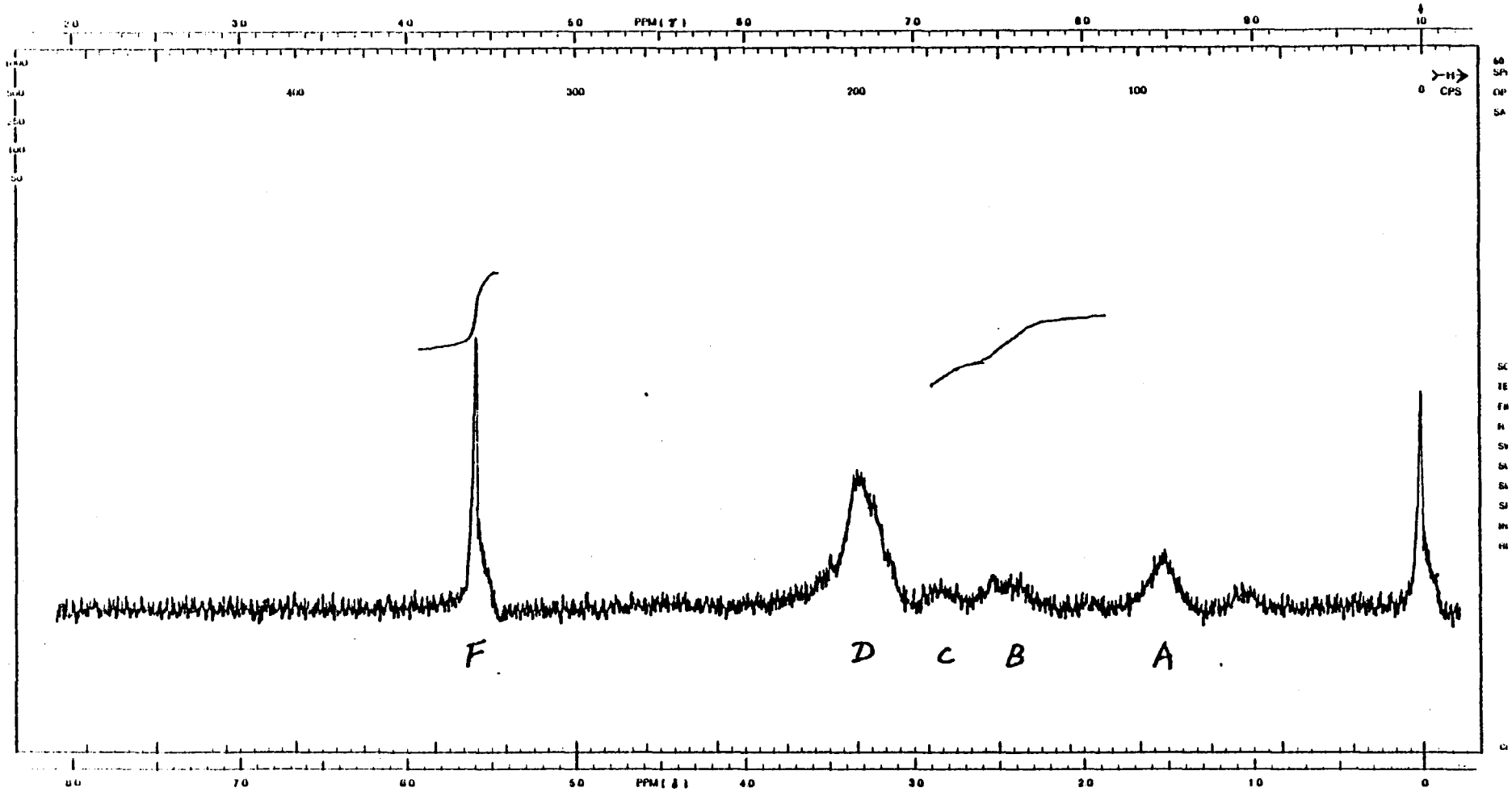

60 MHz Proton NMR spectrum of peak #2 of Epirez 5022 with 1,1,2,2-tetra chloroethane (TCE) added as internal standard.

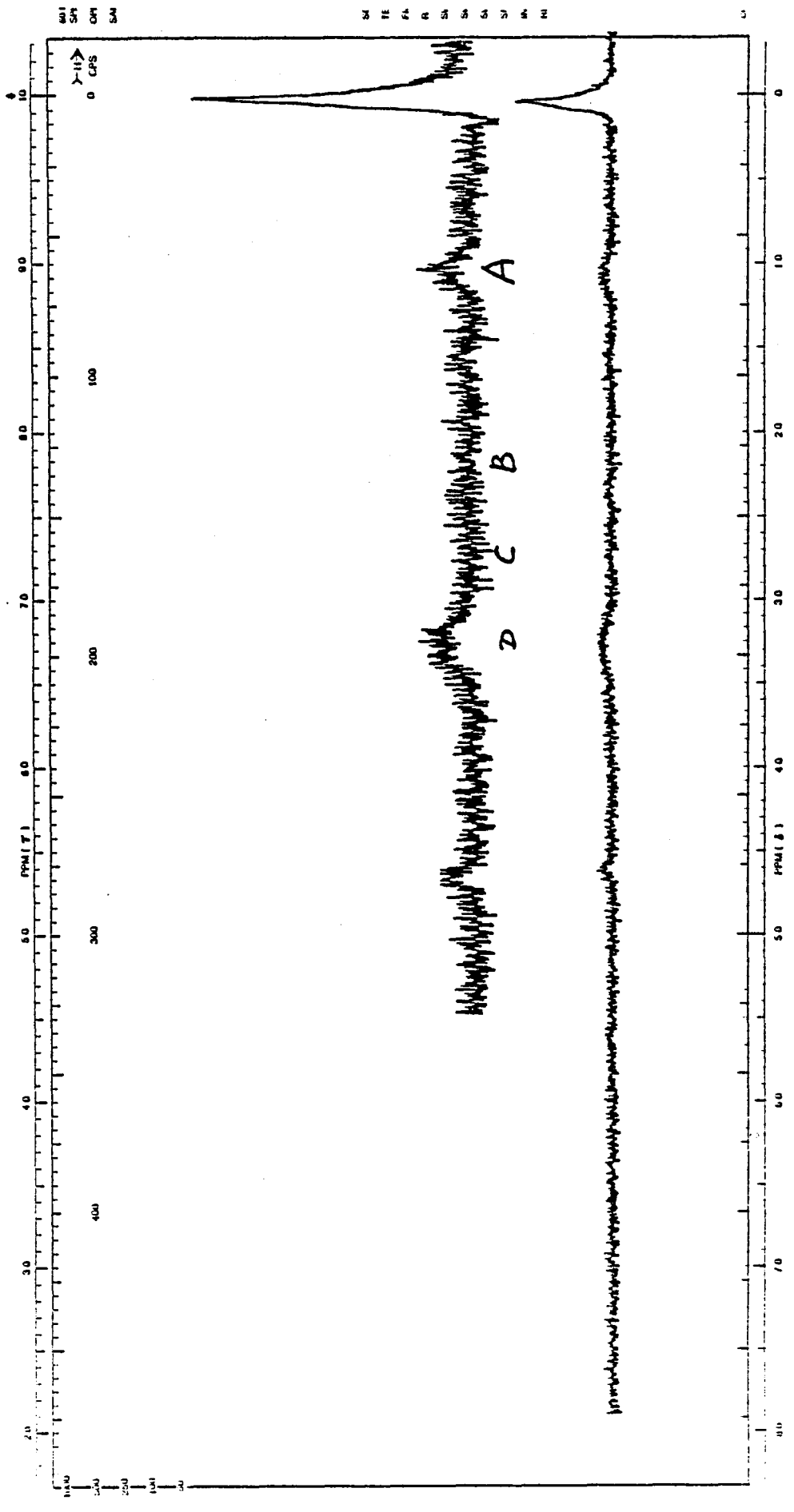

60 MHz Proton NMR spectrum of peak #1 of Epirez 5022

Table 2 Comparison of the Epoxy Equivalent Weight of four fractions of Epirez 5022 by NMR and HBr/AcOH titration with theoretical values.

Components	Theoretical Values	Proton NMR	HBr-Acetic Acid
Fraction 1	>320		
Fraction 2	247	175	206
Fraction 3	174	151	168
Fraction 4	101	104	108
EpiRez 5022	120-140	126	131

Proposed mechanism of synthesis of 1,4-Butanediol diglycidyl ether and higher oligomeric fractions .

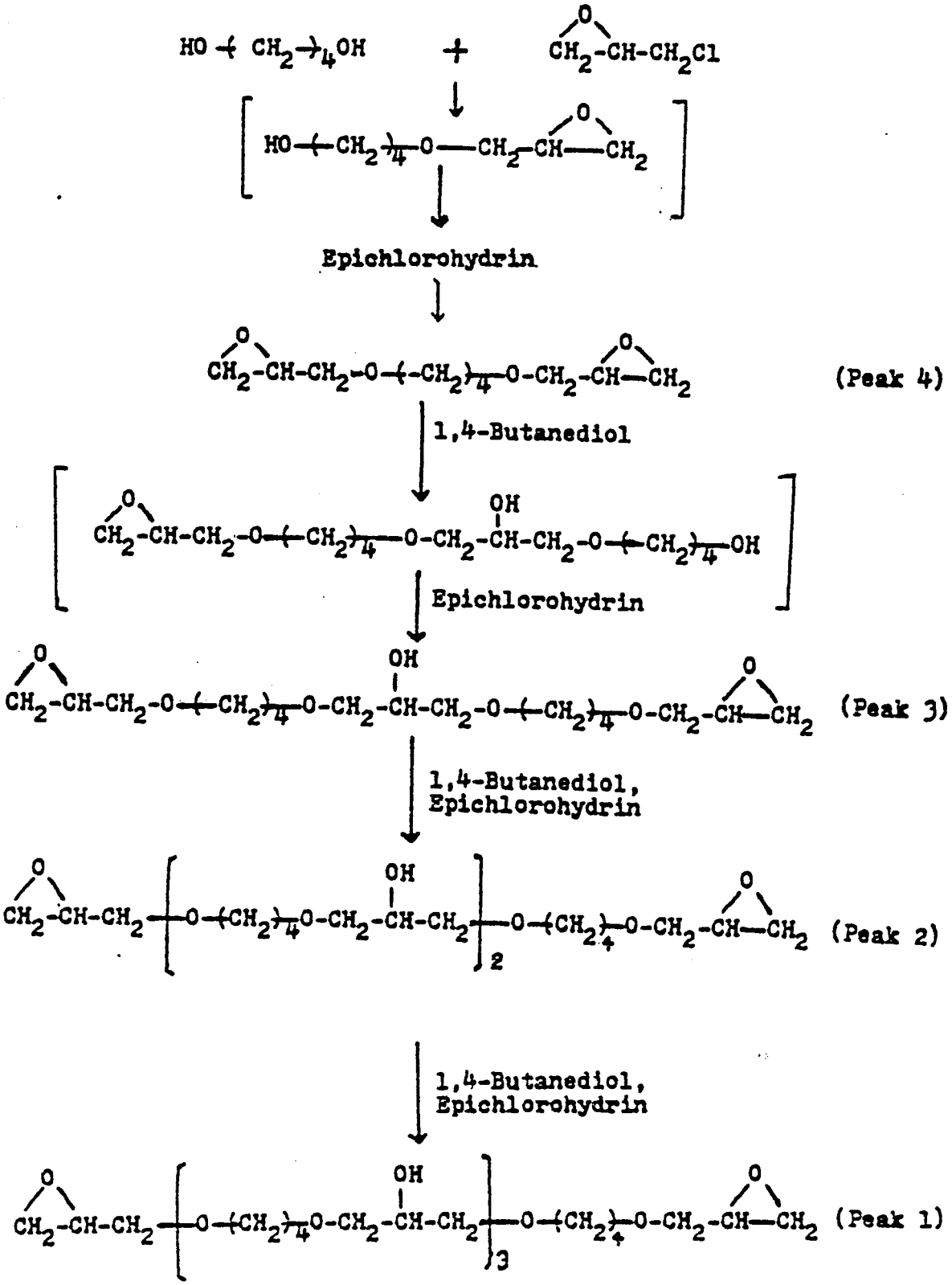

R D - 2

RD-2 analysis by GPC shows a composition similar to Epirez 5022 but with lower percentages of higher oligomeric fractions ($n \geqslant 3$) .

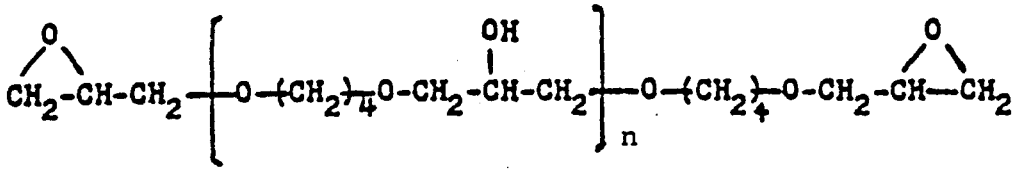

n = 0 MN = 202

n = 1 MN = 348

n = 2 MN = 494

n = 3 MN = 640

It contains a lower percentage of Xylene than Epirez 5022 .

Its FT-IR spectrum shows a reduced intensity of OH bands which agree with its lower content of high, OH containing oligomeric fractions.

The weight percentage composition of RD-2 based on its fractional peak areas is shown in table 3 .

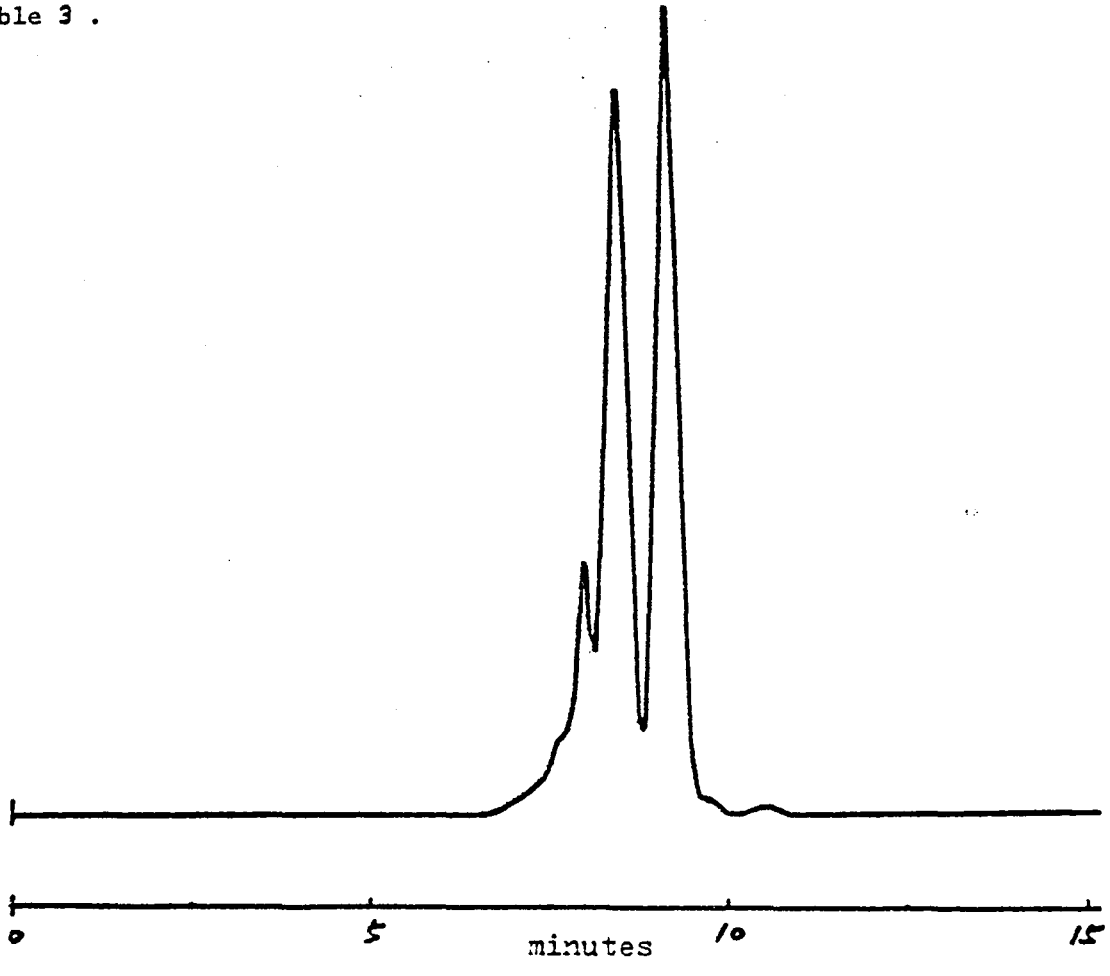

Table 3 **GPC Separation of RD-2. Column, Ultra Styragel 100 Å; Mobile Phase, THF; Flow Rate, 1ml/min; Detector, RI.**

Sample	Peak #	Retention time (mins.)	Composition(%)	Components
RD-2	1	7.6	6.8	Oligomers n⩾3
	2	7.9	13.1	n=2
	3	8.4	37.43	n=1
	4	9.0	42.34	1,4-butanediol diglycidyl ether n=0
	5	10.4	0.33	Xylene

Even in this case the percentage values of every fraction of RD-2 were corrected using the differential refractive index of every fraction ofRD-2, values are shown in table 3 A .

Table 3 A Fractions of RD-2 .

Fraction #	Retention time (min.)	MN	Differential RI	Weight % (corrected)	Component	n
1	7.6	640	1.6	2.84	Oligomers	⩾3
2	7.9	494	1.6	10.06	Oligomer	2
3	8.4	348	1.3	35.11	Oligomer	1
4	9.0	202	1.0	51.26	1,4-butanediol diglycydil ether	0
5	10.4	106	-	0.33	Xylene	

Using these new corrected values of weight percentage for every fraction of RD-2 it was calculated :

$$\overline{MN} = \sum_{n=0}^{3} MN_n N_n \Big/ \sum_{n=0}^{3} N_n = 261$$

$$\overline{MW} = \sum_{n=0}^{3} (MN_n)^2 N_n \Big/ \sum_{n=0}^{3} MN_n N_n = 295$$

where N_n = Weight $\%_n$ / MN_n

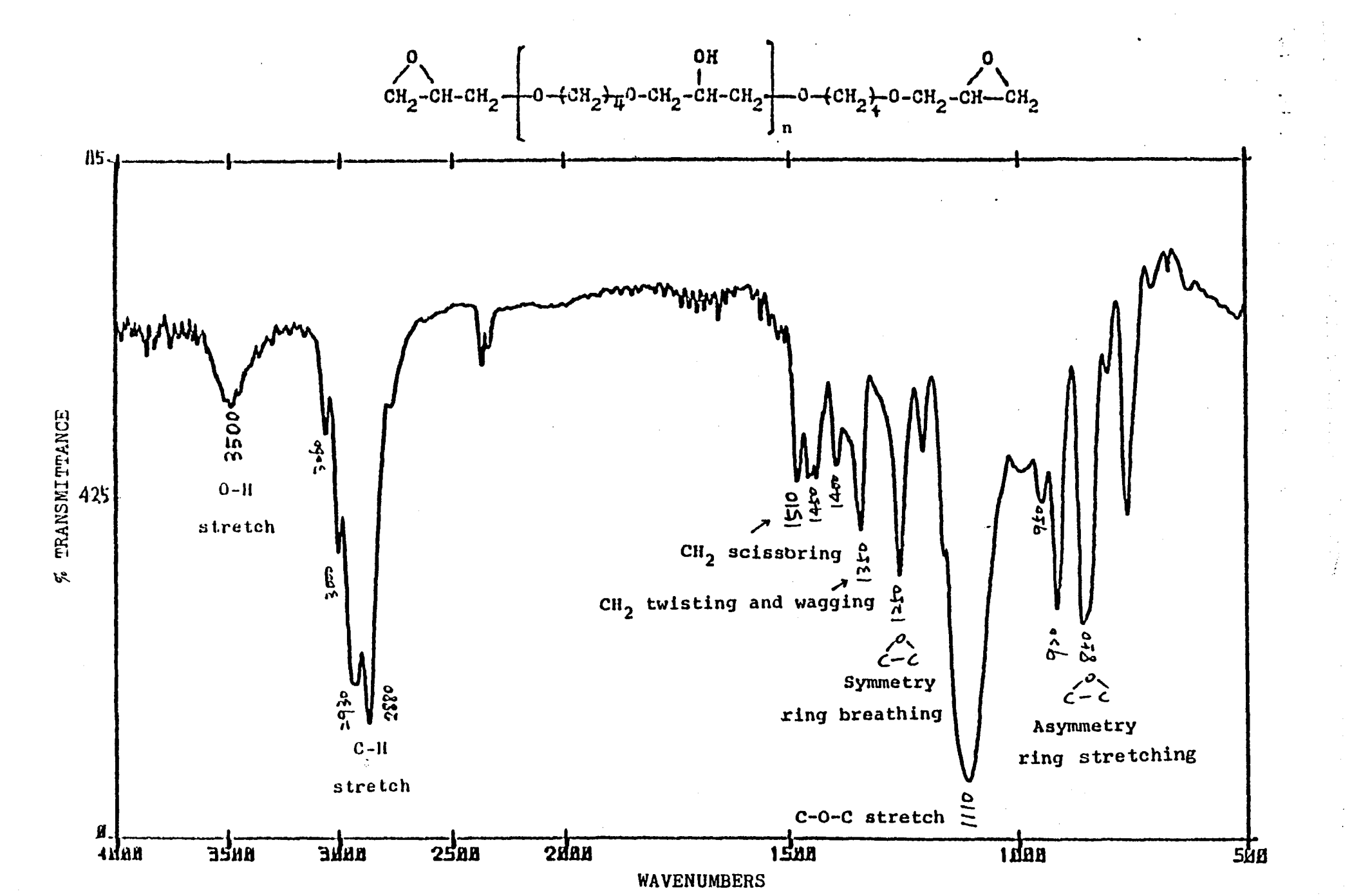

The FT-IR Spectrum of RD-2

Infrared Band Specification

RD-2 (Diglycidyl Ether of 1,4-Butanediol)

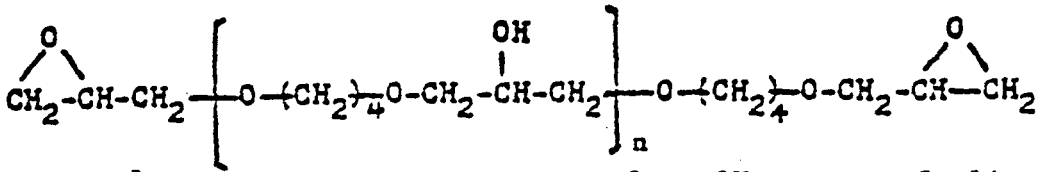

3500 cm^{-1} = OH Stretch due to secondary OH groups of oligomeric fractions, opened epoxide rings and moisture.

3060 cm^{-1} = terminal epoxide CH_2 stretch. R-CH(O)-CH_2

3000 cm^{-1} = Methine C-H stretch R-CH(O)-CH_2

2930 cm^{-1} = CH_2 asymmetry stretch

2880 cm^{-1} = CH_2 symmetry stretch

1510,1450,1400 cm^{-1} = CH_2 scissoring vibration, deformation

1350 cm^{-1} = CH_2 twisting and wagging

1250 cm^{-1} = Symmetry ring breathing

1100 cm^{-1} = C-O-C stretch

950-760 cm^{-1} = Asymmetry ring stretching

E P O N 8 2 6 and E P O N 8 2 8

These two epoxy resins, based on the diglycydil ether of bisphenol A (DGEBA), showed , by GPC analysis , similar composition with the 828 being richer in high oligomeric fractions (n = 1 , 2) and thus having a higher $\overline{MN}$ and $\overline{MW}$.

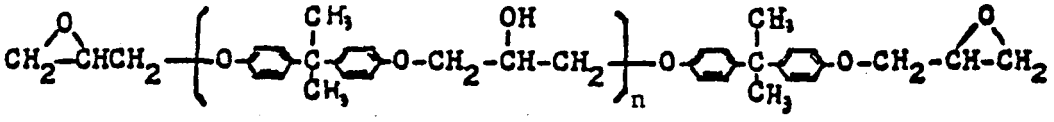

GPC analysis also shows the presence of some DGEBA with one epoxy ring open (peak #3). THese results agree with the ones reported in the literature (1) , (2) .

GPC chromatogram of Epon 826

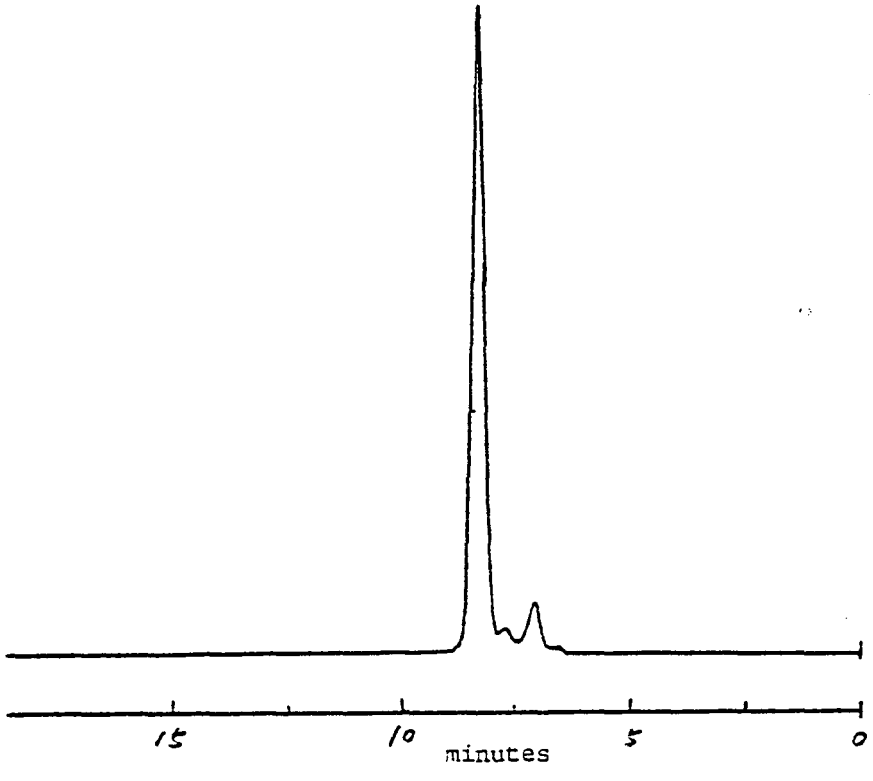

Table 4 GPC Separation of Epon 826. Column, Ultra Styragel 100 Å; Mobile Phase, THF; Flow Rate, 1ml/min, Detector, UV 254 nm.

Sample	Peak #	Retention time (mins.)	Composition(%)	Components
Epon 826	1	6.5	1.04	n = 2
	2	7.0	7.39	n = 1
	3	7.6	4.02	dihydroxy species
	4	8.2	87.55	n = 0

GPC chromathogram of Epon 828

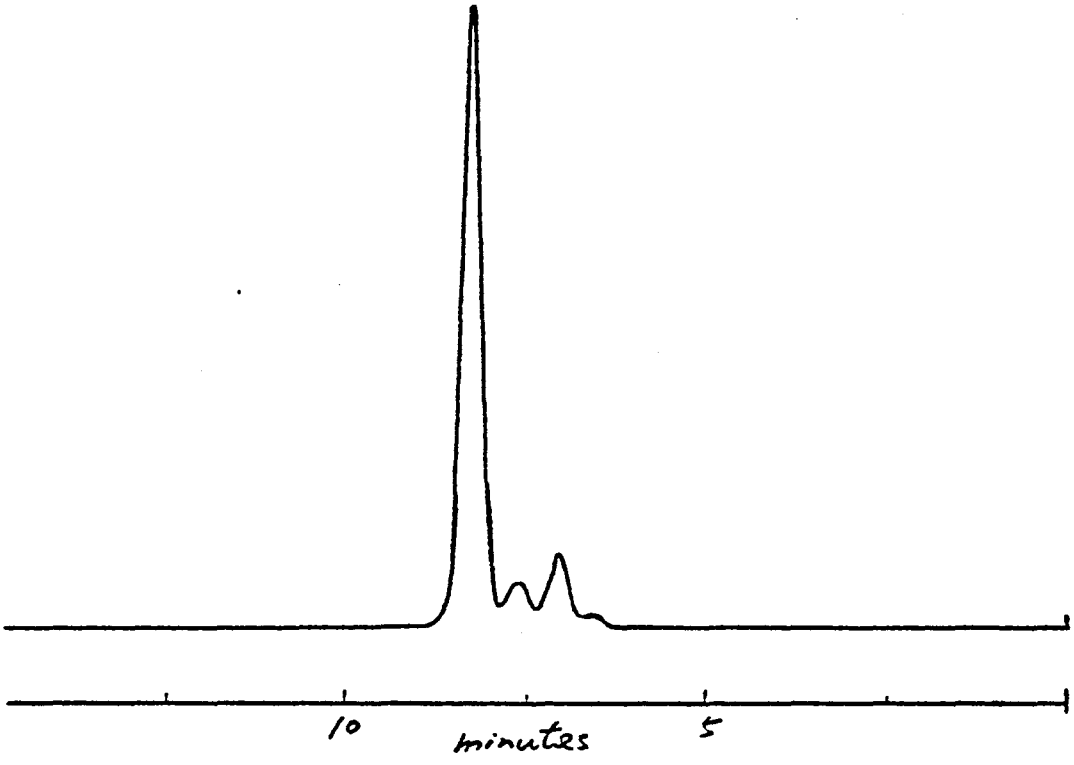

Table 5 GPC Separation of Epon 828. Column, Ultra Styragel 100Å; Mobile Phase, THF; Flow Rate, 1ml/min; Detector, UV 254 nm.

Sample	Peak #	Retention time (mins.)	Composition(%)	Components
Epon 828	1	6.5	2.22	n = 2
	2	7.0	10.51	n = 1
	3	7.6	8.08	dihydroxy species
	4	8.2	87.55	n = 0

Epon 826

Fraction #	Weight %	MN	n	
1	1.04	908	2	
2	7.39	624	1	
3	4.02	358	0	(dihydroxy DGEBA)
4	87.55	340	0	

$$\overline{MN} = \sum_{n=0}^{2} MN_n N_n / \sum_{n=0}^{2} N_n = 356 \quad *$$

$$\overline{MW} = \sum_{n=0}^{2} (MN_n)^2 N_n / \sum_{n=0}^{2} MN_n N_n = 368$$

Literature value $\overline{MN}$ = (EEW · 2)= (178~186 · 2) = 356~372

Epon 828

Fraction #	Wheigh %	MN	n	
1	2.22	908	2	
2	10.51	624	1	
3	8.08	358	0	(dihydroxy DGEBA)
4	79.19	340	0	

$$\overline{MN} = \sum_{n=0}^{2} MN_n N_n / \sum_{n=0}^{2} N_n = 365 \quad *$$

$$\overline{MW} = \sum_{n=0}^{2} (MN_n)^2 N_n / \sum_{n=0}^{2} MN_n N_n = 385$$

Literature value: $\overline{MN}$ = (EEW · 2) = (185~192 · 2) = 370~384

*The reason why the experimental value of $\overline{MN}$ is at the lower limit of the literature value is due to the impossibility of considering the the oligomeric fraction with n=3 (MN = 1192) which lies beyond the exclusion limit of a 100 Å pore size Ultrastyragel GPC column (MN = 1000) .

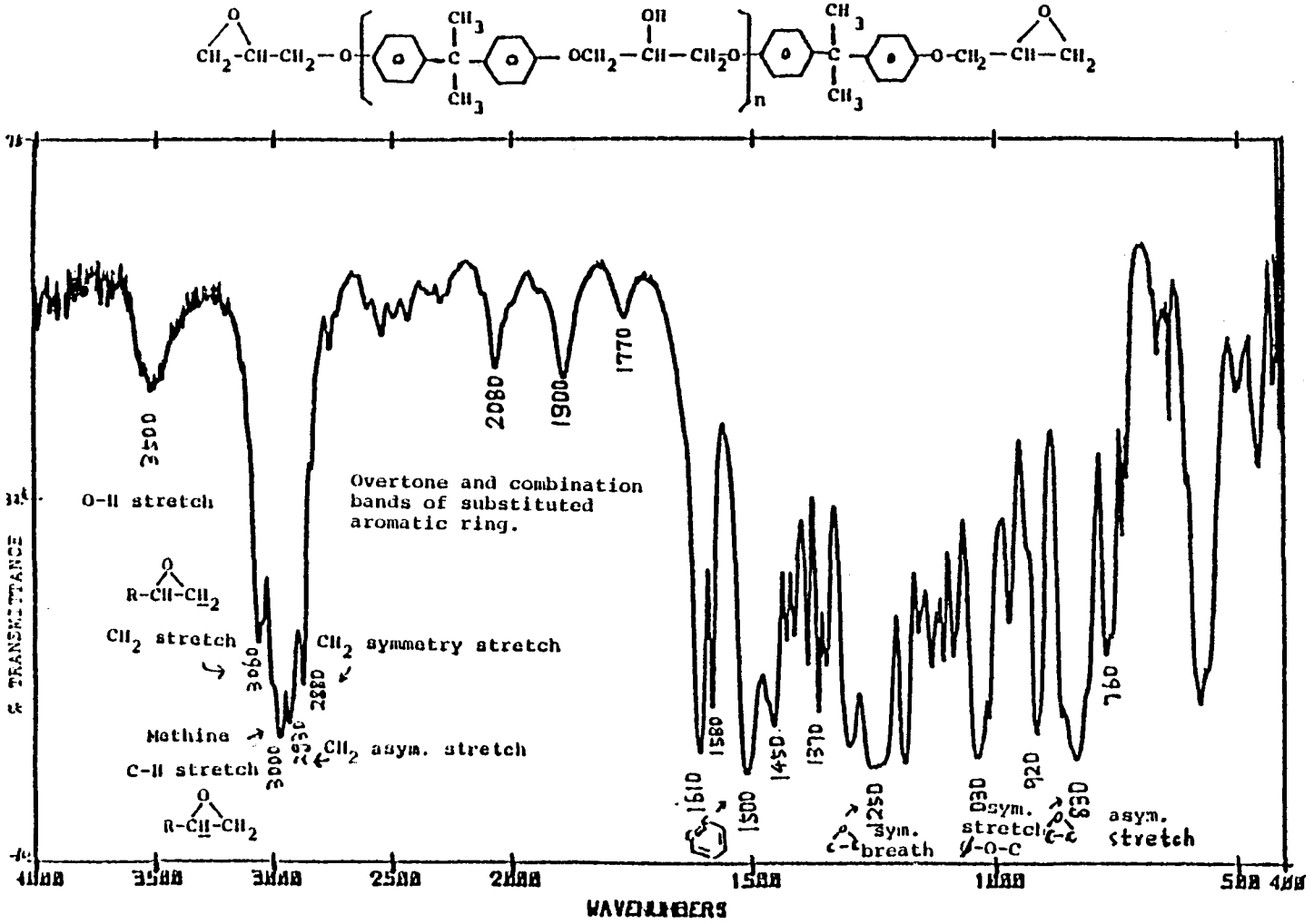

The FT-IR Spectrum of Epon 826

$$EEW = \frac{I_F}{I_B}\left(\frac{\text{Weight of Resin}}{\text{Weight of TCE}}\right)\left(\text{Molecular Weight of TCE}\right)$$

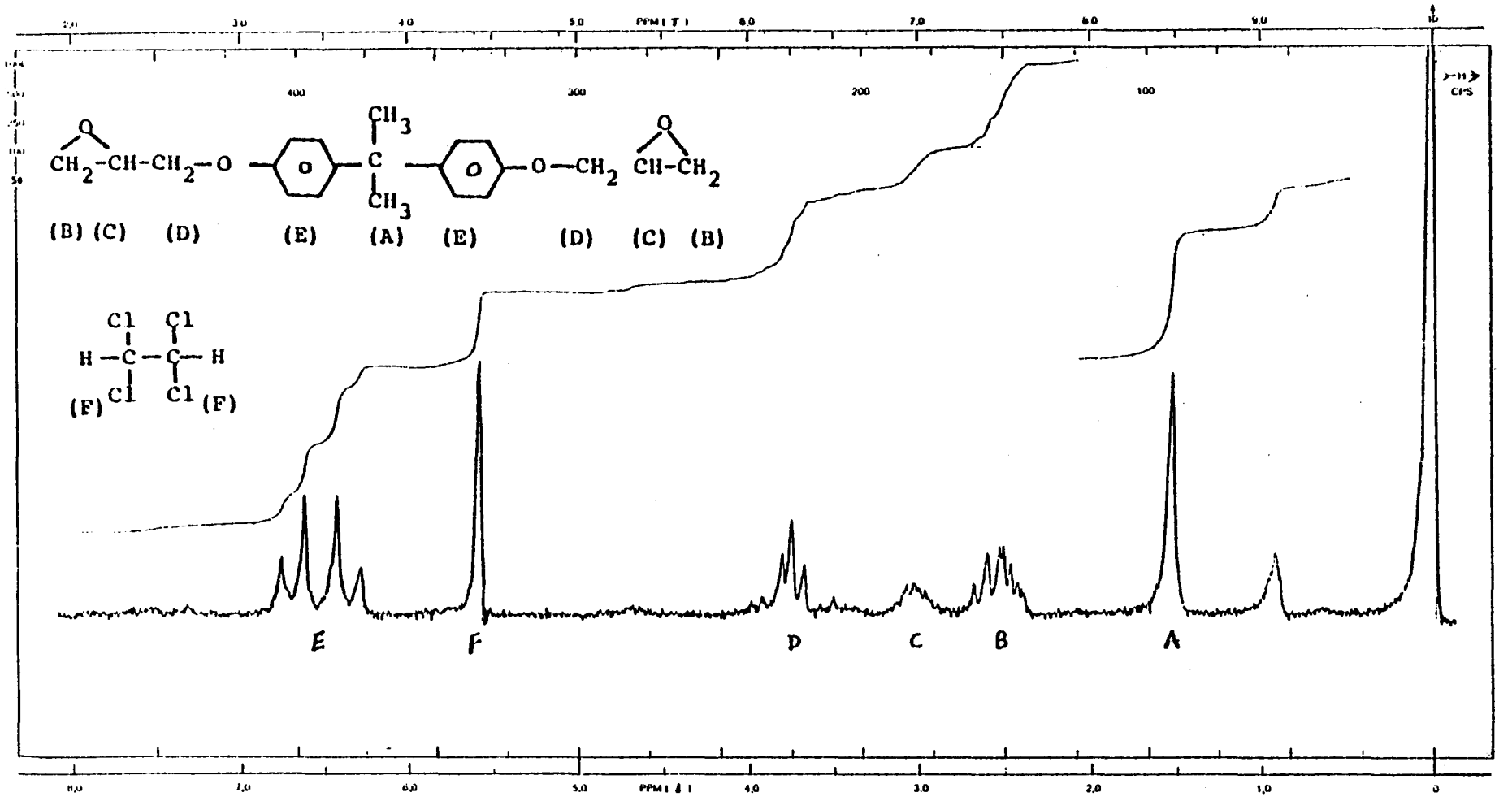

60 MHz proton NMR spectrum of Epon 826 with 1,1,2,2-tetrachloroethane (TCE) added as internal standard.

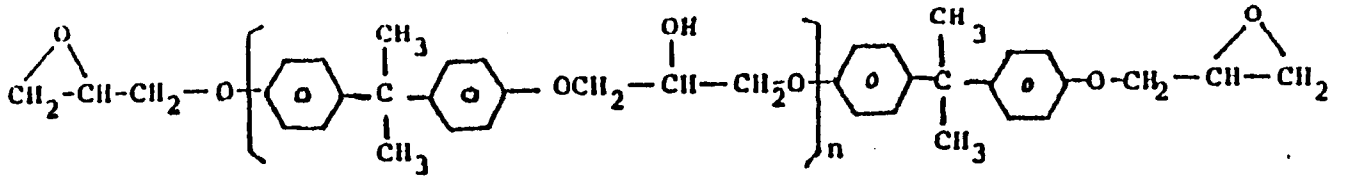

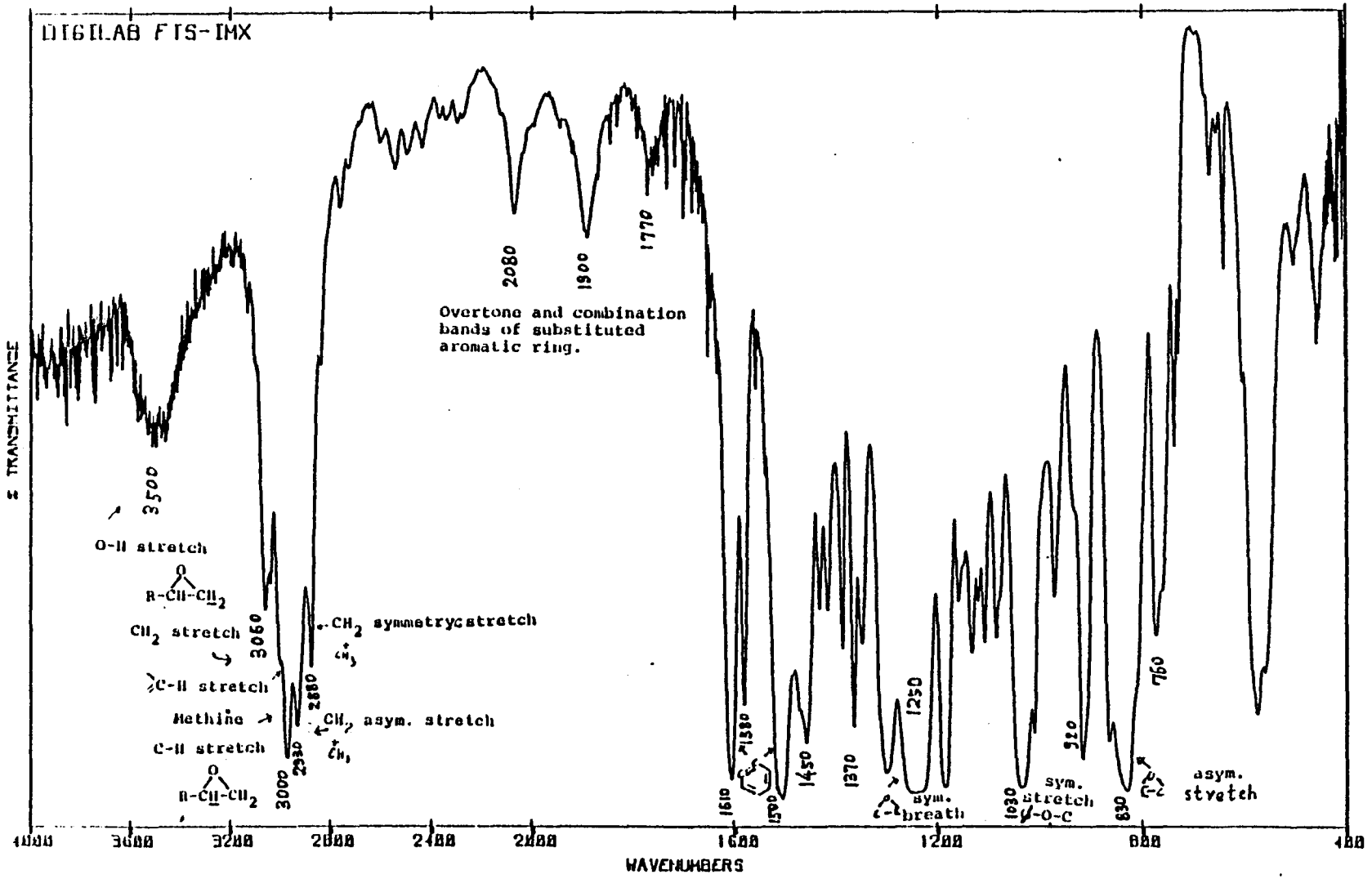

FT-IR spectrum of EPON 828

Determination of the Epoxide Equivalent Weight of Glycidyl Ethers by Proton NMR Spectrometry

(1) Sample Preparation

Into a 1-ml volumetric flask with a ground glass stopper weigh about 200 mg of resin and 200 mg 1,1,2,2-tetrachloroethane (TCE) as internal standard. Dilute to 1 ml with carbon tetrachloride. Stopper and shake for 1 min. Pipeit into a 5-mm NMR tube and add 2 or 3 drops of tetramethylsilane and close tube. Obtain intergrals and calculate the EEW of the Material.

(2) Results and calculation

For example, Epon 826

The assignment of each peak is shown in the following structures:

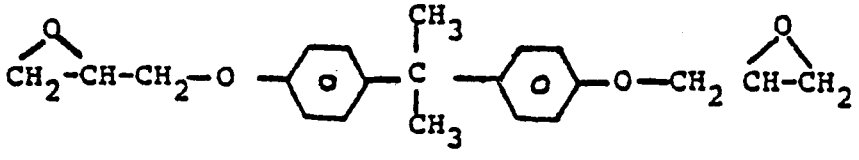

(B) (C) (D) (E) (A) (E) (D) (C) (B)

and

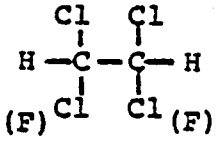

(F) (F)

The structure of Epon 826 is

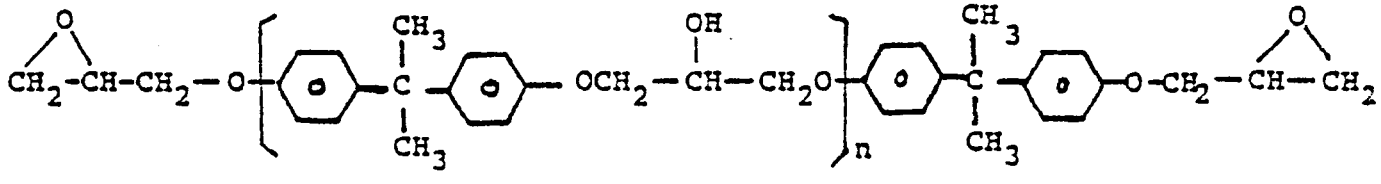

The ratio of the integrals, A:B:C:D:E, in NMR spectrum should be 6:4:2:4=8 if n=0 while the ratio of the integrals of a DGEBA resin where n=1 should be 12:4:2:8:16. The hydroxyl proton and the proton attached to the carbon bearing the hydroxy group are not included in the ratio. The proton NMR spectrum of Epon 826 is shown in Figure and consists of five distinct areas as denoted by the letters at the bottom of the spectrum. The singlet at F(5.6 ppm) is the standard TCE. The EEW is calculated by comparing the integral (I_F) of the two protons of TCE with the integral (I_B) of the two methylene protons of the epoxide group.

$$EEW = \frac{I_F}{I_B}\left(\frac{\text{Weight of Resin}}{\text{Weight of TCE}}\right)\left(\frac{\text{Molecular Weight}}{\text{of TCE}}\right)$$

Table 6 Comparsion of the Epoxy Equivalent Weight Obtained by Proton Magnetic Resonance and HBr-Acetic Acid Methods with Literature Values

Resin	Literature Value	Proton NMR	HBr-Acetic acid
Epon 826	178-186	185	183
EpiRez 5022	120-140	126	131
RD-2	120-140	133	134

T O N O X and T O N O X 6 0 / 4 0

These two epoxy curing agents appear to be a mixture of several aromatic amines. Tonox 60/40 differs from Tonox by having about 42 % of m-phenylene diamine (m-PDA) . Tonox was principally composed of three components the main one being methylene dianiline (MDA), 2,4-bis(aminobenzyl)aniline as confirmed by the same retention time of a purchased sample of the same chemical, which was also characterized by FT-IR ; the third peak, of high molecular mass, appeared to be composed of higher oligomers of MDA .

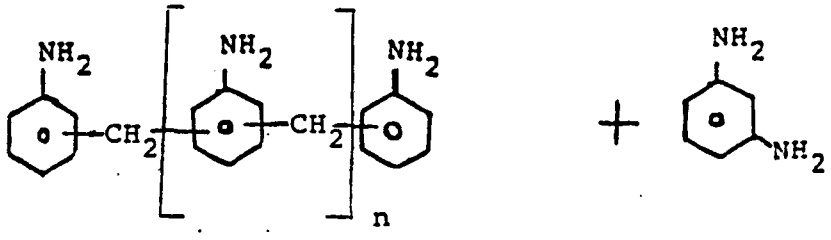

n = 0 MDA

n = 1 2,4-bis(aminobenzyl)aniline

n ⩾ 2 Oligomers

These results agree with those reported in literature (3) .

Tonox 60/40

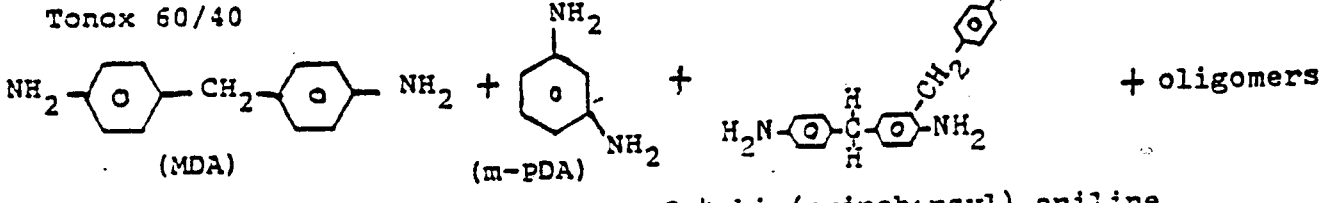

(MDA) (m-PDA) 2,4-bis(aminobenzyl) aniline + oligomers

Tonox

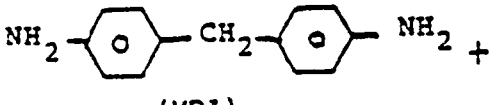

(MDA) + 2,4-bis(aminobenzyl) aniline + oligomers

GPC Chromatogram of Tonox 60/40

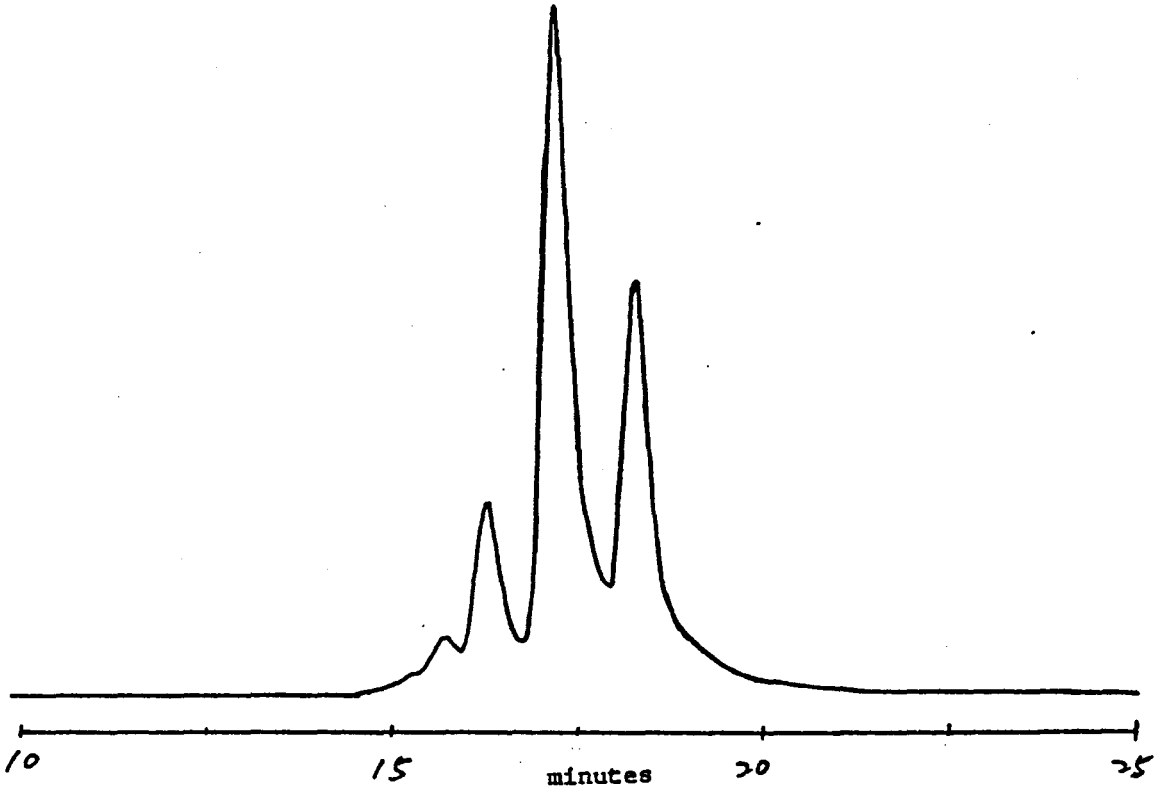

Table 7, GPC Separation of Tonox 60/40. Column, Ultra Styragel 500 Å + 100 Å; Mobile Phase, THF; Flow Rate, 1ml/min; Detector, UV 254 nm.

Sample	Peak #	Retention time (mins.)	Weight %	Components
Tonox 60/40	1	15.7	3.22	Oligomers
	2	16.3	11.25	2,4-bis(aminobenzyl)-aniline
	3	17.2	42.81	MDA
	4	18.3	42.72	m-PDA

GPC chromatogram of Tonox

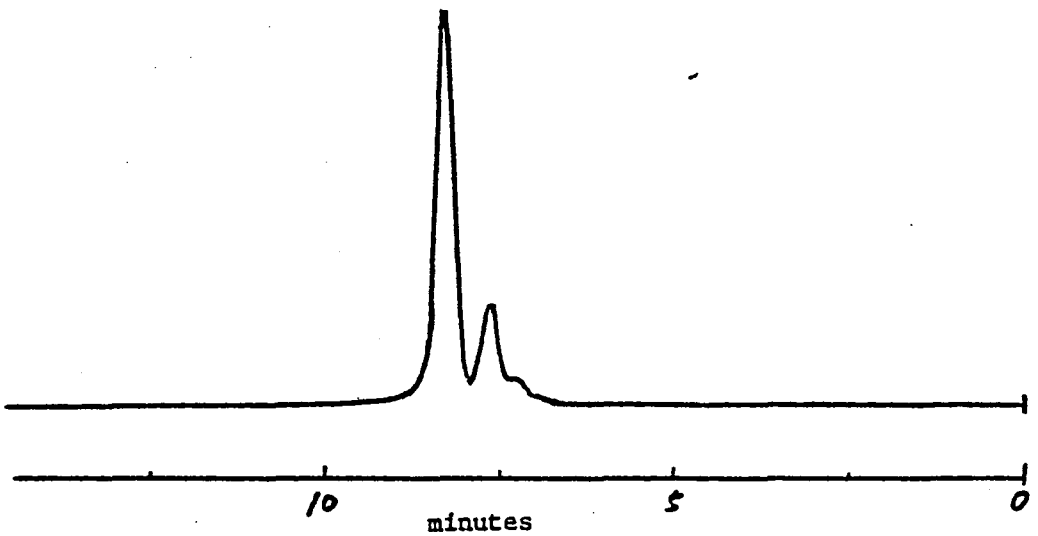

Table 8 GPC Separation of Tonox. Column, Ultra Styragel 100 Å; Mobile Phase, THF; Flow Rate, 1ml/min, Detector, UV 254 nm.

Sample	Peak #	Retention time (mins.)	Weight %	Components
Tonox	1	7.3	4.69	Oligomers
	2	7.7	18.49	2,4-bis(aminobenzyl)-aniline
	3	8.4	76.81	MDA

Infrared Studies

(1) Sample Preparation

The viscous liquid sample of Tonox 60/40 was smeared on the surface of a potassium bromide plate uniformly, then the spectra taken in a Digilab-FTS-20B infrared spectrometer.

The solid sample of MDA or m-pDA was mixed with dried potassium bromide by grinding in a small agate pestle and mortar, then made into a transparent disc by using a mini-press die and the spectra was run by FT-IR.

(2) Infrared Band Specification

4,4'-Methylenedianiline(MDA)

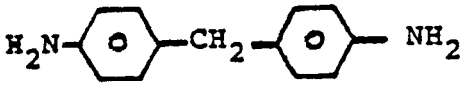

~3420 cm^{-1} = N-H free stretch

~3220 cm^{-1} = N-H bonded stretch

3040 cm^{-1} = Aromatic C-H stretch

2920 cm^{-1} = CH_2 asymmetry stretch

2830 cm^{-1} = CH_2 symmetry stretch

1630 cm^{-1} = N-H bending

1520 cm^{-1} = Aromatic C=C stretch

1440 cm^{-1} = C-H deformation

1320-1080 cm^{-1} = C-N stretch

920-760 cm^{-1} = N-H wagging

620-500 cm^{-1} = C-C bending

m-phenylenediamine (m-PDA)

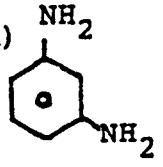

3335 cm^{-1} = N-H free stretch

3220 cm^{-1} = N-H bonded stretch

3050, 3015 cm^{-1} = Aromatic C-H stretch

1610 cm^{-1} = N-H bending

1500 cm^{-1} = Aromatic C=C stretch

1320-1060 cm^{-1} = C-N stretch

840-680 cm^{-1} = N-H wagging

Tonox 60/40

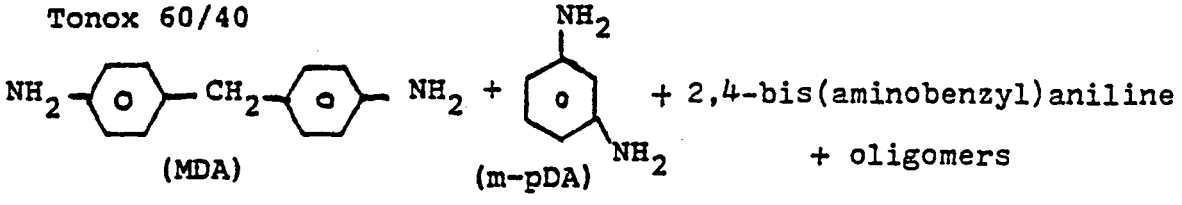

(MDA) (m-pDA) + 2,4-bis(aminobenzyl)aniline + oligomers

3345 cm^{-1} = N-H free stretch

3220 cm^{-1} = N-H bonded stretch

3040 cm^{-1} = Aromatic C-H stretch

2900 cm^{-1} = CH_2 asymmetry stretch

2830 cm^{-1} = CH_2 symmetry stretch

1620 cm^{-1} = N-H bending

1520 cm^{-1} = Aromatic C=C stretch

1310-1080 cm^{-1} = C-N stretch

840-680 cm^{-1} = N-H wagging

570,500 cm^{-1} = C-C bending

FT-IR spectrum of MDA

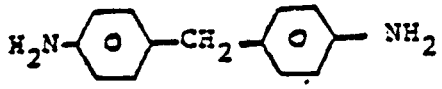

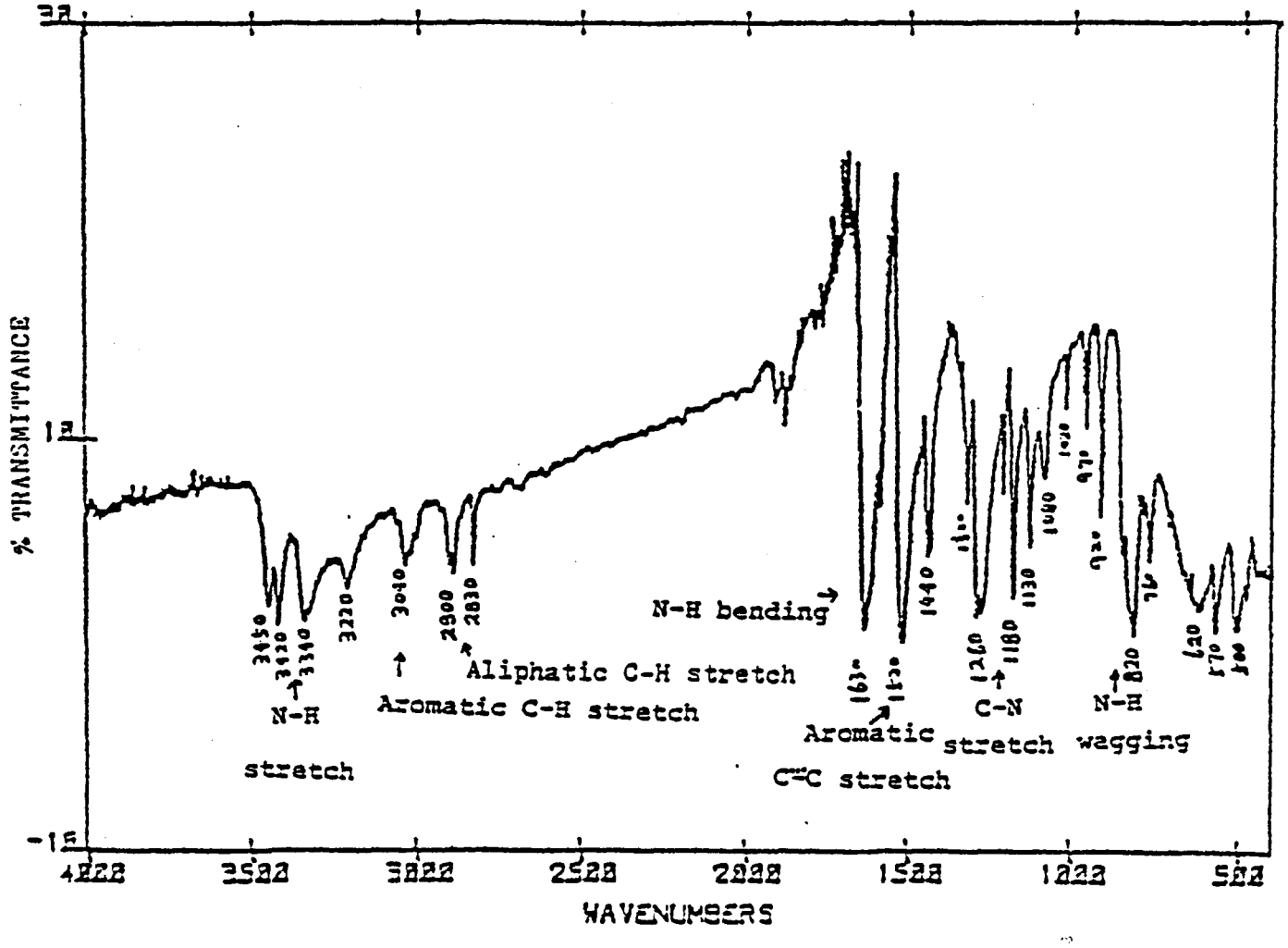

The FT-IR Spectrum of 4,4'-Methylenedianiline

FT-IR spectrum of m-PDA

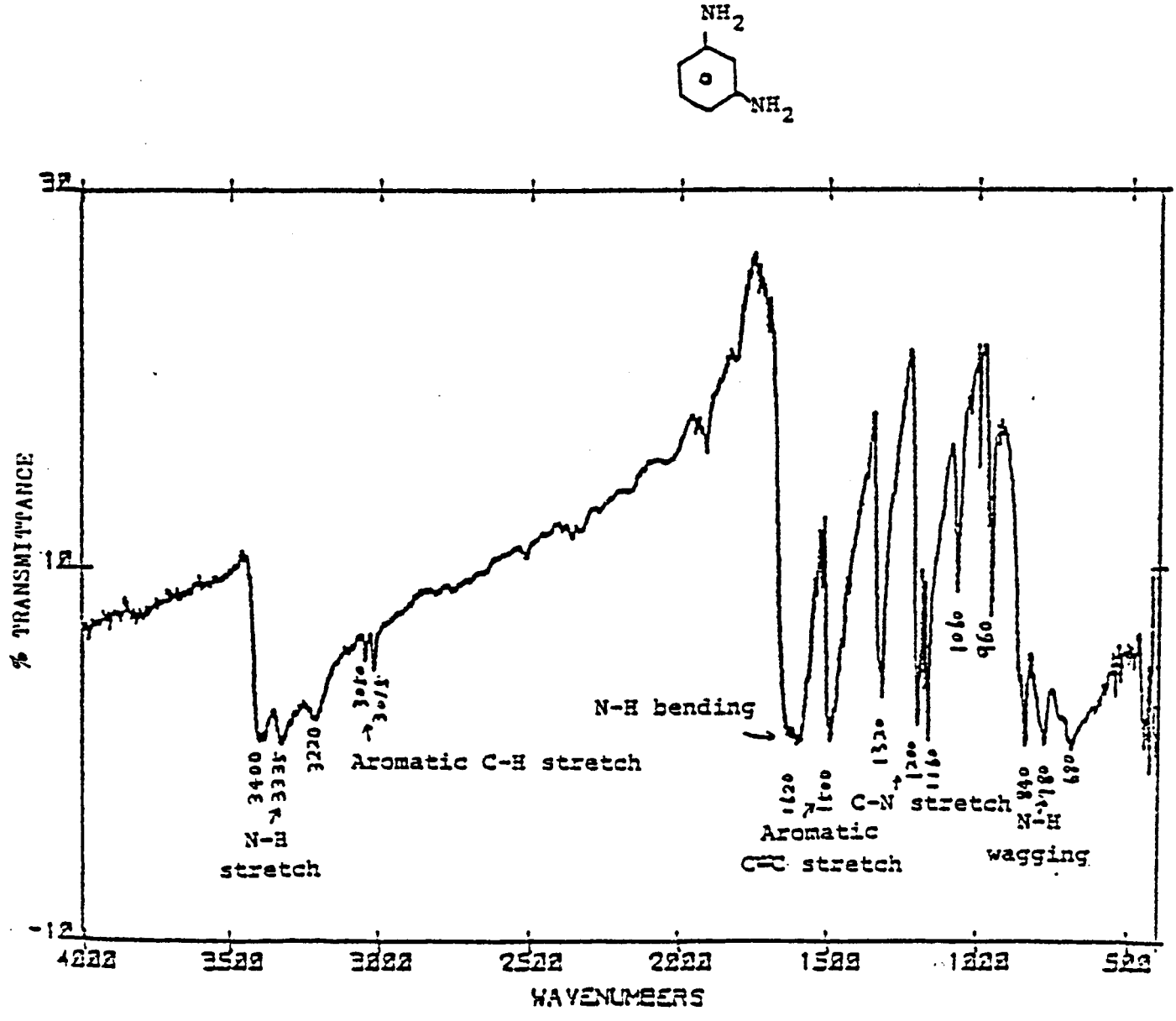

The FT-IR Spectrum of meta-Phenylenediamine

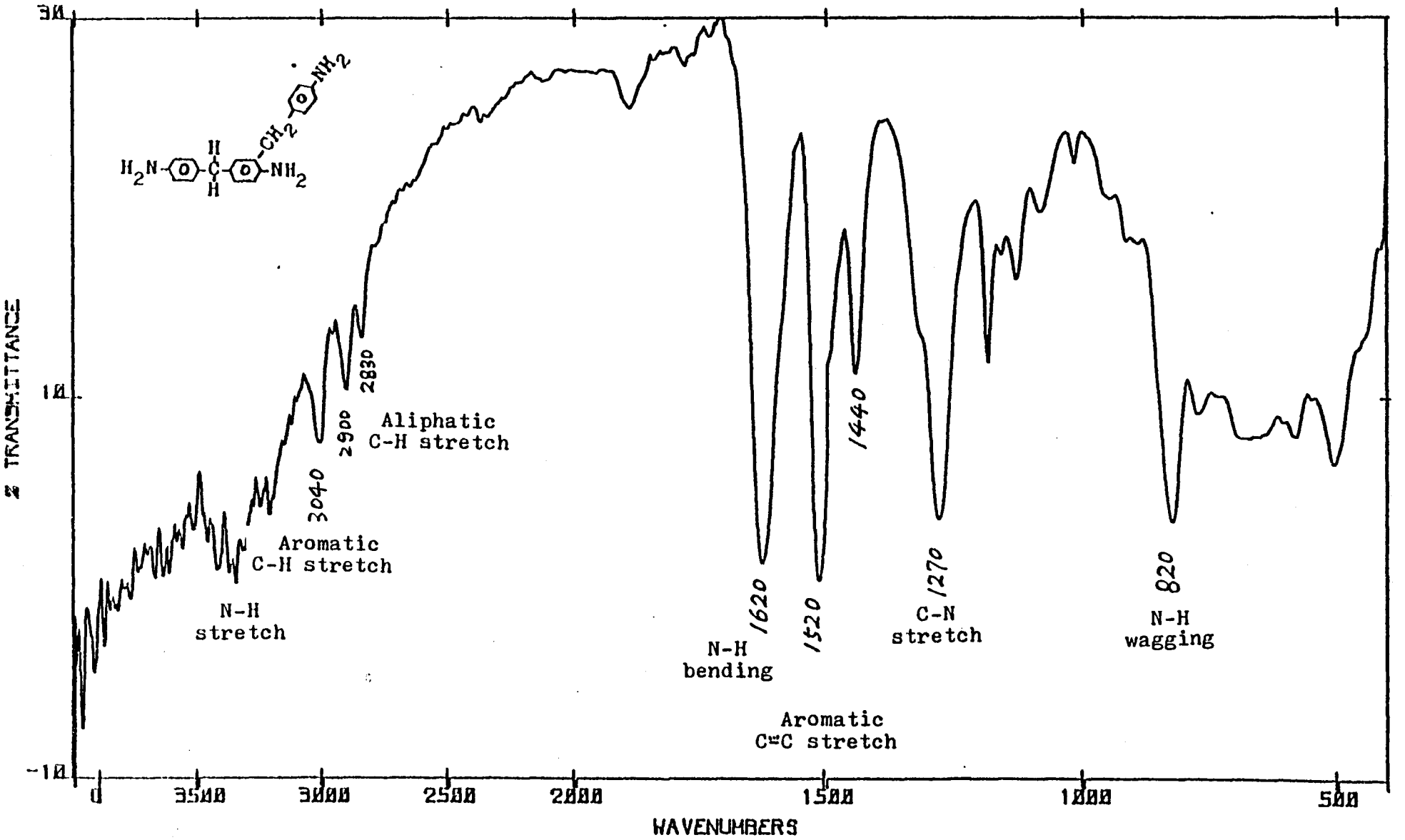

The FT-IR spectrum of 2,4-bis(aminobenzyl) aniline

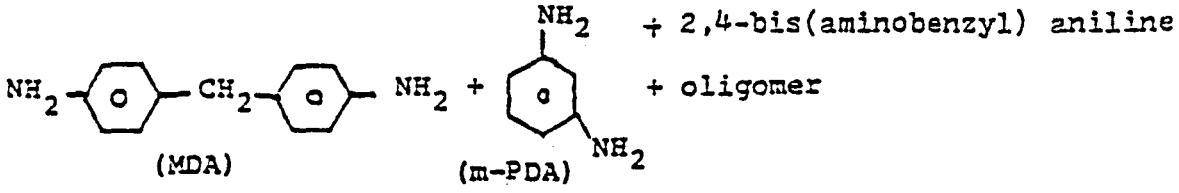

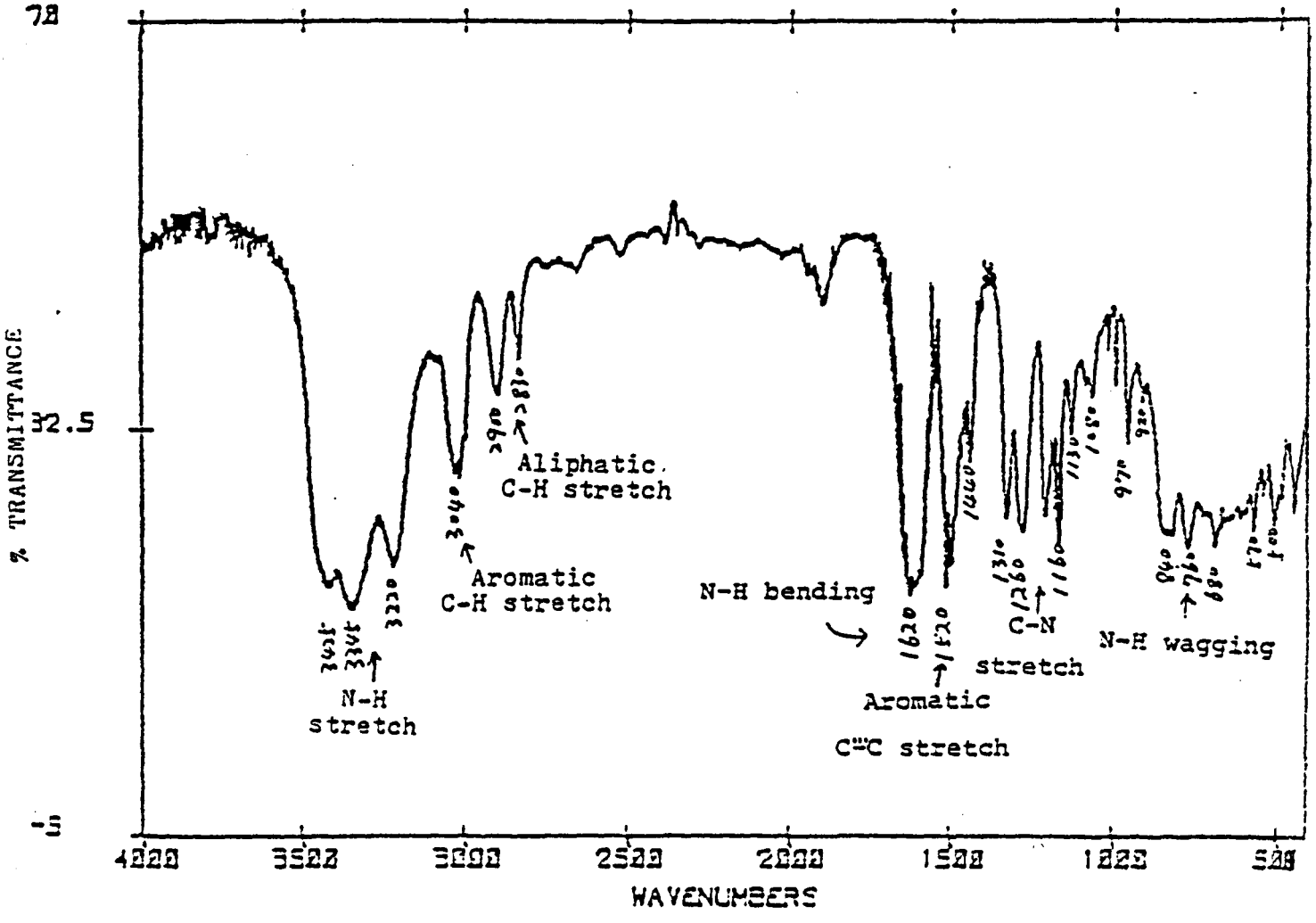

The FT-IR Spectrum of Tonox 60/40

Proton-NMR Studies

(1) Sample preparation

4,4'-Methylenedianiline (MDA), m-phenylenediamine(m-pDA), and Tonox 60/40 were dissolved in chloroform-d, solvent with TMS standard respevtively,then run on a 60 MHz H-NMR spectrometer.

(2) Band Characterization

There are four different kinds of hydrogens for MDA at δ3.25, δ3.54, δ6.2, δ6.5, which has been related to each hydrogen position in the structure

m-pDA also showed four kinds of hydrogen absorptions at δ3.25, δ5.65, δ5.8, δ6.5 in the spectrum. The H-NMR spectrum of Tonox 60/40 showed six absorptions at δ3.25, δ3.54, δ5.6, δ5.8, δ6.2, δ6.5. Obviously, this is a combined spectrum of MDA with m-pDA. The weak absorption of MDA at δ6.5 was combined with the stronger absorption of m-pDA at δ6.5.

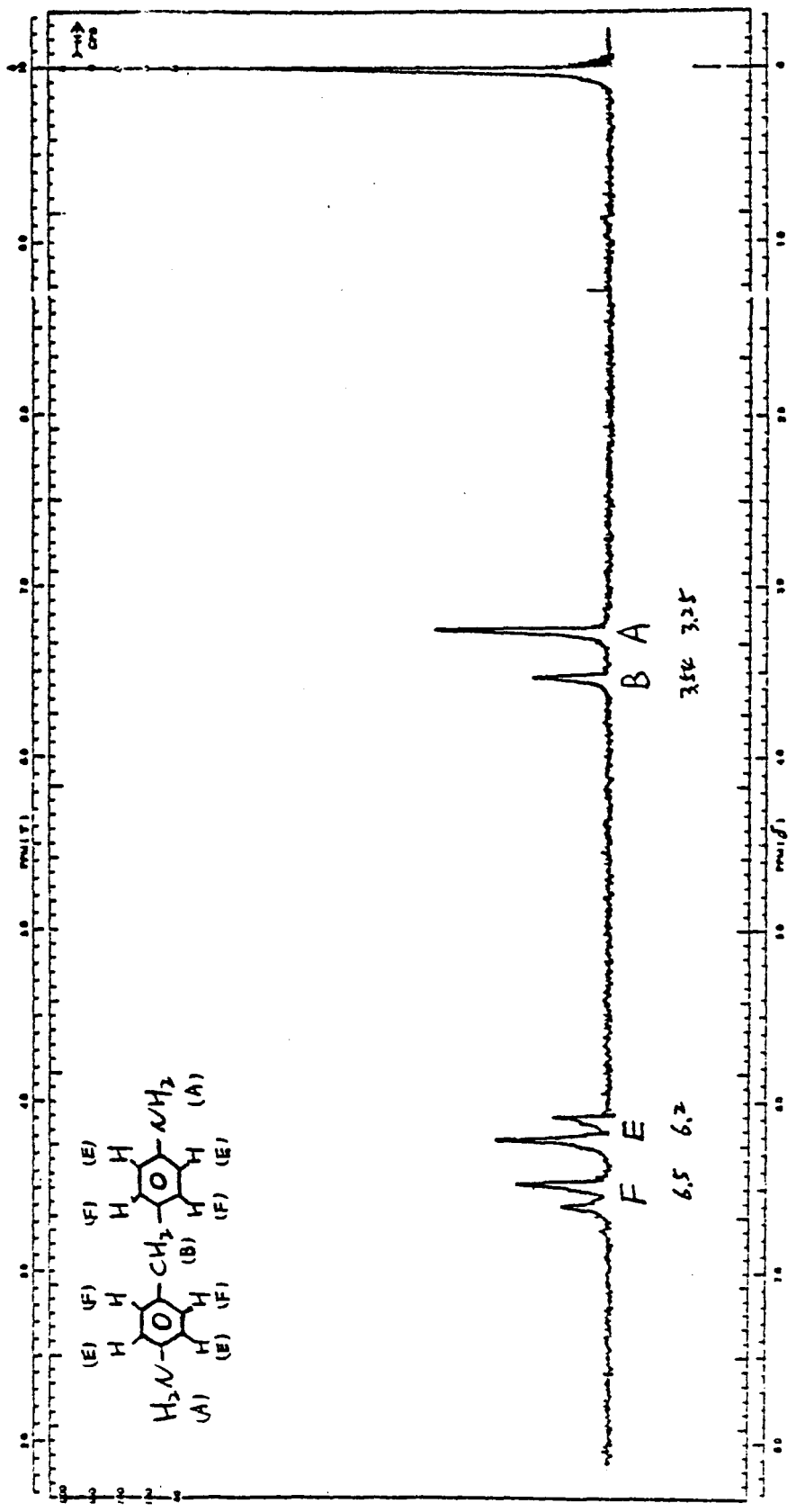

60 MHZ NMR Spectrum of MDA

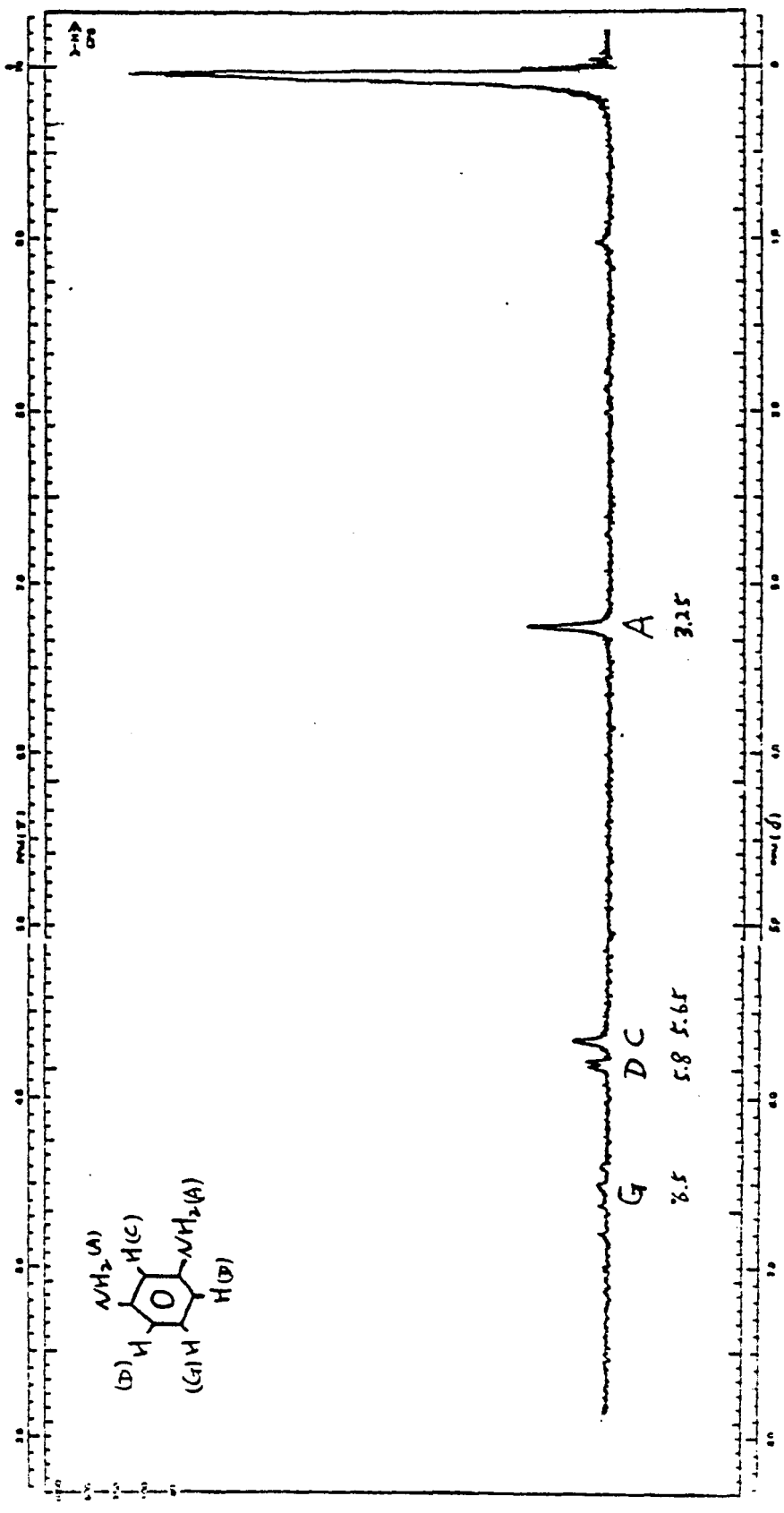

60 MHZ NMR Spectrum of m-PDA

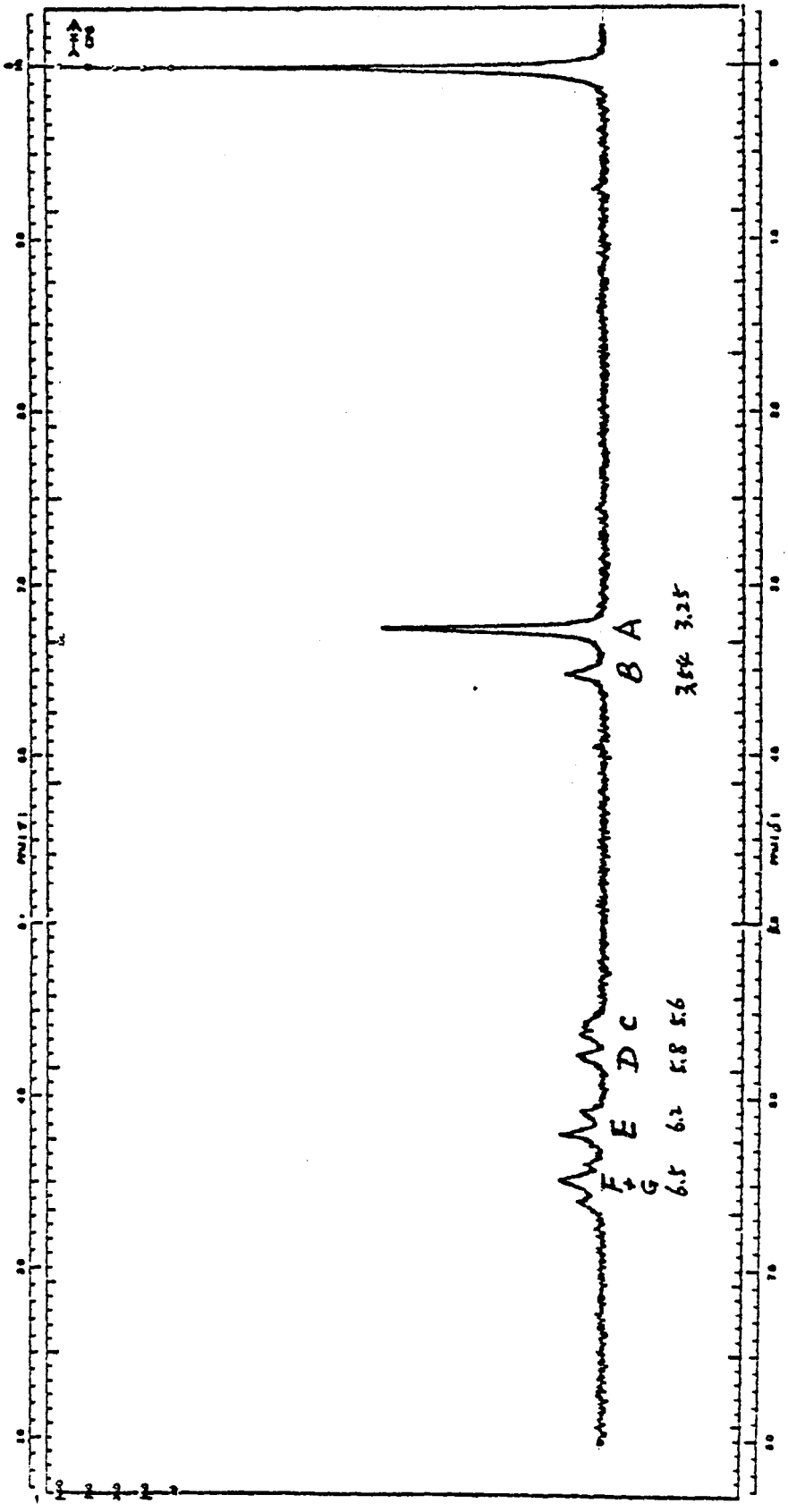

60 MHZ NMR Spectrum of Tonox 60/40

STRUCTURE SCHEME FOR ALL RAW MATERIALS

EPOXY RESINS:

Epon 826, Epon 828 (Diglycidyl Ether of Bisphenol A)

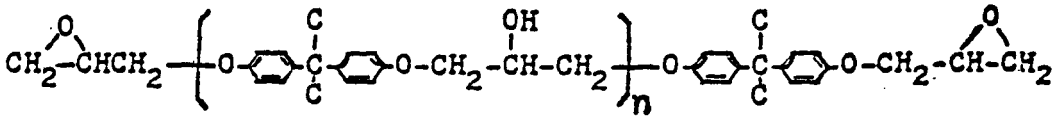

EPOXY DILUENTS:

EpiRez 5022, RD-2 (Diglycidyl Ether of 1,4-Butanediol)

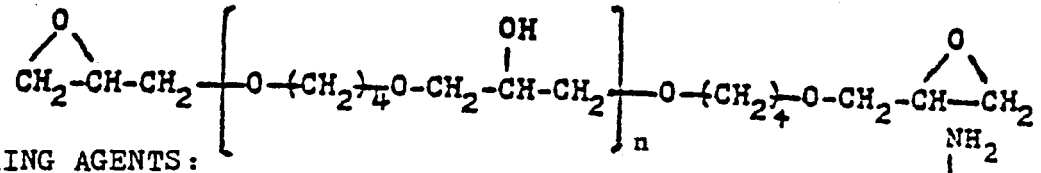

CURING AGENTS:

Tonox 60/40

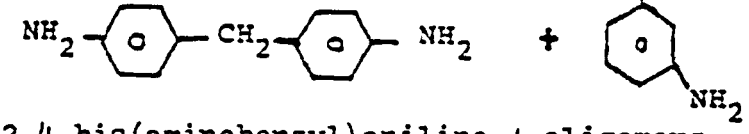

+ 2,4-bis(aminobenzyl)aniline + oligomers

Tonox

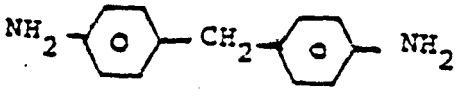

+ 2,4-bis(aminobenzyl)aniline + oligomers

4,4'-Methylenedianiline (MDA)

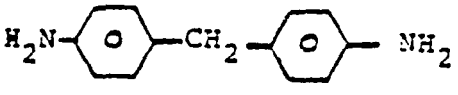

m-Phenylenediamine (m-PDA)

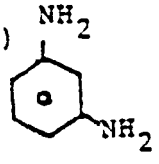

2,4-bis(aminobenzyl)aniline

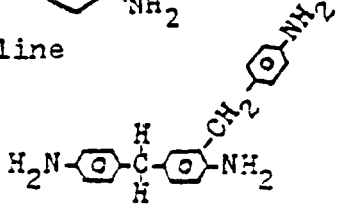

Determination of the amount of curing agent to be added to the epoxy resin for curing .

(a) The epoxy equivalent weight (EEW) and hydrogen equivalent weight (HEW) used to calculate the curing agent concentration is as following:

Material	EEW	HEW
Epon 826	183	
EpiRez 5022	131	
RD-2	134	
Tonox 60/40		37.6
Tonox		50.51
MDA		49.5
m-pDA		27

(b) Curing agent concentration = $\frac{\text{HEW}}{\text{EEW}} \times 100$

(c) An example using these calculations for curing agent concentration is as follows: (A/E=1)

If 100% Epon 826, then it needs Tonox 60/40 = $\frac{37.6}{183}$ = 20.55%

If 100% EpiRez, then it needs Tonox 60/40 = $\frac{37.6}{131}$ = 28.70%

For 80% Epon 826, then it needs Tonox 60/40 = 20.55%x0.8= 16.44%

20% EpiRez 5022, then it needs Tonox 60/40 = 28.70%x0.2= 5.74%

Total 22.18%

Therefore, the formula is:

Epon 826 = 80 grams

EpiRez 5022 = 20 grams

Tonox 60/40 = 22.18 grams (A/E=1)

BIBLIOGRAPHY

1. G.L. Hagnauer, Ind. Res. Dev., 23 (4), 128 (1981)

2. G.L. Hagnauer and D.A. Dunn, Ind. Eng. Chem., Prod. Res. & Dev., 21 (1), 68 (1982)

3. P.R. Young and G.F. Skyes, Natl. SAMPE Tech Conf., 12, 602 (1980)

PART III

CURE KINETICS OF HBRF 55A RESIN FORMULATIONS

KINETIC STUDY OF CURING REACTIONS .

INTRODUCTION

Differential Scanning Calorimetry (DSC) was used to investigate the kinetics of curing reactions of epoxy resins (diglycidyl ether of bisphenol A , DGEBA and butanediol diglycidyl ether, DGBE) with aromatic diamines (methylene dianiline, MDA and m-phenylene diamine, m-PDA) and a commercial product containing a mixture of these diamines (Tonox 60/40).The heat released during the isothermal cure at various temperatures was measured as a function of time and it was assumed to be directly proportional to the extent of cure (Fig.1).

The autocatalytic behavior of these systems has been described in literature (1,2,3,4,9,10) and it is accepted that the kinetics of the curing reaction of epoxides with amines can be successfully described using the following kinetic equation (5,6) :

$$\dot{\alpha} = d\alpha / dt = (k_1 + k_2\alpha^m)(1-\alpha)^n \qquad (1)$$

where $\dot{\alpha}$ is the rate of reaction, α the degree of cure, or extent of reaction, k_1 a kinetic constant expressing the reaction between a primary amine and an epoxide group, k_2 a

rate constant of the subsequent reactions between a secondary amine, an hydroxyl and an epoxide group and two epoxide groups ,reaction which may be anionically started by the tertiary amine formed during the curing reaction (7). The sum of the kinetic exponents m and n is assumed to be two . This equation can successfully describe the autocatalytic behavior of these systems using amounts of amine hydrogens and epoxide groups in the vicinity of the stoichiometric ratio and assuming the same reactivity for every amine hydrogen.

The kinetic constant k_1 was obtained by extrapolation of the heat flow curve at t=0 :

$$k_1 = (d\alpha / dt)_{t=0} \qquad (2)$$

and the remaining kinetic parameters were calculated as reported (5) using the rate and extent of reaction at the peak of the isothermal heat flow curve.(See Appendix 1)

The kinetic parameters were also calculated using a non linear regression of $\dot{\alpha}/(1-\alpha)^n$ over α^m.(See Appendix 2)

The extent of reaction α was taken as the heat evolved at a certain time (Q_t) divided by the total heat of reaction evolved (Q_{Ult}) :

$$\alpha_t = Q_t / Q_{Ult} \qquad (3)$$

For some systems the cure was incomplete at a given

isothermal temperature even after the heat flow curve levelled to the baseline, therefore the total heat of reaction was taken as :

$$Q_{Ult} = Q_{Iso} + Q_{Res} \qquad (4)$$

where Q_{Iso} is the heat evolved during the isothermal curing and Q_{Res} is a residual heat which is released by dynamic run of the sample after the isothermal cure .

EXPERIMENTAL

The formulations used in this study were composed of a DGEBA resin (Shell's Epon 826) containing a small amount of higher oligomeric fractions (8.7 %),DGBE reactive epoxy diluent (Celanese's Epirez 5022) containing pure DGBE (51.2 %) and higher oligomeric fractions (n=1,34.3 %; n=2,9.2 %; n$\geqslant$3 4.3 %), purified MDA and m-PDA and a commercial mixture of them (Uniroyal's Tonox 60/40) also containing some oligomeric fractions (m-PDA, 40 %; MDA,42%; 2,4-bis(aminobenzyl)aniline plus oligomers, 18 %).

The mixtures prepared were:

1) DGEBA MDA A/E = 1.0 2) DGEBA m-PDA A/E = 1.0

3) DGBE MDA A/E = 1.0 4) DGBE m-PDA A/E = 1.0

5) DGEBA/DGBE (80/20) MDA A/E = 1.0

6) DGEBA/DGBE (80/20) m-PDA A/E = 1.0

7)	DGEBA	Tonox 60/40	A/E = 1.0
8)	DGBE	Tonox 60/40	A/E = 1.0
9)	DGEBA/DGBE (80/20)	Tonox 60/40	A/E = .9
10)	DGEBA/DGBE (80/20)	Tonox 60/40	A/E = 1.0
11)	DGEBA/DGBE (80/20)	Tonox 60/40	A/E = 1.1
12)	DGEBA/DGBE (80/20)	Tonox 60/40	A/E = 1.2

The epoxy-amine mixture were prepared at room temperature by adding the curing agent with continuous stirring until a clear homogeneous solution was obtained; the solution was then degassed under vacuum and samples (5-10 mg) prepared were sealed in hermetic aluminum pans and tested immediately. Samples aged even a few hours at room temperature gave unreliable results due to the onset of a slow curing reaction . Weight losses were negligible in all cases . A Du Pont 1090 Thermal Analyzer connected with a 910 DSC module was used to measure the heat flow as a function of time after calibration with high purity Indium (Du Pont thermetric standard). A steady isothermal baseline was established at the preset curing temperature using two empty sample pans.

The sample pan was then introduced in the DSC cell and the data acquisition initiated. Thermal equilibrium between sample and reference pans was achieved in less than one minute from the start of reaction.The reaction was considered to be complete when the rate curve levelled off to the baseline .

Isothermal experiments were conducted in the temperature range of 373-413 ^{o} K (100-140 ^{o} C).Isothermally cured samples were then quenched and scanned from -50 to +350^{o} C at an heating rate of 10 ^{o} C per minute to measure Q_{Res}.Data collected by DSC were processed by a Digital PDP-11 computer to obtain the rate and extent of cure as function of time, and calculate the kinetic parameters of the reaction. The value of $(d\alpha / dt)_{t=0}$, which is subject to an experimental error due to the lack of thermal equilibrium of the sample during the first few seconds of analysis, was optimized by a computer program in order to minimize differences between experimental and calculated results using equation (1).
The program also calculates all actvation energies and frequency factors and its flow chart is shown in Appendix 3.

RESULTS AND DISCUSSION

The "S" shaped curves of evolution of α with the time at different temperaturesof curing (Fig. 2) clearly show the autocatalytic curing kinetic of these systems and confirm the validity of equation (1). All systems studied show a similar behavior, with differences in the temperature dependence of values of rate constants (k_1,k_2), kinetic exponent m , maximum reaction rate ($\dot{\alpha}_p$), conversion at maximum reaction rate (α_p), time to achieve maximum reaction rate (t_p) and time to achieve half of the maximum conversion (t_{50}) (Tables 1-12).

An Arrhenius relationship can describe the temperature variation of k_1, k_2, $\dot{\alpha}_p$, t_p and t_{50} (Fig 3, 4, 6, 7) while α_p and m (Fig 5) decrease linearly with temperature in the range studied. Temperature dependence of α_p, t_p and t_{50} allows measurements of global activation energies (Ea_p, Et_p, Et_{50}) which do not distinguish between different types of reaction. This result was confirmed by monitoring the disappearance of the absorbtion band at 915 cm^{-1} characteristic of the epoxy ring by FT-IR spectroscopy (8) . Temperature dependence of rate constants k_1 and k_2 allows to distinguish between the primary amine-epoxide and the subsequent reactions which have different activation energies (E_1,E_2) and frequency factors (A_1,A_2) (Tables 1a - 12 a).

The values of activation energies and frequency factors were calculated with a computer program ; its flowchart is shown in Appendix 3.

All the systems studied show an E_1 value in the range between 13 and 15 Kcal/mole, indicating similarity of the transition state of the attachement of primary amine on epoxy ring.

Frequency factor A_1 of the curing reaction DGEBA with m-PDA is higher than DGEBA with MDA due to the higher viscosity of this solution which limits the mobility of the molecules . The reaction between DGBE and m-PDA shows a lower value of E_1 and A_1 compared with the reaction of DGBE with MDA . E_1 is probably lower because the small m-PDA molecule can be accomodated in the transition state more easily than the bigger MDA molecule. E_2 is slightly smaller in DGBE systems showing the tendency of these systems to give lower energy transition states.

Systems where the epoxy component contained a mixture of DGEBA and DGBE , cured with either MDA or m-PDA , showed E_1,E_2 ,A_1,A_2 values very close to the theoretical values calculated as the composition weighted average of the values of the bicomponent formulations.

DGEBA cured with Tonox 60/40, which contains a high percentage of oligomeric fractions showed activation energies and frequency factors lower than theoretical value; this behavior is even more evident in the system DGBE cured

with Tonox 60/40 where the values obtained experimentally are quite different from the theoretical ones.

These results may be explained by the presence of a high amount of oligomeric fractions in Tonox 60/40 ,which decreases the activation energy and the frequency factor . This behavior is especially evident in the curing of DGBE with Tonox 60/40 because in this case the reagents participating to the reaction interacts synergistically.

To clarify the effect on the curing kinetics of the presence of oligomeric fractions in the curing agent a study was performed on the system DGBE plus 2,4-bis(aminobenzyl)-anyline .

Activation energy and frequency factor for the primary reaction in this system are quite lower than the others, while E_2 and A_2 are in the same range (Table 13 and 13a).The lower value of the parameters E_1 in this system may be explained with the higher basicity of the amino groups of 2,4-bis(aminobenzyl)-aniline while the lower A_1 coefficent suggests the idea of a reduced mobility of this molecule .

Temperature dependance of k_1 and k_2 for the system DGEBA/DGBE cured with Tonox 60/40 (A/E = .9, 1.0, 1.1, 1.2) is shown in Fig. 8 and Fig. 9 .

The curing kinetics of the mixture DGEBA / DGBE (80:20) with Tonox 60/40 A/E = 1.0 show E_1 slightly lower and A_1 lower than the percentage composition weighted average of the

bicomponents formulations. This behavior may be explained with the presence of a high percentage of oligomeric fractions in the curing agent which, as explained in the former pharagraph, reduces the mobility of the molecules in the reaction medium and decreases the activation energy.

The formulations with A/E = .9,1.1,1.2 show a value of E_1 very close to the formulation A/E = 1.0 .Departures from the stoichiometric ratio affects the value of A_1 which increases by increasing the concentration of mobile amino groups.

E_2 values are similar for all four formulation and A_2 increases by increasing the A/E ratio from .9 to 1.1 but decreases above this value, due to the lower availability of epoxy rings needed for the reaction with the secondary amine.

The Q_{Iso} evolved during the curing of every system studied did not change in function of temperature outside the error range of the technique used except for the system DGEBA with MDA,thus showing Q_{Res}. The high viscosity and Tg_{∞} of this system prevent high conversion (Fig. 2) at curing temperatures much lower than its Tg_{∞} .

System DGEBA/DGBE with Tonox 60/40 releases the maximum Q_{Iso} for the formulation A/E = 1.1 showing the maximum number of functional groups reacted in this case.

REFERENCES

1) Prime B.,in" Thermal Characterization of Polymeric Materials", E.Turi,Editor,Chapter 5, Academic Press N.Y. 1982 .

2) Horie K.,Hiura H.,Sawada M., Mita I. and Kambe H.; J.Polym. Sci (A-1), 8, 1357 (1970).

3) Kamal M.R., Souror S. and Ryan M. ; Soc. Plast. Eng. Tech. Papers, 19, 187 (1973) .

4) Souror S. and Kamal M.R. ; Thermochimica Acta, 14,41 (1976)

5) Ryan M.E. and Dutta A. ; Polymer, 20, 203 (1979) .

6) Hagnauer G.L., LaLiberte B.R. and Dunn D.A. ; Epoxy resins chemistry II , ACS Sym. Ser., 221, 229 (1982).

7) Mijovic J., Kim K. and Slaby J.; J. Appl. Polym. Sci., 29, (4), 1449 (1984) .

8) Golub M.A. and Hsu M.S. ; To be published.

9) C.C.Foun, A. Moroni, E.M. Pearce, J. Mijovic ; ACS PMSE Preprints , 51,411-20 (1984).

10) C.C.Foun, A. Moroni, E.M. Pearce, J. Mijovic ; Proceedings of the 13th NATAS Conference , Philadelphia 1984, pg. 418-23.

Table 1. Temperature dependence of kinetic variables.
System : DGEBA with MDA A/E = 1.0 .

Kinetic Variables	Temperature dependence	correlation coefficient
k_1 (min^{-1})	1.99 E+6 exp(-6.11 E+4 / RT)	-.9981
k_2 (min^{-1})	1.28 E+5 exp(-4.40 E+4 / RT)	-.9978
m	1.99 - 2.89 E-3 *T	-.9395
$\dot{\alpha}_p$ (min^{-1})	2.27 E+5 exp(-4.98 E+4 / RT)	-.9996
α_p	1.17 - 1.98 E-3 *T	-.9732
t_p (min)	9.96 E-8 exp(6.03 E+4 / RT)	.9999
t_{50} (min)	2.56 E-6 exp(5.04 E+4 / RT)	.9964

Table 1a. Activation energies and frequency factors.
System : DGEBA with MDA.

Activation Energy (Kcal/mole)			Frequecy Factor (min^{-1})		
E_1	=	14.60	A_1	=	1.99 E+6
E_2	=	10.52	A_2	=	1.28 E+5
$E\dot{a}_p$	=	11.90	$A\dot{a}_p$	=	2.27 E+5
Et_p	=	14.41			
Et_{50}	=	12.01			

Table 2. Temperature dependence of kinetic variables.
System : DGEBA with m-PDA A/E = 1.0 .

Kinetic Variables	Temperature dependence	correlation coefficient
k_1 (min^{-1})	6.99 E+6 exp(-6.40 E+4 / RT)	-.9998
k_2 (min^{-1})	1.79 E+5 exp(-4.45 E+4 / RT)	-.9934
m	2.58 - 4.57 E-3 *T	-.9935
$\dot{\alpha}_p$ (min^{-1})	3.65 E+5 exp(-5.05 E+4 / RT)	-.9966
α_p	1.46 - 2.85 E-3 *T	-.9962
t_p (min)	1.39 E-8 exp(6.52 E+4 / RT)	.9991
t_{50} (min)	7.85 E-7 exp(5.30 E+4 / RT)	.9964

Table 2a. Activation energies and frequency factors.
System : DGEBA with m-PDA.

Activation Energy (Kcal/mole)			Frequecy Factor (min^{-1})		
E_1	=	15.30	A_1	=	6.99 E+6
E_2	=	10.63	A_2	=	1.79 E+5
$E\dot{\alpha}_p$	=	12.07	$A\dot{\alpha}_p$	=	3.65 E+5
Et_p	=	15.59			
Et_{50}	=	12.67			

Table 3. Temperature dependence of kinetic variables .
System : DGBE with MDA A/E = 1.0 .

Kinetic Variables	Temperature dependence	correlation coefficient
k_1 (min^{-1})	7.54 E+6 exp(-6.20 E+4 / RT)	-.9994
k_2 (min^{-1})	.39 E+5 exp(-4.06 E+4 / RT)	-.9976
m	2.43 - 4.03 E-3 *T	-.9982
$\dot{\alpha}_p$ (min^{-1})	4.87 E+5 exp(-5.16 E+4 / RT)	-.9989
α_p	1.75 - 3.72 E-3 *T	-.9976
t_p (min)	2.16 E-9 exp(7.04 E+4 / RT)	.9993
t_{50} (min)	1.02 E-6 exp(5.20 E+4 / RT)	.9985

Table 3a. Activation energies and frequency factors.
System : DGBE with MDA.

Activation Energy (Kcal/mole)			Frequecy Factor (min^{-1})		
E_1	=	14.81	A_1	=	7.55 E+6
E_2	=	9.12	A_2	=	.38 E+5
$E\dot{a}_p$	=	12.34	$A\dot{a}_p$	=	4.87 E+5
Et_p	=	16.81			
Et_{50}	=	12.43			

Table 4. Temperature dependence of kinetic variables.
System : DGBE with m-PDA A/E = 1.0 .

Kinetic Variables	Temperature dependence	correlation coefficient
k_1 (min^{-1})	1.52 E+6 exp(-5.54 E+4 / RT)	-.9973
k_2 (min^{-1})	.56 E+5 exp(-4.12 E+4 / RT)	-.9980
m	1.48 - 1.59 E-3 *T	-.9666
$\dot{\alpha}_p$ (min^{-1})	3.19 E+5 exp(-4.93 E+4 / RT)	-.9994
α_p	1.15 - 2.28 E-3 *T	-.9612
t_p (min)	1.87 E-8 exp(6.19 E+4 / RT)	.9958
t_{50} (min)	1.40 E-6 exp(4.99 E+4 / RT)	.9990

Table 4a. Activation energies and frequency factors.
System : DGBE with m-PDA.

Activation Energy (Kcal/mole)			Frequecy Factor (min^{-1})		
E_1	=	13.23	A_1	=	1.51 E+6
E_2	=	9.85	A_2	=	.56 E+5
$E\dot{a}_p$	=	11.78	$A\dot{a}_p$	=	3.19 E+5
Et_p	=	14.79			
Et_{50}	=	11.923			

Table 5. Temperature dependence of kinetic variables.
System : DGEBA/DGBE (80/20) with MDA A/E = 1.0 .

Kinetic Variables	Temperature dependence	correlation coefficient
k_1 (min^{-1})	3.33 E+6 exp(-6.10 E+4 / RT)	-.9995
k_2 (min^{-1})	1.26 E+5 exp(-4.39 E+4 / RT)	-.9977
m	1.95 - 2.71 E-3 *T	-.9553
$\dot{\alpha}_p$ (min^{-1})	2.26 E+5 exp(-4.94 E+4 / RT)	-.9987
α_p	1.23 - 2.19 E-3 *T	-.9829
t_p (min)	9.07 E-8 exp(5.97 E+4 / RT)	.9986
t_{50} (min)	3.38 E-7 exp(5.61 E+4 / RT)	.9964

Table 5a. Activation energies and frequency factors.
System : DGEBA/DGBE (80/20) with MDA

Activation Energy (Kcal/mole)			Frequecy Factor (min^{-1})		
E_1	=	14.56	A_1	=	3.33 E+6
E_2	=	10.48	A_2	=	1.26 E+5
$E\dot{a}_p$	=	11.79	$A\dot{a}_p$	=	2.26 E+5
Et_p	=	14.26			
Et_{50}	=	13.40			

Table 6. Temperature dependence of kinetic variables.
System : DGEBA/DGBE (80/20) with m-PDA A/E = 1.0 .

Kinetic Variables	Temperature dependence	correlation coefficient
k_1 (min^{-1})	7.03 E+6 exp(-6.19 E+4 / RT)	-.9989
k_2 (min^{-1})	2.86 E+5 exp(-4.64 E+4 / RT)	-.9963
m	1.24 - 1.06 E-3 *T	-.9405
$\dot{\alpha}_p$ (min^{-1})	7.28 E+5 exp(-5.26 E+4 / RT)	-.9976
α_p	0.96 - 1.64 E-3 *T	-.9874
t_p (min)	3.61 E-8 exp(6.12 E+4 / RT)	.9971
t_{50} (min)	3.28 E-7 exp(5.54 E+4 / RT)	.9923

Table 6a. Activation energies and frequency factors.
System : DGEBA/DGBE (80/20) with m-PDA

Activation Energy (Kcal/mole)			Frequecy Factor (min^{-1})		
E_1	=	14.79	A_1	=	7.03 E+6
E_2	=	11.08	A_2	=	2.86 E+5
$E\dot{a}_p$	=	12.55	$A\dot{a}_p$	=	7.28 E+5
Et_p	=	14.63			
Et_{50}	=	13.23			

Table 7. Temperature dependence of kinetic variables.
System : DGEBA with Tonox 60/40 A/E = 1.0 .

Kinetic Variables	Temperature dependence	correlation coefficient
k_1 (min^{-1})	3.18 E+6 exp(-6.09 E+4 / RT)	-.9971
k_2 (min^{-1})	1.42 E+5 exp(-4.40 E+4 / RT)	-.9995
m	2.15 - 3.22 E-3 *T	-.9791
$\dot{\alpha}_p$ (min^{-1})	1.46 E+5 exp(-4.80 E+4 / RT)	-.9997
α_p	1.34 - 2.45 E-3 *T	-.9958
t_p (min)	8.15 E-8 exp(6.02 E+4 / RT)	.9994
t_{50} (min)	1.83 E-6 exp(5.08 E+4 / RT)	.9991

Table 7a. Activation energies and frequency factors.
System : DGEBA with Tonox 60/40 A/E = 1.0

Activation Energy (Kcal/mole)			Frequecy Factor (min^{-1})		
E_1	=	14.56	A_1	=	3.18 E+6
E_2	=	10.59	A_2	=	1.42 E+5
$E\dot{\alpha}_p$	=	11.46	$A\dot{\alpha}_p$	=	1.46 E+5
Et_p	=	14.38			
Et_{50}	=	12.14			

Table 8. Temperature dependence of kinetic variables.
System : DGBE with Tonox 60/40 A/E = 1.0 .

Kinetic Variables	Temperature dependence	correlation coefficient
k_1 (min^{-1})	1.16 E+6 exp(-5.50 E+4 / RT)	-.9996
k_2 (min^{-1})	1.07 E+5 exp(-4.39 E+4 / RT)	-.9738
m	1.44 - 1.54 E-3 *T	-.8623
$\dot{\alpha}_p$ (min^{-1})	3.64 E+5 exp(-5.03 E+4 / RT)	-.9934
α_p	0.95 - 1.78 E-3 *T	-.8484
t_p (min)	4.82 E-8 exp(5.92 E+4 / RT)	.9975
t_{50} (min)	1.11 E-6 exp(5.12 E+4 / RT)	.9928

Table 8a. Activation energies and frequency factors.
System : DGBE with Tonox 60/40 A/E = 1.0

Activation Energy (Kcal/mole)			Frequecy Factor (min^{-1})		
E_1	=	13.13	A_1	=	1.16 E+6
E_2	=	10.49	A_2	=	1.07 E+5
$E\dot{a}_p$	=	12.01	$A\dot{a}_p$	=	3.64 E+5
Et_p	=	14.13			
Et_{50}	=	12.22			

Table 9. Temperature dependence of kinetic variables.
System : DGEBA/DGBE(80/20) with Tonox60/40 A/E = .9 .

Kinetic Variables	Temperature dependence	correlation coefficient
k_1 (min^{-1})	.725 E+6 exp(-5.54 E+4 / RT)	-.9978
k_2 (min^{-1})	.868 E+5 exp(-4.30 E+4 / RT)	-.9970
m	1.59 - 1.80 E-3 *T	-.8301
$\&_p$ (min^{-1})	1.33 E+5 exp(-4.77 E+4 / RT)	-.9991
α_p	1.04 - 1.46 E-3 *T	-.9418
t_p (min)	1.74 E-7 exp(5.72 E+4 / RT)	.9998
t_{50} (min)	6.20 E-6 exp(4.67 E+4 / RT)	.9999

Table 9a. Activation energies and frequency factors.
System : DGEBA/DGBE (80/20) with Tonox 60/40 A/E = .9

Activation Energy (Kcal/mole)			Frequecy Factor (min^{-1})		
E_1	=	13.24	A_1	=	.725 E+6
E_2	=	10.26	A_2	=	.868 E+5
Ea_p	=	11.40	Aa_p	=	1.33 E+5
Et_p	=	13.68			
Et_{50}	=	11.16			

Table 10. Temperature dependence of kinetic variables.
System : DGEBA/DGBE (80/20) with Tonox 60/40 A/E = 1.0 .

Kinetic Variables	Temperature dependence	correlation coefficient
k_1 (min^{-1})	1.20 E+6 exp(-5.67 E+4 / RT)	-.9993
k_2 (min^{-1})	1.86 E+5 exp(-4.51 E+4 / RT)	-.9998
m	1.25 - .996 E-3 *T	-.8342
$\dot{a}_p$ (min^{-1})	3.04 E+5 exp(-5.01 E+4 / RT)	-.9999
α_p	.80 - 1.17 E-3 *T	-.9294
t_p (min)	3.25 E-7 exp(5.48 E+4 / RT)	.9981
t_{50} (min)	1.08 E-6 exp(5.20 E+4 / RT)	.9987

Table 10a. Activation energies and frequency factors.
System : DGEBA/DGBE (80/20) with Tonox 60/40 A/E =1.0 .

Activation Energy (Kcal/mole)			Frequecy Factor (min^{-1})		
E_1	=	13.55	A_1	=	1.20 E+6
E_2	=	10.78	A_2	=	1.86 E+5
Ea_p	=	11.96	Aa_p	=	3.04 E+5
Et_p	=	13.08			
Et_{50}	=	12.49			

Table 11. Temperature dependence of kinetic variables.
System : DGEBA/DGBE (80/20) with Tonox 60/40 A/E = 1.1 .

Kinetic Variables	Temperature dependence	correlation coefficient
k_1 (min^{-1})	1.50 E+6 exp(-5.69 E+4 / RT)	-.9997
k_2 (min^{-1})	2.07 E+5 exp(-4.53 E+4 / RT)	-.9990
m	1.43 - 1.41 E-3 *T	-.6318
$\dot{\alpha}_p$ (min^{-1})	3.04 E+5 exp(-4.98 E+4 / RT)	-.9996
α_p	.980 - 1.63 E-3 *T	-.8514
t_p (min)	1.01 E-7 exp(5.82 E+4 / RT)	.9975
t_{50} (min)	1.90 E-6 exp(4.98 E+4 / RT)	.9966

Table 11a. Activation energies and frequency factors.
System : DGEBA/DGBE (80/20) with Tonox 60/40 A/E =1.1 .

Activation Energy (Kcal/mole)			Frequecy Factors (min-1)		
E_1	=	13.60	A_1	=	1.50 E+6
E_2	=	10.80	A_2	=	2.07 E+5
E_{ap}	=	11.88	A_{ap}	=	3.04 E+5
E_{tp}	=	13.92			
Et_{50}	=	11.90			

Table 12. Temperature dependence of kinetic variables.
System : DGEBA/DGBE (80/20) with Tonox 60/40 A/E = 1.2 .

Kinetic Variables	Temperature dependence	correlation coefficient
k_1 (min^{-1})	1.70 E+6 exp(-5.64 E+4 / RT)	-.9999
k_2 (min^{-1})	1.32 E+5 exp(-4.38 E+4 / RT)	-.9998
m	.230 - 1.83 E-3 *T	-.8775
$\dot{\alpha}_p$ (min^{-1})	2.43 E+5 exp(-4.87 E+4 / RT)	-.9997
α_p	.520 - 4.70 E-4 *T	-.6793
t_p (min)	5.88 E-7 exp(5.20 E+4 / RT)	.9990
t_{50} (min)	8.58 E-6 exp(4.45 E+4 / RT)	.9999

Table 12a. Activation energies and frequency factors.
System : DGEBA/DGBE (80/20) with Tonox 60/40 A/E = 1.2 .

Activation Energy (Kcal/mole)			Frequecy Factors (min-1)		
E1	=	13.46	A1	=	1.70 E+6
E2	=	10.47	A2	=	1.32 E+5
Eap	=	11.63	Aap	=	2.43 E+5
Etp	=	12.42			
Et50	=	10.62			

Table 13. Temperature dependence of kinetic variables.
System : DGBE with 2,4-bis(aminobenzyl)-aniline A/E = 1.0 .

Kinetic Variables	Temperature dependence	correlation coefficient
k_1 (min^{-1})	0.21 E+6 exp(-5.02 E+4 / RT)	-.9949
k_2 (min^{-1})	2.28 E+5 exp(-4.76 E+4 / RT)	-.9989
m	1.98 - 3.15 E-3 *T	-.9103
$\dot{\alpha}_p$ (min^{-1})	3.48 E+5 exp(-5.09 E+4 / RT)	-.9980
α_p	0.85 - 1.63 E-3 *T	-.9360
t_p (min)	4.82 E-8 exp(5.95 E+4 / RT)	.9991
t_{50} (min)	3.72 E-6 exp(4.81 E+4 / RT)	.9982

Table 13a. Activation energies and frequency factors.
System : DGBE with 2,4-bis(aminobenzyl)aniline A/E =1.0 .

Activation Energy (Kcal/mole)			Frequecy Factor (min^{-1})		
E_1	=	12.01	A_1	=	0.21 E+6
E_2	=	11.38	A_2	=	2.22 E+5
Ea_p	=	12.17	Aa_p	=	3.48 E+5
Et_p	=	14.21			
Et_{50}	=	11.50			

DSC

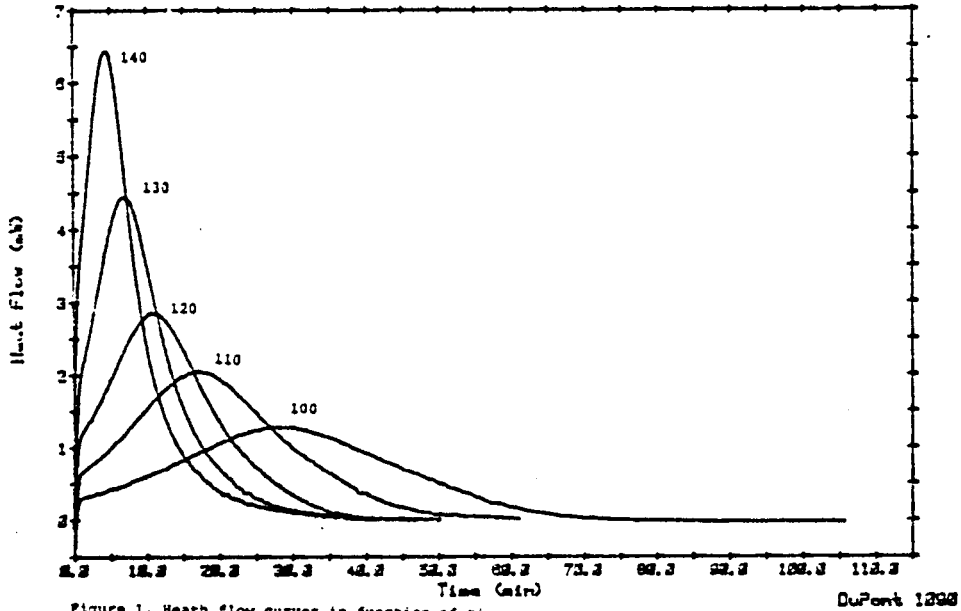

Figure 1. Heath flow curves in function of time.
System DGEBA with MDA A/E = 1.0 .Temperatures 140, 130.120.110,100 °C.

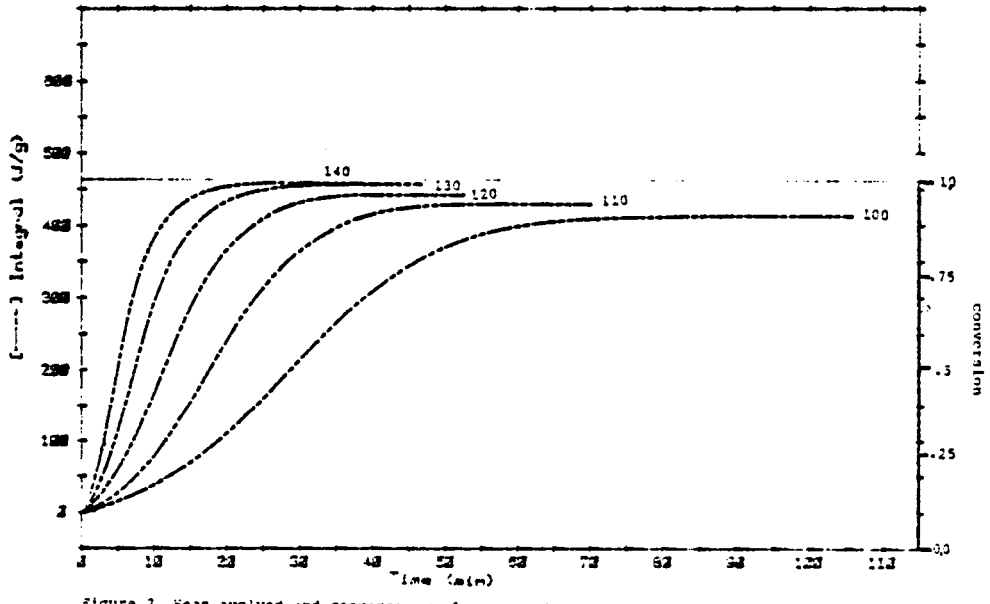

Figure 2 .Heat evolved and conversion in function of time.
System DGEBA with MDA A/E = 1.0. Temperatures 140, 130, 120, 110, 100 °C .

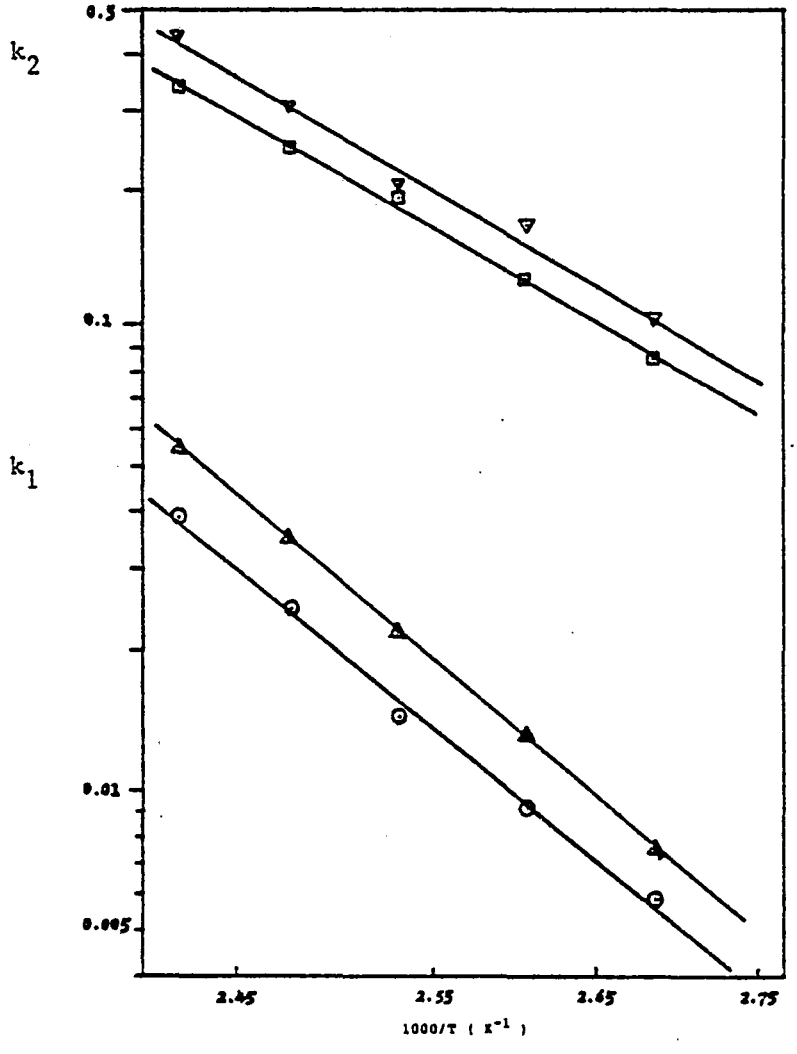

Figure 3. Kinetic rate constants k_1 and k_2 as a function of reciprocal absolute temperature.
Systems: DGEBA with MDA k_1 ⊙ k_2 ⊡
DGEBA with m-PDA k_1 △ k_2 ▽

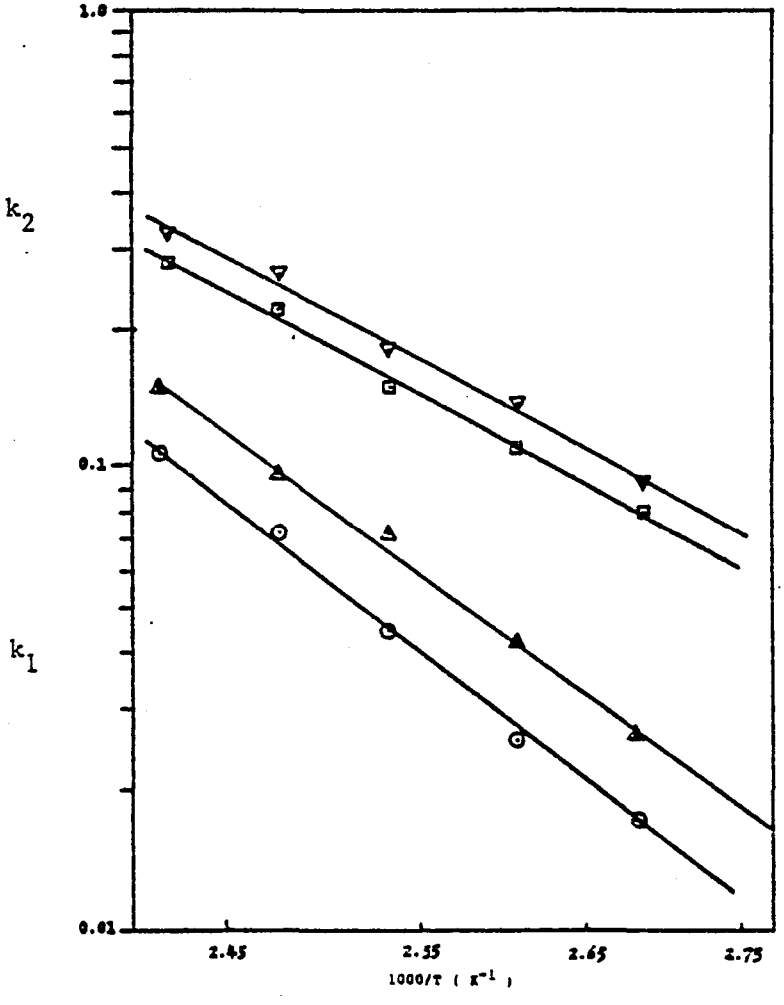

Figure 4. Kinetic rate constants k_1 and k_2 as a function of reciprocal absolute temperature.
Systems: DGBE with MDA k_1 ⊙ k_2 ⊡
DGBE with m-PDA k_1 △ k_2 ▽

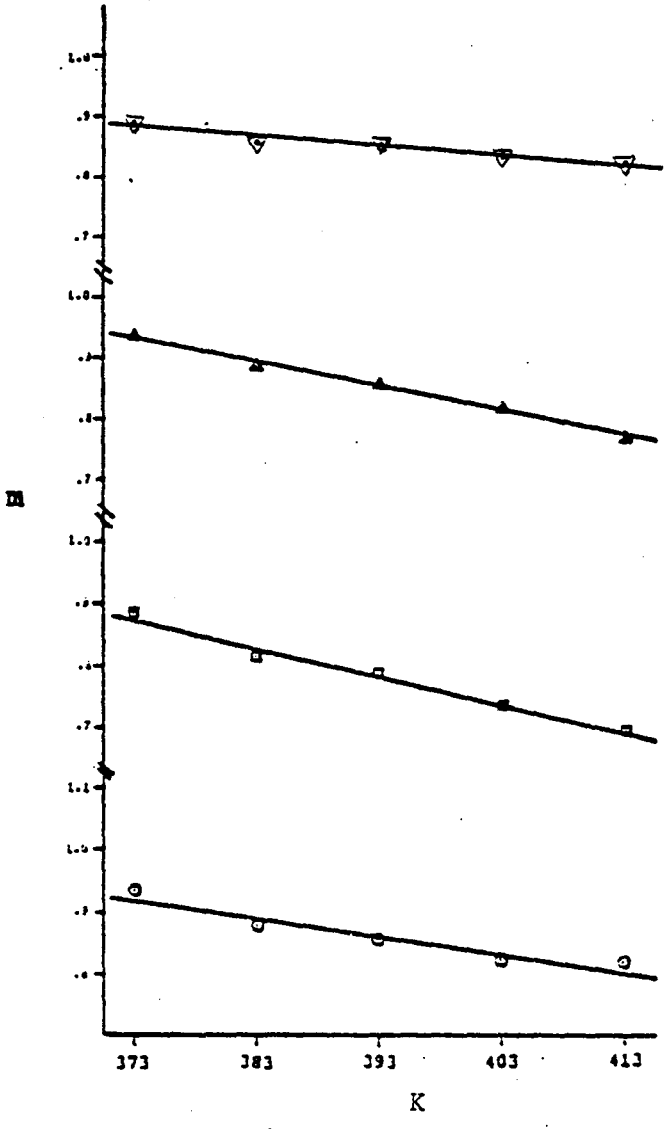

Figure 5. Kinetic exponent m as a function of absolute temperature.
Systems: DGEBA with MDA ⊙ DGEBA with m-PDA ⊡
DGBE with MDA △ DGBE with m-PDA ▽

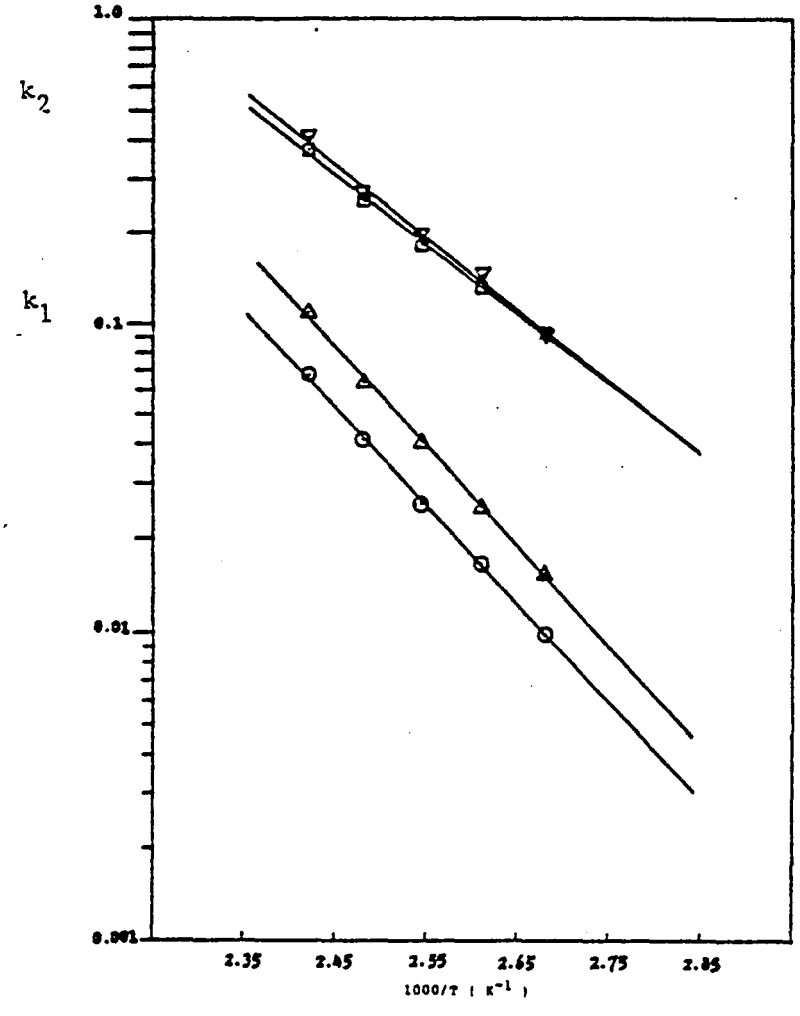

Figure 6. Kinetic rate constants k_1 and k_2 as a function of reciprocal absolute temperature.
Systems: DGEBA / DGBE (80/20) with MDA k_1 ⊙ k_2 ▽
DGEBA / DGBE (80/20) with m-PDA k_1 △ k_2 □

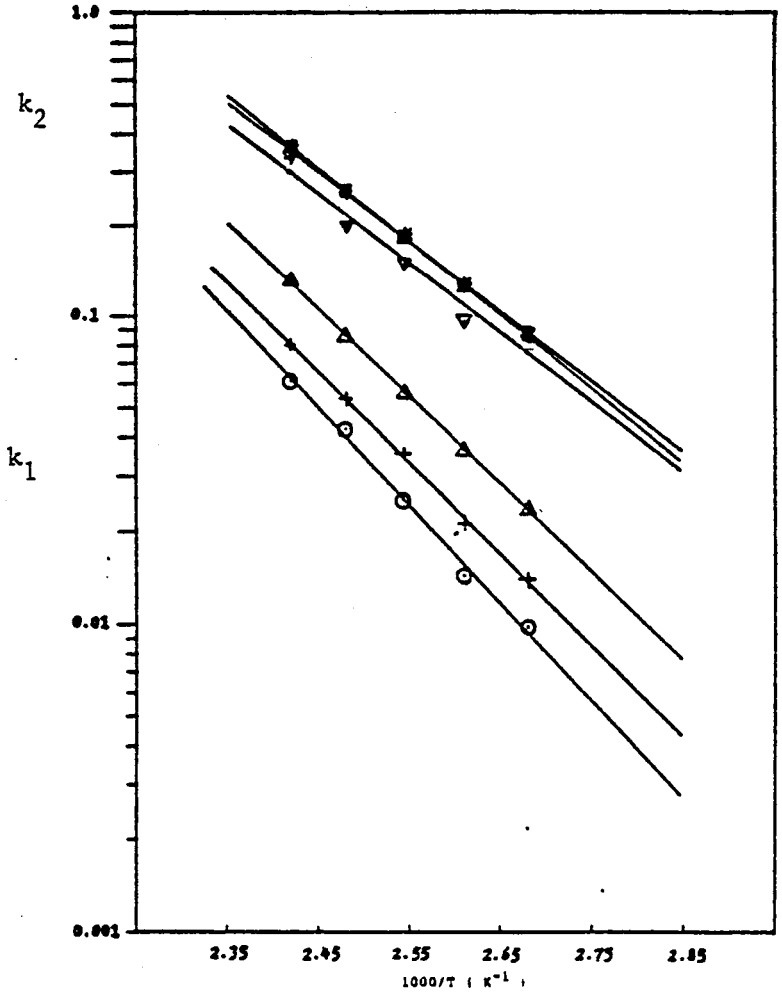

Figure 7. Kinetic rate constants k_1 and k_2 as a function of reciprocal absolute temperature.

Systems:			
DGEBA with Tonox 60/40	k_1 ⊙	k_2 ⊡
DGBE with Tonox 60/40	k_1 △	k_2 ◁
DGEBA / DGBE (80/20) with Tonox 60/40	k_1 +	k_2 *

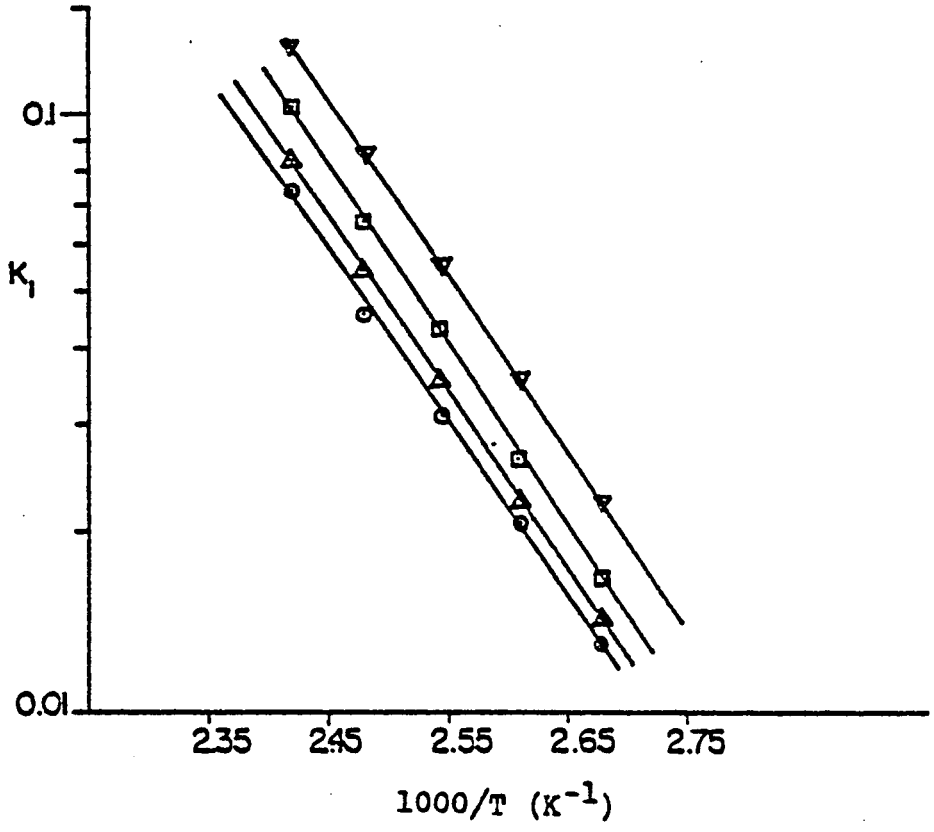

Figure 8. Kinetic rate constants k_1 as a function of reciprocal absolute temperature.
Systems: DGEBA / DGBE (80/20) with Tonox 60/40
A/E = 0.9 ⊙ A/E = 1.0 △
A/E = 1.1 ⊡ A/E = 1.2 ▽

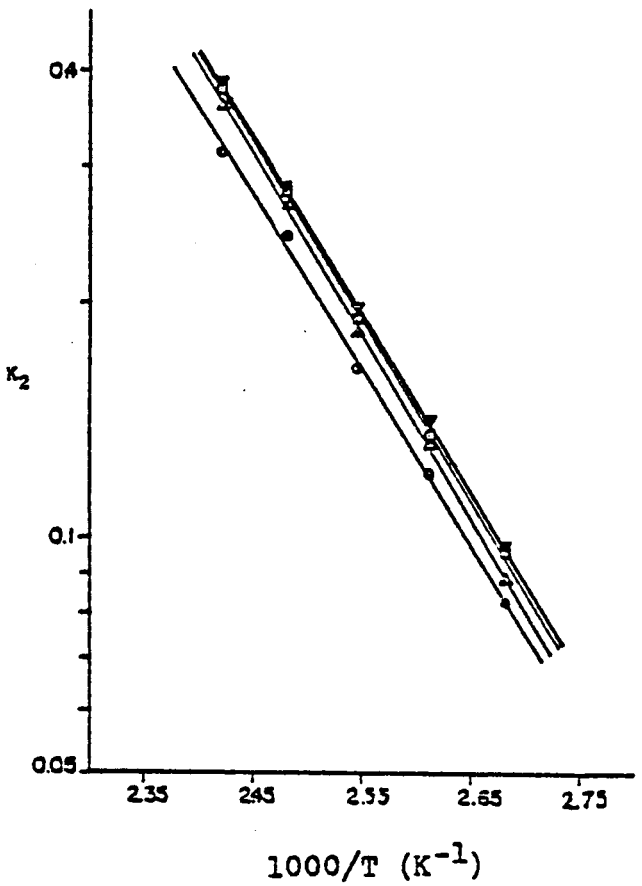

Figure 9. Kinetic rate constants k_2 as a function of reciprocal absolute temperature.
Systems: DGEBA / DGBE (80/20) with Tonox 60/40
A/E = 0.9 ⊙ A/E = 1.0 △
A/E = 1.1 ⊡ A/E = 1.2 ▽

Appendix 1. Method of rearrangement of the kinetic equation (1) to calculate k_1, k_2, m and n.

$$\dot{\alpha} = \frac{d\alpha}{dt} = (K_1 + K_2\alpha^m)(1-\alpha)^n \tag{1}$$

$$m = \frac{\ln\left(\left(\frac{\dot{\alpha}}{(1-\alpha)^n} - K_1\right)\Big/ K_2\right)}{\ln\alpha} \tag{2}$$

$$\left(\frac{d\alpha}{dt}\right)_{t=0} = K_1 \tag{3}$$

$$\frac{d^2\alpha}{dt^2} = 0 \tag{4}$$

$$nK_1\alpha_p^{1-m} + K_2(m+n)\alpha_p - mK_2 = 0 \tag{5}$$

$$m + n = 2 \tag{6}$$

$$K_2 = \frac{(2-m)K_1\alpha_p^{1-m}}{m-2\alpha_p} \tag{7}$$

$$m = \frac{\ln\left(\left(\frac{\dot{\alpha}_p}{(1-\alpha_p)^{2-m}} - K_1\right)\Big/\left(\frac{(2-m)K_1\alpha_p^{1-m}}{m-2\alpha_p}\right)\right)}{\ln\alpha_p} \tag{8}$$

Appendix 2. Graphical rapresentation of the method of non linear regression.

$$\frac{\dot{\alpha}}{(1-\alpha)^n} = k_1 + k_2 \alpha^m$$

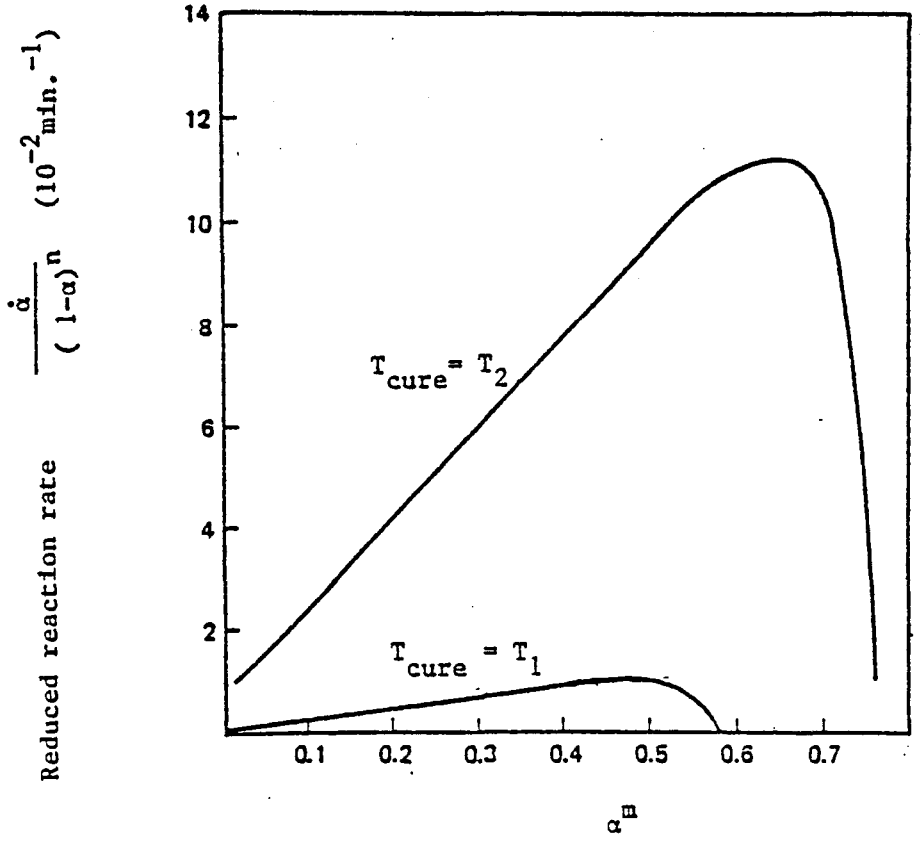

$T_2 > T_1$

Slope = k_2 Intercept = k_1

Appendix 3. Flowchart of the computer program used to calculate and optimize activation energies an frequency factors.

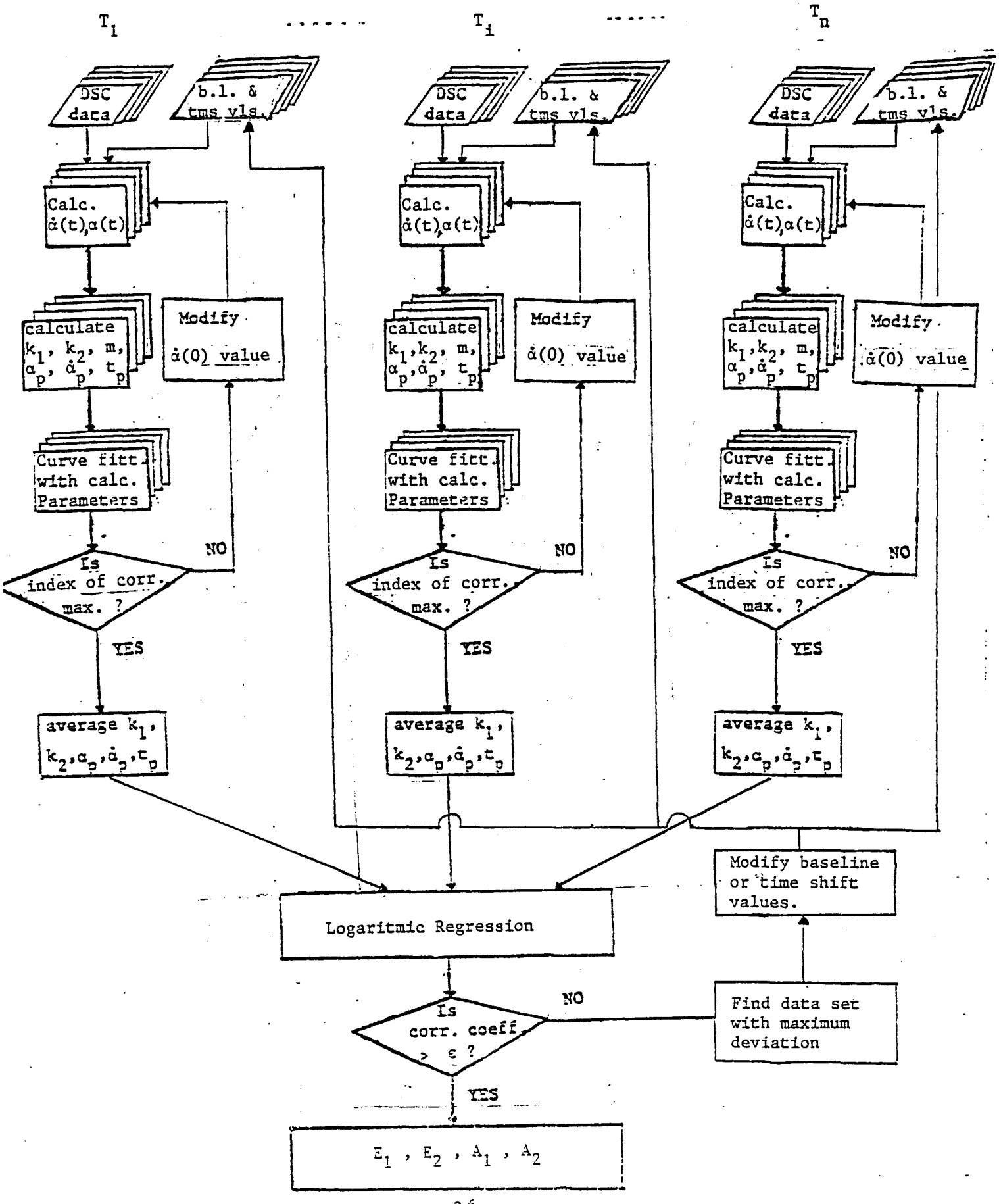

PART IV

PHYSICAL/THERMAL PROPERTIES OF HBRF 55A RESIN FORMULATIONS DURING CURE

A. Measurements of Viscosity During Cure

A series of viscosity measurements were conducted with the formulation containing DGEBA/DGBE (80/20) resin mixture and cured with the stoichiometric amount of the Tonox mixture (A/E=1.0). Rheological measurements were performed using a model R-17 Weissenberg Rheogoniometer which is a cone-and-plate type instrument. Viscosity was measured as a function of steady shear rate, curing time and curing temperature.

In Figures 1-3, viscosity is shown as a function of shear rate for three different temperatures; 26°C, 40°C and 50°C, respectively. In each figure there are data points for several curing times. We conclude that, of the conditions of this study, viscosity is independent of shear rate. The changes in viscosity as a function of time and temperature during cure are summarized in Table 1.

In Figure 4, we show the results of changes in viscosity as a function of curing time with temperature as a parameter. As one would expect, the higher the curing temperature, the lower the initial viscosity and the faster the increase in viscosity as a function of curing time.

In Figure 5, viscosity was plotted as a function of curing temperature with curing time as a parameter. Solid lines connect the isochronous points at different temperatures. At short times, viscosity decreases with increasing temperature. At longer times, however, viscosity increases as the temperature is increased due to an increase in MW of the network.

B. Measurements of Extent of Reaction During Cure

The extent of reaction was measured next in order to correlate it to the simultaneous changes in physical/thermal properties during cure. DuPont's 910 DSC cell in conjunction with the 1090 Thermal Analyzer were used in this study. The heating rate was 20°C/min. A dynamic scan of an "as-prepared" sample provided the reference value of the total heat of reaction (ΔH_T). Other samples were then prepared and maintained at three different temperatures for various periods of time. At desired time intervals, samples were removed and scanned in DSC. The difference in the thus obtained heat of reaction (ΔH_R) and the reference value (ΔH_T) was taken as the heat of reaction during the elapsed period at a given temperature. The ratio of $\Delta H_R/\Delta H_T$ was take to represent the extent of reaction (α). Values of α as a function of curing time and temperature are summarized in Table 2. In Figure 6, the extent of cure is plotted as a function of curing time with temperature as a parameter. A cross-plot showing the observed relationship between changes in viscosity and the extent of reaction at 40°C, is given in Figure 7.

C. Measurements of Heat Capacity During Cure

A series of measurements of heat capacity was performed next. DSC unit describe in part B was used to generate data. A baseline was established first and then a standard sample with known heat capacity was run. Finally, the resin samples were run and their heat capacities calculated. In Table 3, we summarize the calculated values

of Cp obtained from DSC data at different temperatures and times. Plots of heat capacity as a function of curing time with temperature as a parameter, are shown in Figure 8. A decrease in heat capacity with increased curing time was observed for every temperature. In Figure 9, we show heat capacity as a function of curing temperature. Solid lines connect sets of isochronal points obtained at different temperatures. It is interesting to note that the rate of heat capacity change increases as the curing temperature is increased. Finally, in Figure 10, we show the heat capacity for sample cured at 40°C for 1.5 hr, in the range between 20° and 70°C. The corresponding equation is included on Figure 10.

Next, heat capacity of the composite (Cp_c) was calculated using the equation:

$$Cp_c = W_f Cp_f + W_m Cp_m$$

where W_f and W_m are the weight fractions, and Cp_f and Cp_m heat capacities of the fiber and the matrix, respectively. Changes in Cp_c during cure are shown as dashed lines in Figures 8 and 10. The values of heat capacity and density of the fiber were obtained from the literature.

Measurements of Density During Cure

A series of density measurements were performed next. During the initial stages of cure, density of the liquid resin was measured with a hydrometer. In Figure 11, we show density of the resin as a function of curing time with curing temperature as a parameter. An abrupt increase in density occurs during gelation. In Figure 12,

changes in density are shown as a function of the extent of cure. We also calculated changes in the density of composite. A typical value of carbon fiber density obtained from the literature is ρf = 1.80 g/cm^3. Assuming that ρf does not change during the resin cure in the temperature range between 20°C and 50°C, we proceeded to calculate the changes in composite density (ρc) during cure. The following equation was used:

$$\rho_c = \rho_f V_f + \rho_m V_m$$

where ρ_f and ρ_m are densities, and V_f and V_m the volume fractions of the fiber and the matrix, respectively. Changes in ρ_c during cure are shown as dashed lines in Figure 11.

Measurement of Thermal Conductivity During Cure

Our initial studies have shown that the thermal conductivity of the resin increases with the extent of cure. However, we have not yet generated absolute values because we are in the process of performing an exact calibration of our equipment.

TABLE 1

Changes in Viscosity (μ, poise) as a Function of Curing Temperature and Curing Time

	Curing Temperature		
Curing Time hr.	26°C	40°C	50°C
1.5	11.4	3.3	1.8
2.5		4.4	3.1
3.0	14.1	5.1	4.1
4.0		7.3	11.8
4.5	19.0	9.0	22.3
5.5		17.1	100.2
6.0	28.0	25.0	250
7.5	44.2	150	gelled
9.0	79.3	1,000	
12.0	350	gelled	
13.5	2,210		
15.0	5,950		
16.0	11,314		
17.0	gelled		

TABLE 2

Changes in Extent of Reaction (α, %) as a Function of Curing Temperture and Curing Time

	Curing Temperature		
Curing Time hr.	26°C	40°C	50°C
1.5		15.0	18.5
3.0		31.1	
4.5		50.4	
5.0	4.1		
6.0		64.3	70.2
7.5		68.3	
8.0	7.0		
9.7	13.9		
14.0	28.5		
16.0	31.3		

TABLE 3

Changes in Heat Capacity (Cp, Cal/g,°C) at 20°C as a Function of Curing Temperture and Curing Time

	Curing Temperature		
Curing Time hr.	26°C	40°C	50°C
1.5	0.7964	0.6203	0.5882
3.0	0.7735	0.5768	0.5530
4.5	0.7481	0.5333	0.4424
6.0	0.6905	0.4563	0.3982
7.5	0.6627	0.4088	
9.0	0.6350		
12.0	0.6175		
14.0	0.5980		
16.0	0.5792		

TABLE 4

Changes in Density (ρ, g/cm^3) as a Function of Curing Temperature and Curing Time

Curing Time hr.	Curing Temperature 26°C	40°C	50°C
0.0	1.137	1.137	1.137
1.5			1.139
2.0	1.140	1.144	1.147
3.5		1.148	
4.5	1.148	1.154	1.166
5.0	1.152	1.159	
6.5			*1.2222(gel)
7.5			*1.2233(gel)
8.0	1.157		
9.0	1.158	1.167	
10.0	1.161		
12.0	1.163		
14.0	1.164	*1.2205(gel)	
16.0	1.165	*1.2234(gel)	
18.0		*1.2250(gel)	
22.0			*1.2268(gel)
25.0		*1.2283(gel)	
40.0	*1.2168(gel)		

*measured with Density Gradient Column

Other data obtained with Hydrometer.

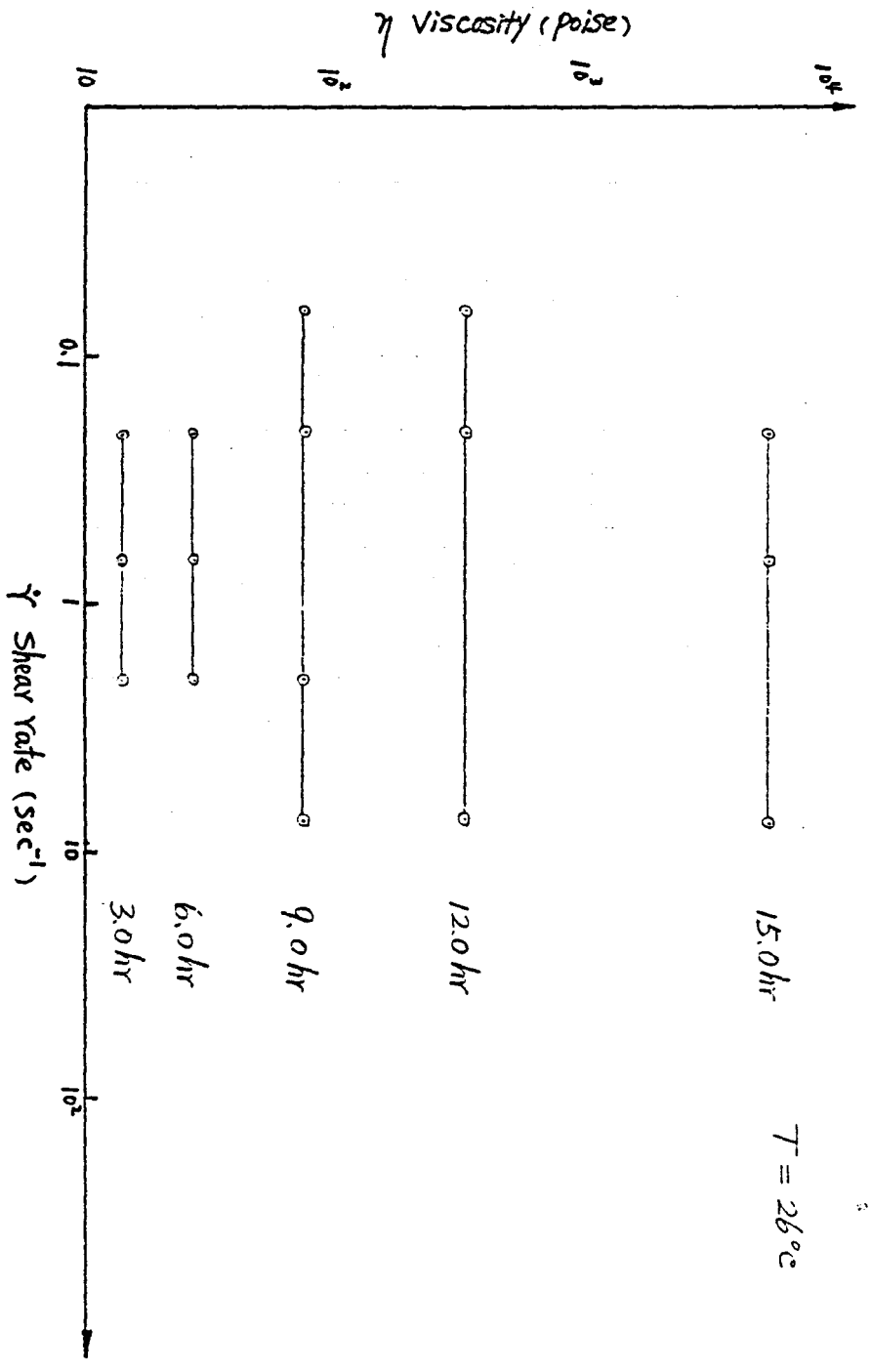
η Viscosity (poise)
10⁴
10³
10²
10
0.1
1
10
10²
γ̇ Shear Rate (sec⁻¹)
15.0 hr
12.0 hr
9.0 hr
6.0 hr
3.0 hr
T = 26°C

Figure 1

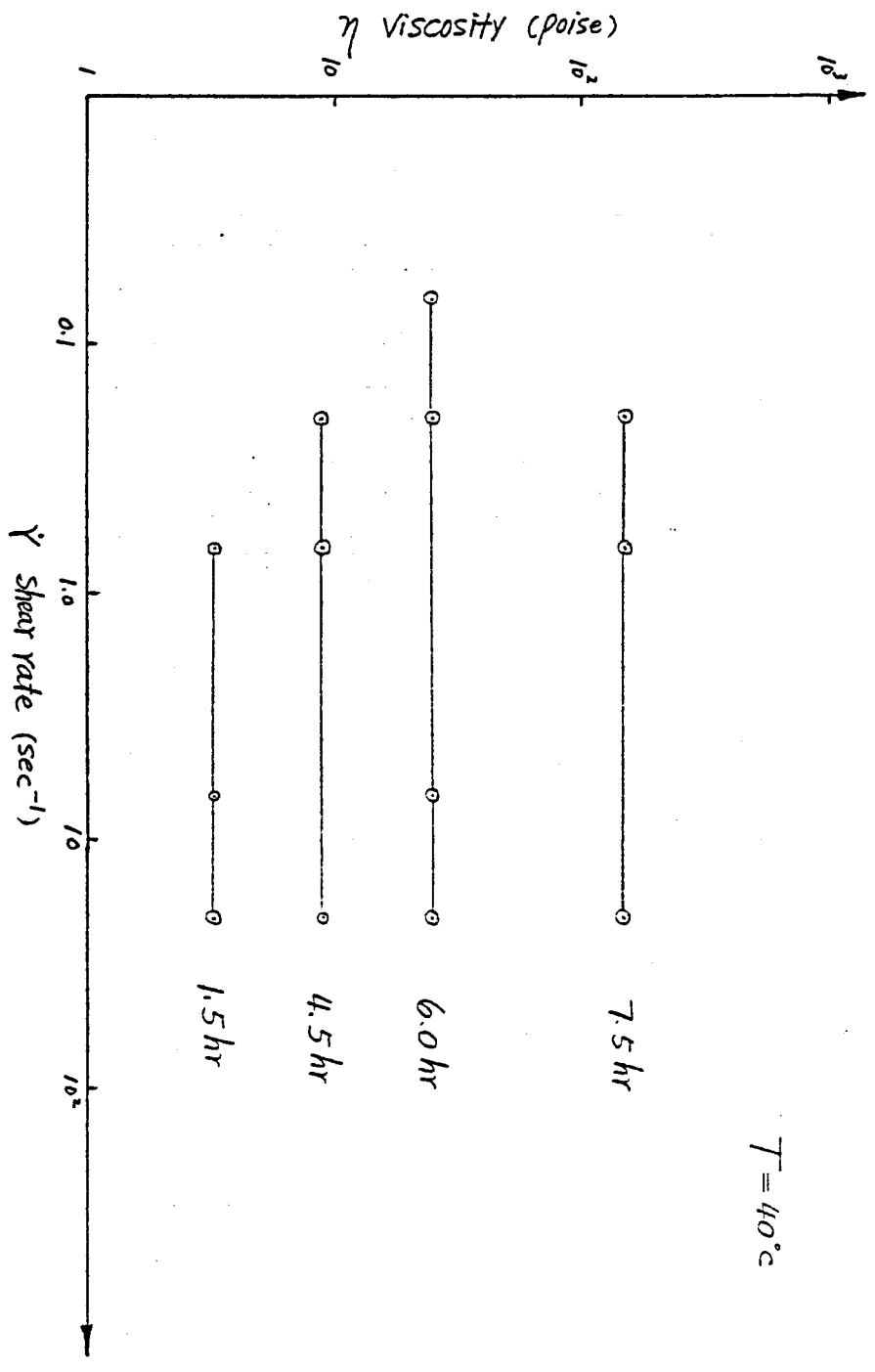
η Viscosity (poise)
1
10
10²
10³
0.1
1.0
10
10²
γ̇ Shear rate (sec⁻¹)
1.5 hr
4.5 hr
6.0 hr
7.5 hr
T = 110°C

Figure 2

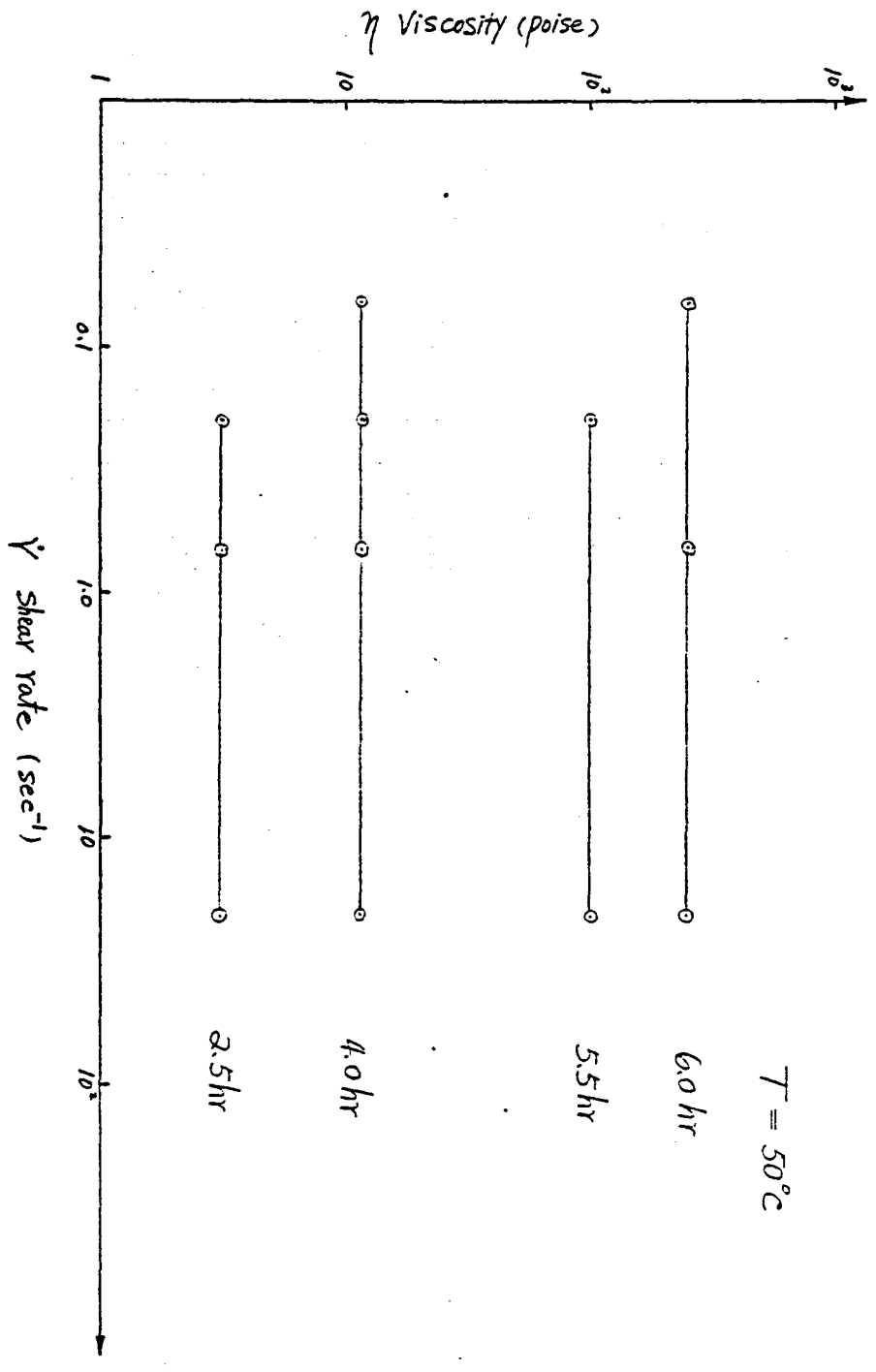
η Viscosity (poise)
1
10
10²
10³
0.1
1.0
10
10²
γ̇ Shear rate (sec⁻¹)
T = 50°C
6.0 hr
5.5 hr
4.0 hr
2.5 hr

Figure 3

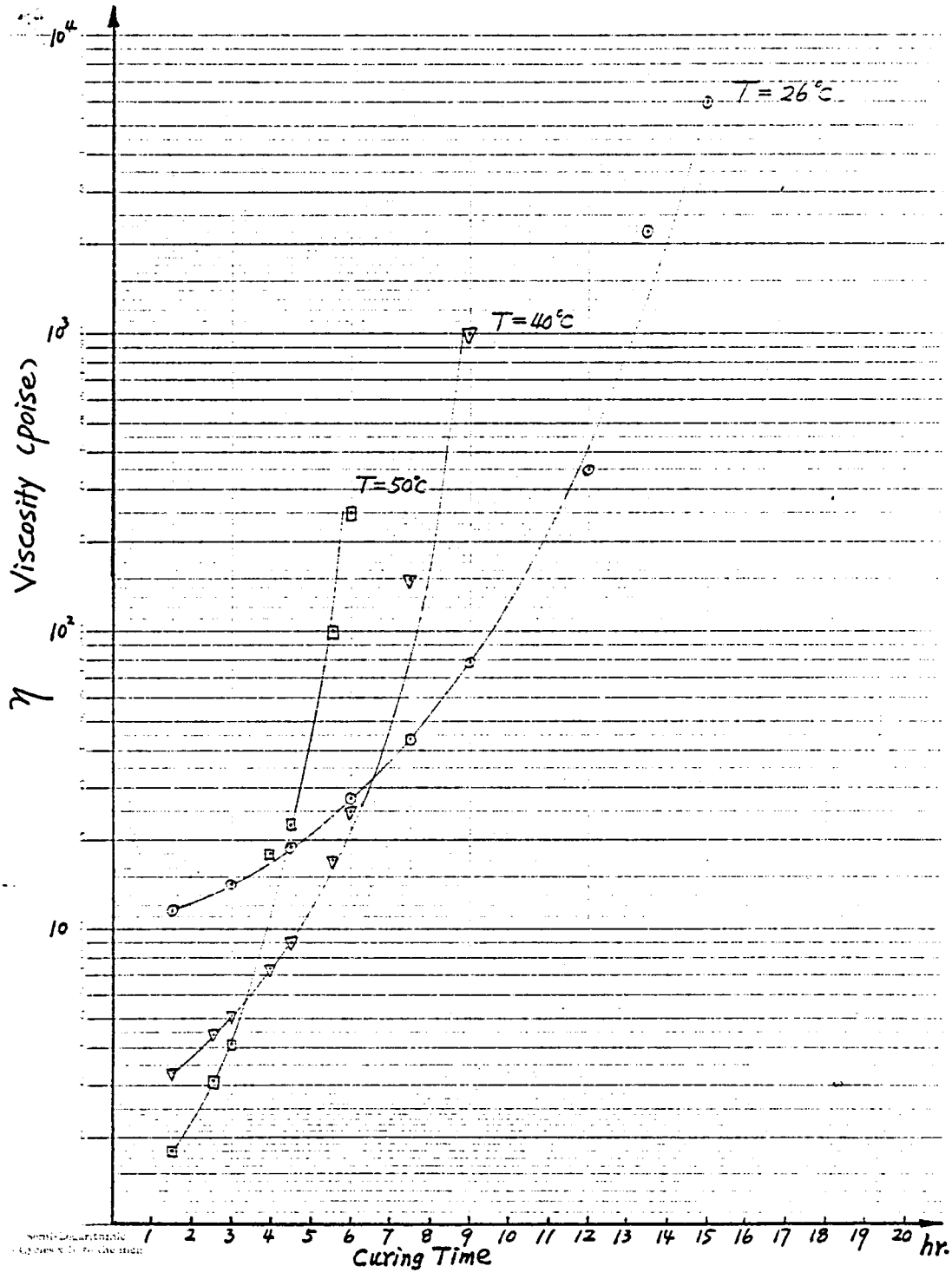
10^4
10^3
10^2
10
η Viscosity (poise)
T = 26°C
T = 40°C
T = 50°C
1 2 3 4 5 6 7 8 9 10 11 12 13 14 15 16 17 18 19 20 hr.
Curing Time

Figure 4

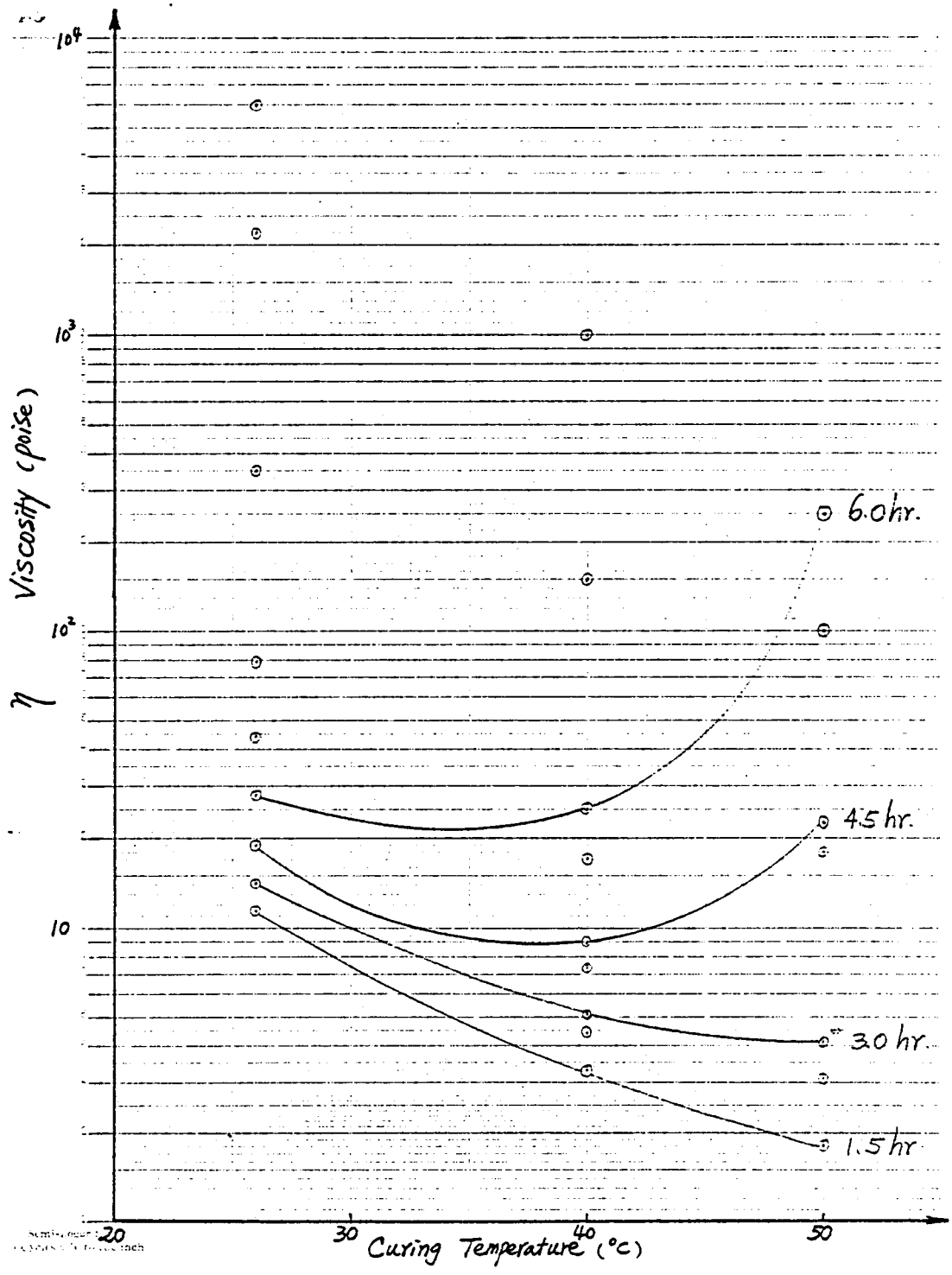
10^4
10^3
10^2
10
η Viscosity (poise)
6.0 hr.
4.5 hr.
3.0 hr.
1.5 hr
20
30
40
50
Curing Temperature (°C)

Figure 5

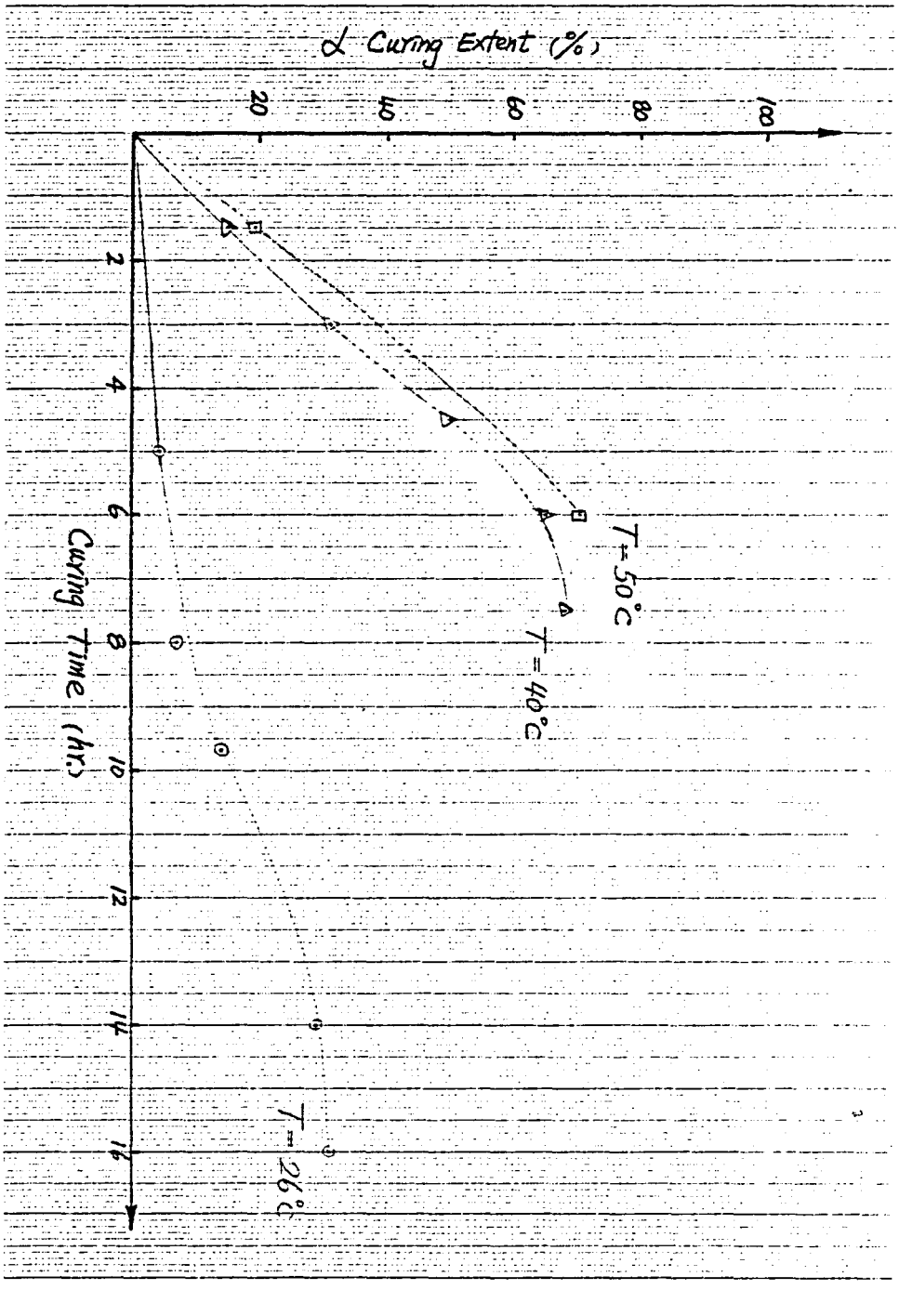
α Curing Extent (%)
20
40
60
80
100
2
4
6
8
10
12
14
16
Curing Time (hr.)
T = 50°C
T = 40°C
T = 26°C

Figure 6

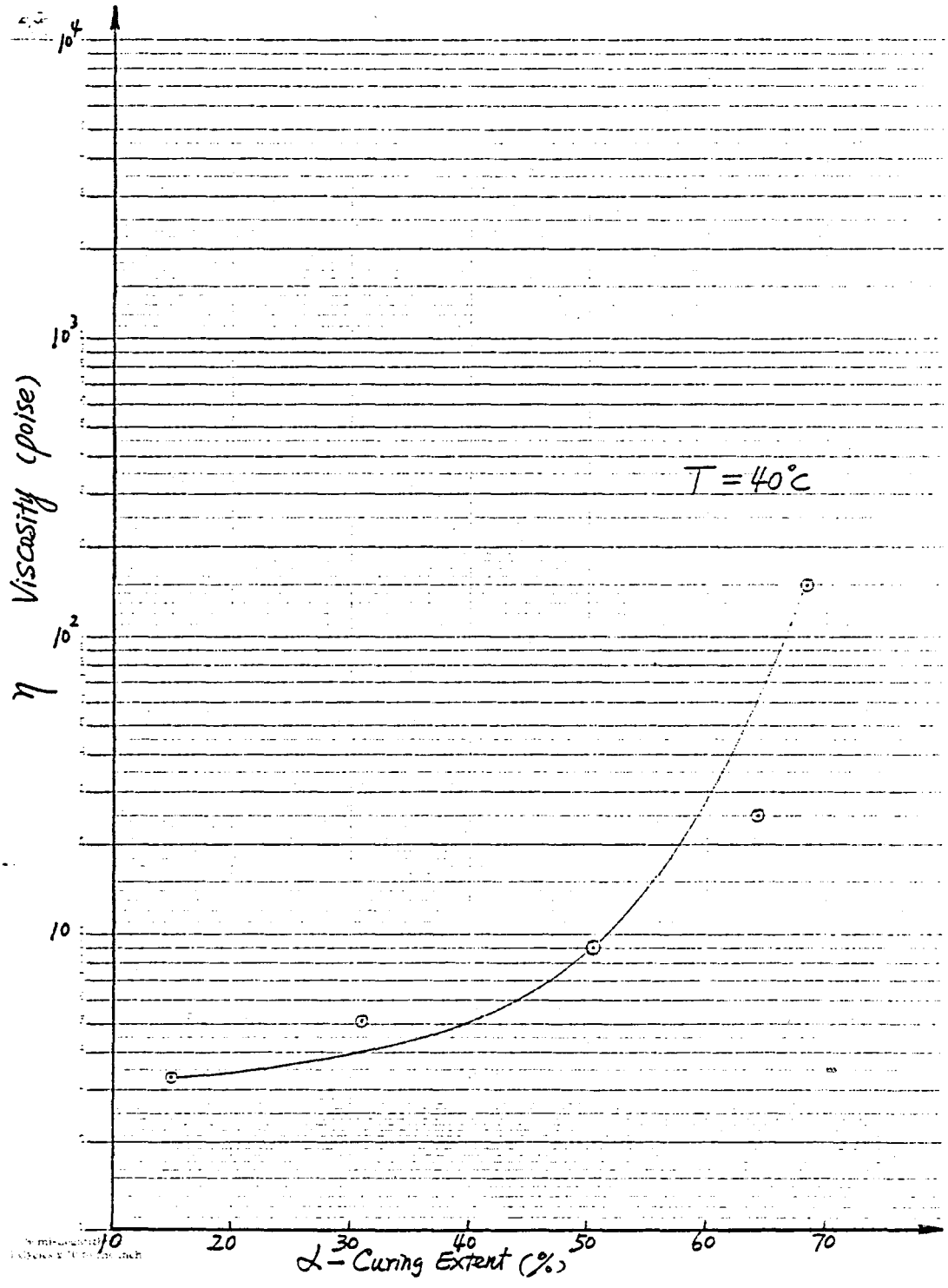
10^4
10^3
10^2
10
η Viscosity (poise)
T = 40°C
10
20
30
40
50
60
70
α – Curing Extent (%)

Figure 7

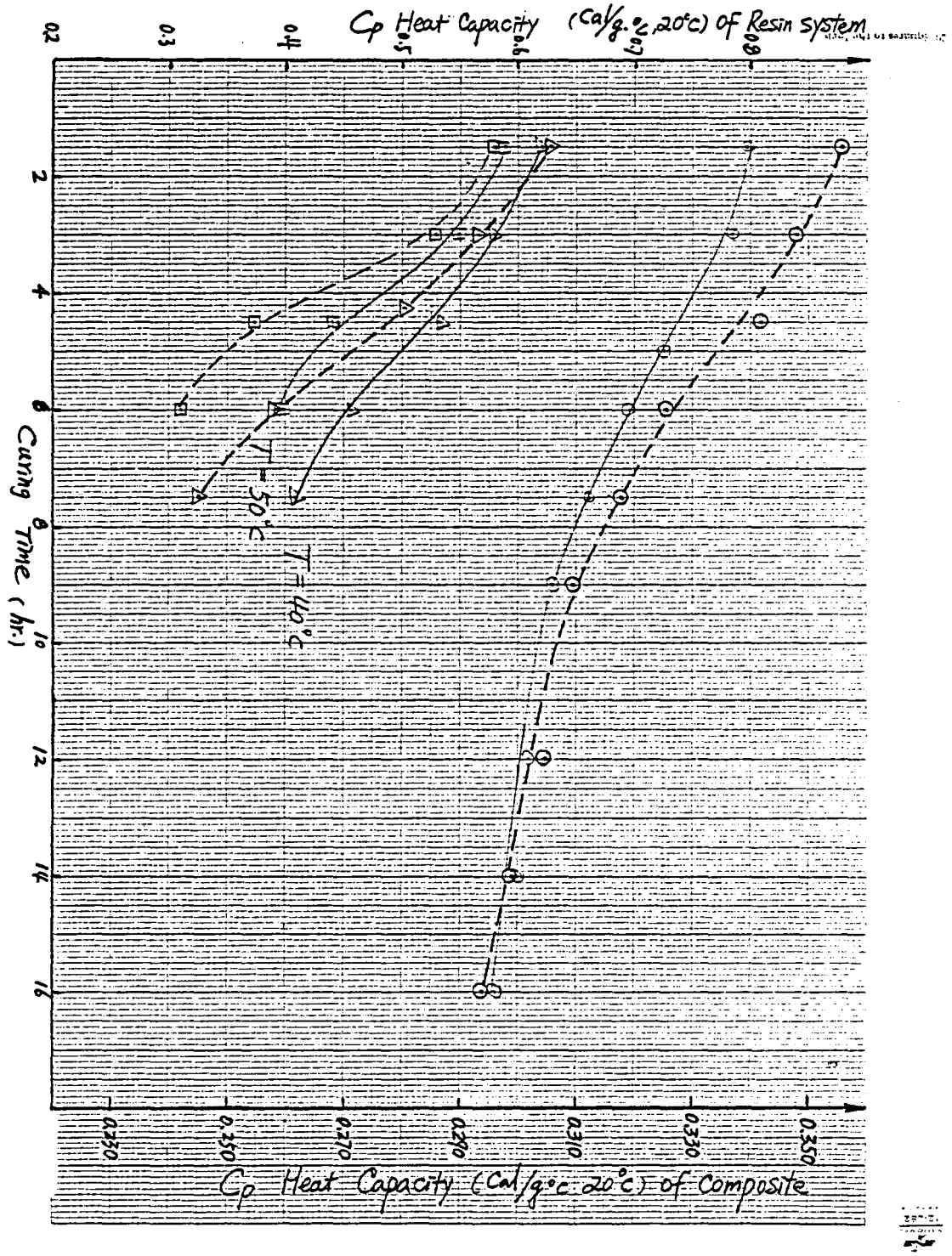
Cp Heat Capacity (Cal/g.°C, 20°C) of Resin System
0.2
0.3
0.4
0.5
0.6
0.7
0.8
Curing Time (hr.)
2
4
6
8
10
12
14
16
T = 50°C
T = 110°C
0.250
0.260
0.270
0.280
0.290
0.300
0.310
0.320
0.330
0.340
0.350
Cp Heat Capacity (Cal/g°C 20°C) of Composite

Figure 8

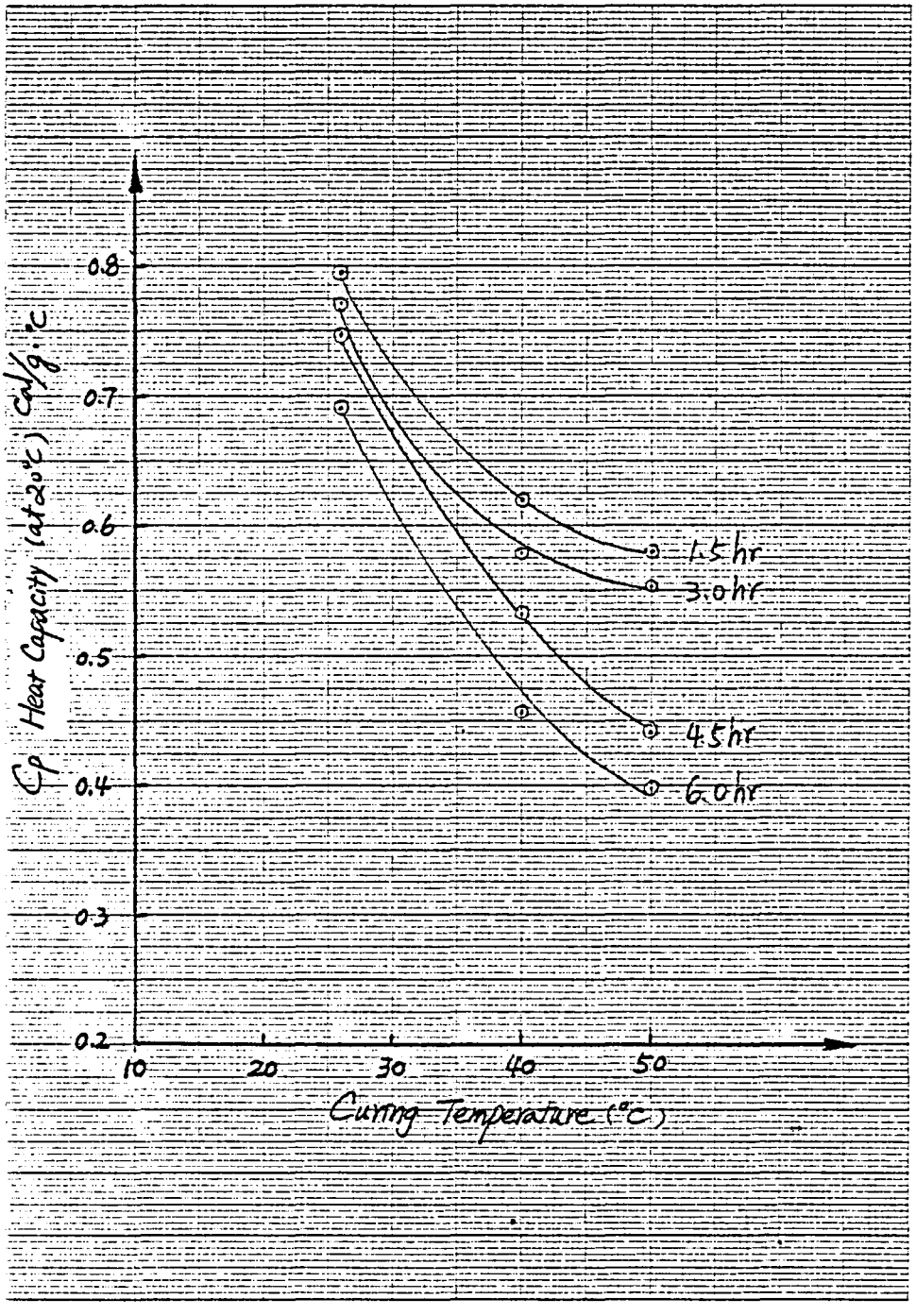
0.8
0.7
0.6
0.5
0.4
0.3
0.2
Cp Heat Capacity (at 20°C) cal/g·°C
1.5 hr
3.0 hr
4.5 hr
6.0 hr
10
20
30
40
50
Curing Temperature (°C)

Figure 9

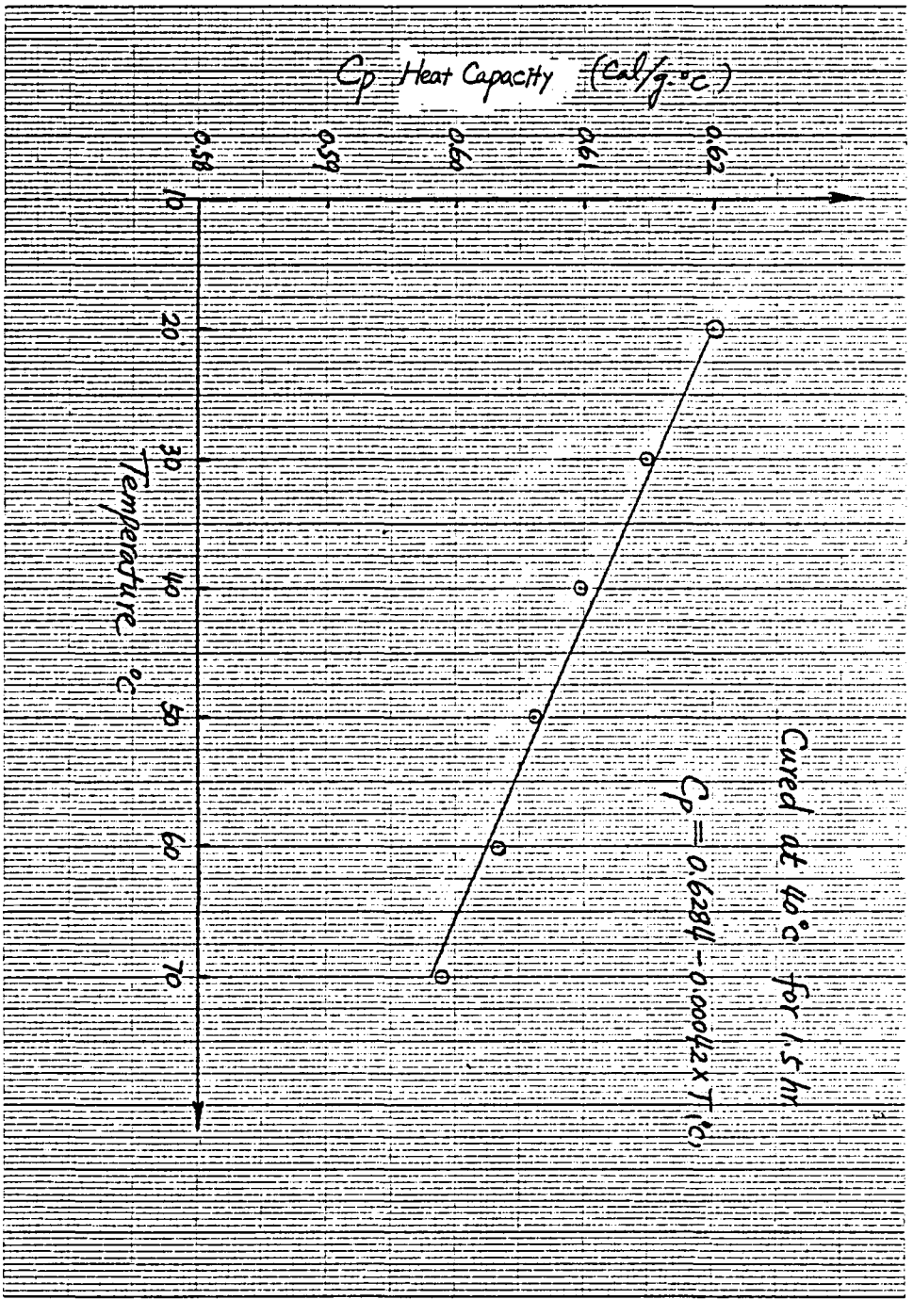
Cp Heat Capacity (cal/g.°C)
0.58
0.59
0.60
0.61
0.62
10
20
30
40
50
60
70
Temperature °C
Cured at 40°C for 1.5 hr
Cp = 0.6284 - 0.00042 x T(°C)

Figure 10

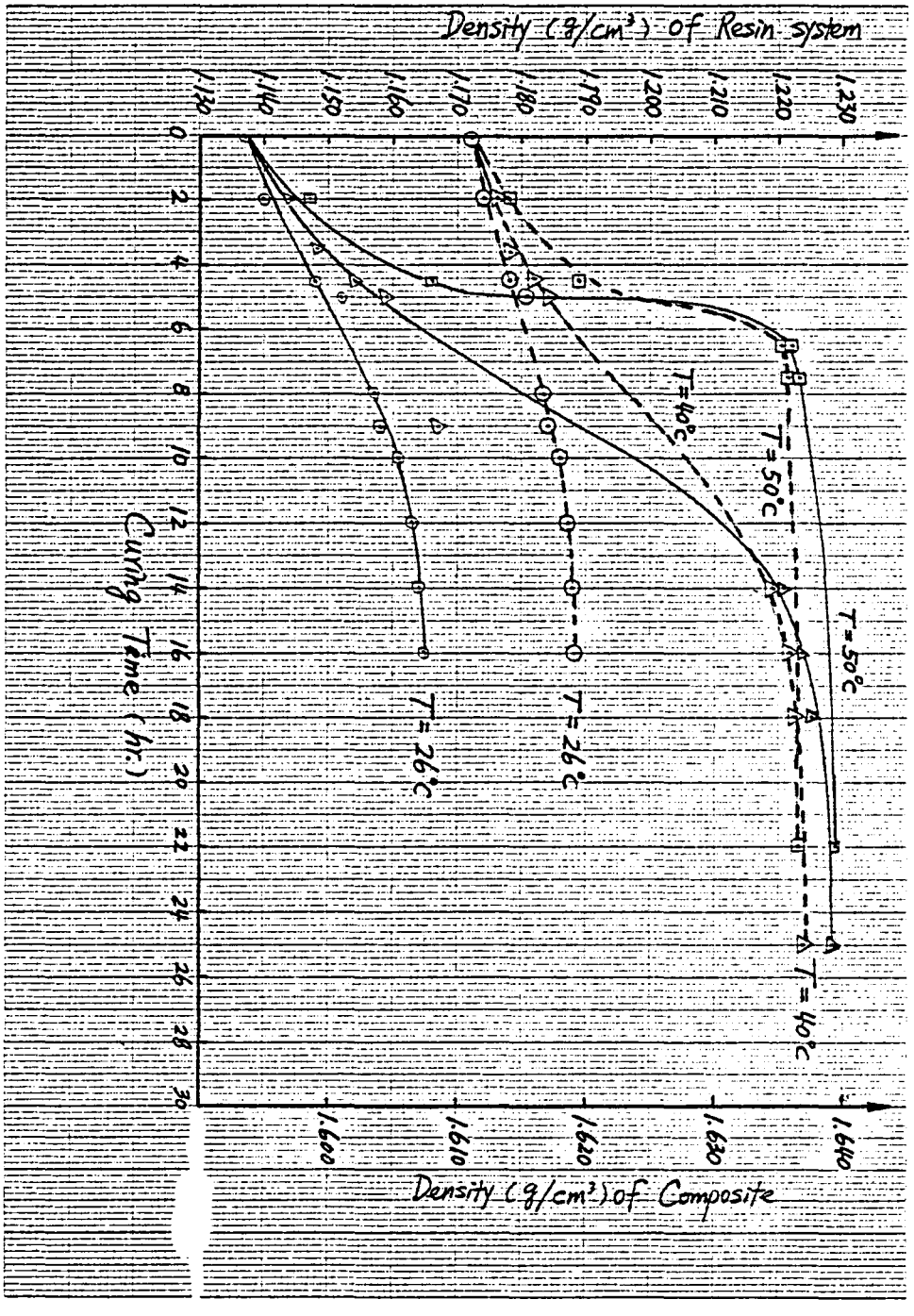
Density (g/cm³) of Resin system
1.130
1.140
1.150
1.160
1.170
1.180
1.190
1.200
1.210
1.220
1.230
0
2
4
6
8
10
12
14
16
18
20
22
24
26
28
30
Curing Time (hr.)
T = 50°C
T = 40°C
T = 26°C
T = 50°C
T = 40°C
T = 26°C
1.600
1.610
1.620
1.630
1.640
Density (g/cm³) of Composite

Figure 11

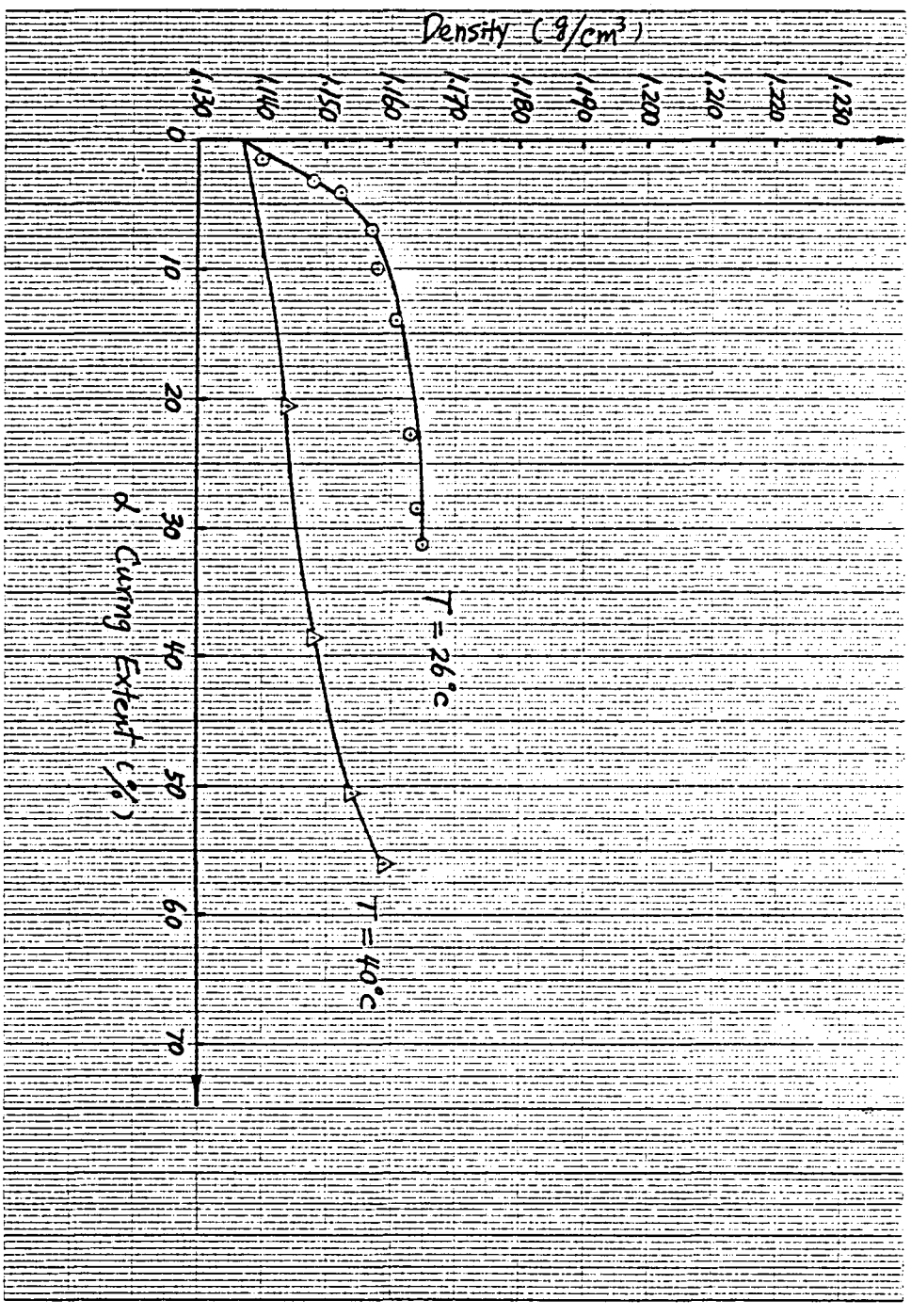
Density (g/cm³)
1.130
1.140
1.150
1.160
1.170
1.180
1.190
1.200
1.210
1.220
1.230
0
10
20
30
40
50
60
70
α Curing Extent (%)
T = 26°C
T = 40°C

Figure 12

End of Document